Universidad de Málaga

Escuela Técnica Superior de Ingeniería de Telecomunicación

TESIS DOCTORAL

Analysis of SC-FDMA and OFDMA Performance over Fading Channels

Autor:

Juan Jesús Sánchez Sánchez

Directores:

María del Carmen Aguayo Torres

Unai Fernández Plazaola

Final Version (20-05-2011)

UNIVERSIDAD DE MÁLAGA
ESCUELA TÉCNICA SUPERIOR DE INGENIERÍA DE TELECOMUNICACIÓN

Reunido el tribunal examinador en el día de la fecha, constituido por:

Presidente: Dr. D. _____

Secretario: Dr. D. _____

Vocales: Dr. D. _____

Dr. D. _____

Dr. D. _____

para juzgar la Tesis Doctoral titulada *Analysis of SC-FDMA and OFDMA Performance over Fading Channels* realizada por D. Juan Jesús Sánchez Sánchez y dirigida por los Prof. Dr. Dª. Mª. Carmen Aguayo Torres y D. Unai Fernández Plazaola, acordó por

_____ otorgar la calificación de

_____ y para que conste,

se extiende firmada por los componentes del tribunal la presente diligencia.

Málaga a ____ de _____ del ____

El Presidente: El Secretario:

Fdo.: _____ Fdo.: _____

El Vocal: El Vocal: El Vocal:

Fdo.: _____ Fdo.: _____ Fdo.: _____

To my family. To my friends with all the letters

Acknowledgments

I wish to express my gratitude to Dra. Carmen del Castillo Vázquez for her guidance and advice when it took to tackle with mathematics way beyond my knowledge. I would also like to thank Dr. Eduardo Martos Naya and D. José Francisco Paris Ángel for their valuable comments and the interesting discussion.

Lastly, I gratefully acknowledge the financial support by the Junta de Andalucía (Proyecto de Excelencia P07-TIC-03226) and by the Spanish Government (Plan Nacional de I+D+I, TEC2010-18451).

Table of Contents

List of Figures

List of Tables

List of Acronyms

3GPP LTE	3rd Generation Partnership Project Long Term Evolution
AM	Adaptive Modulation
AWGN	Additive White Gaussian Noise
BER	Bit Error Rate
BPSK	Binary Phase Shift Keying
CATV	Community Antenna Television
CB	Coherence Bandwidth
CDF	Cumulative Distribution Function
CEP	Components of Error Probability
CHF	Characteristic Function
CLT	Central Limit Theorem
CP	Cyclic Prefix
CQI	Channel Quality Indicator
CR	Coherence Ratio
DCT	Discrete Cosine Transform
DFT	Discrete Fourier Transform
DVB-T	Digital Video Broadcast - Terrestrial
ETU	Extended Typical Urban
EVA	Extended Vehicular A
FFT	Fast Fourier Transform
GCLT	Generalized Central Limit Theorem
IBI	Inter-Block Interference
ICI	Inter-Carrier Interference
IDFT	Inverse Discrete Fourier Transform
IFFT	Inverse Fast Fourier Transform
ISI	Inter-Symbolic Interference
ITU	International Telecommunications Union
LOS	Line Of Sight
LTE	Long Term Evolution
MCM	Multi-Carrier Modulation
MGF	Moment-Generating Function
MIMO	Multiple-Input Multiple-Output
MMSE	Minimum Mean Square Error
M-QAM	Multilevel QAM

non-LOS	non-Line Of Sight
OFDM	Orthogonal Frequency-Division Multiplexing
OFDMA	Orthogonal Frequency-Division Multiple Access
PA	Pedestrian A
PAPR	Peak-to-Average Power Ratio
PB	Pedestrian B
PDF	Probability Density Function
PDP	Power Delay Profile
PSK	Phase Shift Keying
QAM	Quadrature Amplitude Modulation
RCS	Radar Cross Section
SC-FDE	Single-Carrier modulation with Frequency-Domain Equalization
SER	Symbol Error Rate
SINR	Signal to Interference plus Noise Ratio
SNR	Signal to Noise Ratio
TDE	Time-Domain Equalization
UMTS	Universal Mobile Telecommunications System
VA	Vehicular A
VB	Vehicular B
ZF	Zero-Forcing

Abstract

Next generation of wireless mobile systems will allow the provision of advanced multimedia services with ubiquitous access thanks to the higher data rates offered. However, it is necessary for the transmission technologies to be able to cope with problems deriving from high-data-rate transmissions over wireless channels that are limited in bandwidth and power.

Hitherto, Orthogonal Frequency-Division Multiplexing (OFDM) has been the more widely used technique due to its robustness against frequency selective fading channels. However, it suffers from a high Peak-to-Average Power Ratio (PAPR) which may be particularly troublesome in uplink transmissions because of the costly high-power linear amplifiers that are needed in user terminals. These features are inherited by Orthogonal Frequency-Division Multiple Access (OFDMA), the multiple access technique based on OFDM.

Single Carrier Frequency-Division Multiple Access (SC-FDMA) has become an alternative to these techniques since, due to its low PAPR, it was chosen as the uplink multiple access scheme in 3rd Generation Partnership Project Long Term Evolution (3GPP LTE). This technique can be described as a version of OFDMA in which pre-coding and inverse pre-coding stages are added at the transmitter and receiver ends respectively. The reduction of PAPR in the uplink transmission results in a relaxation on the constraints regarding power efficiency in user terminals and, hence, in lower manufacturing costs.

This dissertation is aimed to provide a mathematical analysis of the performance for a SC-FDMA system over a fading channels in terms of Bit Error Rate (BER) and

spectral efficiency. With this purpose, we first introduce the considered technologies and the mathematical grounds necessary to perform the aforementioned analysis.

Then, we undertake the analysis of the BER for OFDM and SC-FDMA based on characterizing the enhanced complex noise in the detection stage after linear equalization in the frequency domain. For the considered fading channels (namely, Rayleigh, Rice and Nakagami-μ) this noise is shown to have circular symmetry. We show how, in this case and under the assumption of independent bit-mapping, it is possible to derive BER expressions based on the marginal characteristic function of the enhanced noise. The core of the dissertation is based on the performance analysis for Nakagami-μ channels in terms of BER. In order to validate obtained BER closed-form expressions through simulations, we particularize them for Rayleigh fading channels (i.e., Nakagami-μ with $\mu = 1$) and compare the analytical results to simulations values. Later, more realistic channel models, based on ITU and 3GPP specifications, are used to check the suitability of the provided expression to approximate actual BER values.

The final contribution is based on the study of spectral efficiency for SC-FDMA after ZF and MMSE frequency equalization. As before, closed-form expressions are derived for an ideal scenario and validated through simulations. Their suitability to approximate spectral values for more realistic scenarios is also evaluated.

Resumen

Gracias a la alta velocidad de transmisión que ofertarán, los sistemas de comunicaciones móviles e inalámbricas de la próxima generación facilitarán la provisión de servicios multimedia avanzados de manera ubicua. No obstante, es necesario que las tecnologías de transmisión empleadas sean capaces de resolver los problemas derivados de la transmisión de altas tasas de datos sobre canales limitados en ancho de banda y potencia.

Hasta el momento, OFDM (*Orthogonal Frequency-Division Multiplexing*) ha sido la técnica de transmisión más empleada debido a su robustez frente a canales con desvanecimientos selectivos en frecuencia. Sin embargo, sufre de una alta tasa de potencia pico a potencia media (*Peak-to-Average Power Ratio, PAPR*), una característica no deseable para la transmisión en el enlace ascendente ya que son necesarios amplificadores de potencia lineales en los terminales de usuario con lo que se incrementa el coste de estos últimos. Esta problemática también aparece cuando se combina esta tecnología con acceso múltiple en OFDMA (Orthogonal Frequency-Division Multiple Access).

Recientemente SC-FDMA (*Single Carrier Frequency-Division Multiple Access*) se ha convertido en una atractiva alternativa a OFDMA debido a su baja PAPR. Esta característica ha hecho que fuera elegida para su implantación en el enlace ascendente en la especificación *Long Term Evolution* (LTE) del *3rd Generation Partnership Project* (3GPP). Podemos describir esta técnica como una versión de OFDMA en la que una etapa de precodificación y precodificación inversa se añaden respectivamente al transmisor y al receptor. La reducción de la PAPR en la transmisión en el enlace ascendente se traduce en una relajación en las restricciones en

cuanto a eficiencia de potencia en los terminales de usuario y, por tanto, en una reducción en los costes de fabricación de los mismos.

El objetivo de esta tesis es realizar un análisis matemático de las prestaciones de SC-FDMA en términos de tasa de error de bit (*Bit Error Rate, BER*) y eficiencia espectral cuando se emplea esta tecnología para transmitir sobre un canal con desvanecimiento selectivo en frecuencia. Con tal propósito, se realiza primero una revisión de las tecnologías consideradas para después presentar los fundamentos matemáticos necesarios para realizar el mencionado análisis.

A continuación se lleva a cabo el análisis de la BER para OFDM y SC-FDMA tomando como punto de partida el estudio del ruido complejo, mejorado por el empleo de ecualización lineal en el dominio de la frecuencia, a la entrada del detector. Para los canales con desvancimientos considerados (esto es, Rayleigh, Rice y Nakagami-μ) se demuestra que este ruido es circularmente simétrico. Además, para dicho caso y asumiendo mapeo independiente de los bits, es posible derivar expresiones para la BER a partir de la función característica correspondiente a la densidad de probabilidad marginal del ruido complejo mejorado. El núcleo de esta disertación es el análisis de las prestaciones para la transmisión sobre canales Nakagami-μ en términos de BER. Para validar las expresiones cerradas obtenidas, estas han sido particularizadas para un canal Rayleigh (canal Nakagami-μ con $\mu = 1$) y se han comparado los resultados analíticos resultantes de su evaluación con aquellos obtenidos mediante simulaciones. A continuación, se ha comprobado la adecuación de las expresiones cerradas para aproximar valores reales de BER obtenidos para modelos de canales realistas definidos por la ITU (International Telecommunications Union) y el 3GPP.

La contribución final se basa en el estudio de la eficiencia espectral para SC-FDMA cuando se aplica ecualización lineal en frecuencia (ZF o MMSE). De nuevo se obtienen primero expresiones cerradas para un escenario ideal para luego validarlas mediante simulaciones. Su validez a la hora de aproximar valores de eficiencia espectral para escenarios realistas es también evaluada.

Chapter 1

Introduction

1.1 Motivation and Contributions

With each generation of wireless mobile systems, higher data rates are aimed in order to provide advanced multimedia services with ubiquitous access. Thus, modern broadband mobile technologies must cope with problems deriving from high-data-rate transmissions over wireless channels that are limited in bandwidth and power. Hitherto, the most popular multi-carrier communication technique used to overcome these limitations is the Orthogonal Frequency-Division Multiplexing (OFDM) due to its robustness against frequency selective fading channels. However, it suffers from a high Peak-to-Average Power Ratio (PAPR) which may be particularly troublesome in uplink transmissions as costly high-power linear amplifiers are needed in user terminals. These features are inherited by Orthogonal Frequency-Division Multiple Access (OFDMA), the multiple access technique based on OFDM,

Single Carrier Frequency-Division Multiple Access (SC-FDMA) has become an alternative to these techniques since, due to its low PAPR, it was chosen as the uplink multiple access scheme in 3rd Generation Partnership Project Long Term Evolution (3GPP LTE) [3GPP 08]. This technique is based on the use of Single-Carrier modulation with Frequency-Domain Equalization (SC-FDE) [Pancaldi 08] and it can be

described as a version of OFDMA in which pre-coding and inverse pre-coding stages are added at the transmitter and receiver ends respectively. The reduction of PAPR in the uplink transmission results in a relaxation on the constraints regarding power efficiency in user terminals and, hence, in lower manufacturing costs.

This thesis is aimed to provide a mathematical analysis of the performance for a SC-FDMA system over fading channels in terms of Bit Error Rate (BER) and spectral efficiency. The obtained results will be, first, validated through simulations and, then, compared to those obtained with OFDMA. These comparisons will allow us to determine the difference in performance between OFDM and SC-FDMA.

1.2 Related Publications

Some of the contributions listed were partially published as follows:

- J. J. Sánchez-Sánchez, U. Fernández-Plazaola, and M. C. Aguayo-Torres, IB2Com 2010. Extended Best Papers. River, 2011, ch. BER Analysis for SC-FDMA and OFDM in Nakagami-m Fading Channels (Work in progress).

- J. J. Sánchez-Sánchez, M. C. Aguayo-Torres, and U. Fernández-Plazaola, "BER Analysis for Zero-Forcing SC-FDMA over Nakagami-m Fading Channels", IEEE Transactions on Vehicular Technology (Under review).

- J. J. Sánchez-Sánchez, C. Castillo-Vázquez, M. C. Aguayo-Torres, and U. Fernández-Plazaola, "Application of Student t and Behrens-Fisher Distributions to the Analysis of Enhanced Noise after ZF-FDE", IET Communications (Under review).

- J. J. Sánchez-Sánchez, U. Fernández-Plazaola, and M. C. Aguayo-Torres, "BER analysis for OFDM with ZF-FDE in Nakagami-m fading channels",

Proceedings of the Fifth International Conference on Broadband and Biomedical Communications (IB2Com), 2010.

- J. J. Sánchez-Sánchez, M. C. Aguayo-Torres, and U. Fernández-Plazaola, "Analysis of SC-FDMA Spectral Efficiency over Rayleigh Fading Channels", in Workshop on Broadband Single Carrier and Frequency Domain Communications at IEEE GLOBECOM 2010, 2010.

- J. J. Sánchez-Sánchez, U. Fernández-Plazaola and M.C. Aguayo-Torres, "Sum of Ratios of Complex Gaussian RVs and its application to a simple OFDM Relay Network", Proceedings of the 71st Vehicular Technology Conference VTC 2010-Spring.

- J. J. Sánchez-Sánchez, U. Fernández-Plazaola, M.C. Aguayo-Torres and J.T. Entrambasaguas, "On the Bivariate Pearson type VII and its application to the BER analysis for SC-FDMA", Proceedings of 2nd International Symposium on Applied Sciences in Biomedical and Communication Technologies, Bratislava, Slovak Republic.

- Juan J. Sánchez-Sánchez, Unai Fernández Plazaola, M.C. Aguayo-Torres, and J.T. Entrambasaguas, "Closed-form BER expression for interleaved SC-FDMA with M-QAM", Proceedings of the 70th Vehicular Technology Conference VTC 2009-Fall.

- J. J. Sánchez-Sánchez, D. Morales, Gerardo Gómez, U. Fernández Plazaola, E. Martos-Naya, J. T. Entrambasaguas, "WM-SIM: A Platform for Design and Simulation of Wireless Mobile Systems", Proceedings of the Second ACM Workshop on Performance Monitoring and Measurement of Heterogeneous Wireless and Wired Networks. Chania, Crete Island, Greece, October 2007.

- J. J. Sánchez, D. Morales-Jiménez, G. Gómez, J. T. Entrambasaguas, "Physical Layer Performance of Long Term Evolution Cellular Technology", Proceedings of the 16th IST Mobile and Wireless Communications Summit, Budapest

(Hungary), July 2007.

1.3 Outline of the Dissertation

The following is the outline of the remainder of the thesis.

In Chapter 2 we describe OFDM multi-carrier modulation technique and compare it with SC-FDE. Then we extend the comparison to the multiple access schemes derived from them, that is, OFDMA and SC-FDMA respectively.

In Chapter 3 we introduce the fundamentals of probability theory paying special attention to those concepts that will be intensively applied through this dissertation. The purpose of this chapter is to serve as a reference for the analyses performed in the following chapters.

Chapter 4 is devoted to study the statistical distribution of the enhanced noise after frequency domain equalization in an OFDM system. We first characterize the wireless mobile communications channel for different fast fading distributions and then we find the probability density function of the resulting noise term after zero-forcing equalization.

The analysis of SC-FDMA BER performance is carried out in Chapter 5, first, for ideal zero-forcing equalization, and then, for the more realistic MMSE equalization. These analyses are extended in Chapter 6 where we investigate the performance of SC-FDMA when adaptive modulation is applied.

In the last chapter, we present a brief summary of this dissertation and comment the main conclusions derived from our research.

Chapter 2

Overview of OFDMA and SC-FDMA

2.1 Introduction

Multi-carrier transmission techniques [Prasad 03] are used in modern wireless mobile systems to provide virtually error-free high bit rates. In order to achieve this purpose, the use of Multi-Carrier Modulation (MCM) has became a popular option. MCM is based on the idea of dividing the transmitted data stream into several symbol streams, with a much lower symbol rate, which are used to modulate several sub-carriers [Hara 03]. MCM presents a relative immunity to multipath fading and has a lesser susceptibility to interference caused by impulse noise than that presented by single-carrier systems. Additionally, it demonstrates enhanced immunity to interference. Thanks to those features, MCM became a key component of several standards (i.e., Digital Video Broadcast - Terrestrial (DVB-T), or IEEE 802.11x and IEEE 802.16x series) [Fazel 03].

The most prominent example of MCM transmission is OFDM. In this technique, a large number of orthogonal sub-carriers are used to transmit information from several parallel streams modulated with a digital modulation scheme [Nee 00]. If these data streams belong to different terminals or users, OFDM becomes OFDMA in which different data signals are transmitted through a common physical media

that is divided into frequency resources units. Both OFDM and OFDMA suffer from power distortion that may be particularly troublesome in uplink transmissions where excessive complexity in user terminal is an issue.

With the purpose of overcoming that limitation in 3GPP LTE [3GPP 08], SC-FDMA was chosen as the uplink multiple access scheme due to its lower power distortion [Myung 08].

2.2 Orthogonal Frequency-Division Multiplexing

The origins of OFDM can be dated back to 1966 when it was first proposed as a patent by Bell Labs [Chang 66]. Later, in 1971, Weinstein and Eckbert proposed in [Weinstein 71] the use of the Discrete Fourier transform (DFT) for its implementation. However, the first description of the use of OFDM for a wireless system came even later, in 1985, with Cimini's work [Cimini 85]. Thanks to the advances in the field of digital signal processing and the efficient implementation of DFT by Fast Fourier Transform (FFT) algorithms, OFDM has become the most widely used alternative system for broadband communications, both wired and wireless.

In OFDM, the available bandwidth is divided into sub-carriers that are orthogonal in the sense that the peak of one sub-carrier coincides with the nulls of the other sub-carriers, thereby avoiding the use of frequency guard bands and increasing spectral efficiency. OFDM multiplexes the data on these orthogonal sub-carriers and transmits them in parallel. This allows dividing the high-speed digital signal to be transmitted into several slower signals that are sent in parallel through separated narrower frequency bands.

The block diagram for an OFDM system (transmitter and receiver) is depicted in Fig. 2.1. The sequence of bits to be transmitted is mapped into a sequence of complex symbols according to the modulation scheme used, typically Quadrature

Amplitude Modulation (QAM) or Phase Shift Keying (PSK). These complex symbols are allocated in orthogonal sub-carriers and transformed by means of M-IDFT that produces an OFDM symbol in the time domain. A Cyclic Prefix (CP) of length greater than the channel response, is added as a guard period, to reduce the temporal dispersion and to eliminate the Inter-Symbolic Interference (ISI) [van de Beek 02]. Additionally, the prefix also helps to preserve the orthogonality among sub-carriers, thereby avoiding Inter-Carrier Interference (ICI) as well. The addition of the cyclic prefix also transforms the time domain convolution between the OFDM symbols and the channel response in a circular convolution. In the frequency domain, this circular convolution becomes a point-wise multiplication between the complex symbol allocated in each sub-carrier and the corresponding channel frequency response. Thereby, it is possible to perform the equalization in the frequency domain. The main advantage of OFDM is its behavior against bad channel conditions, such as the fading caused by multi-path propagation, without using complex equalization filters. Normally, as the bandwidth of the transmitted signal is less than the coherence bandwidth, the channel response in each carrier can be considered flat. Thus, the channel can be modeled as a set of narrowband fading channels, one for each single sub-carrier [Nee 00]. Besides, thanks to its inherent immunity to multipath effects, OFDM provides multipath and interference tolerance in non-Line Of Sight (non-LOS) conditions.

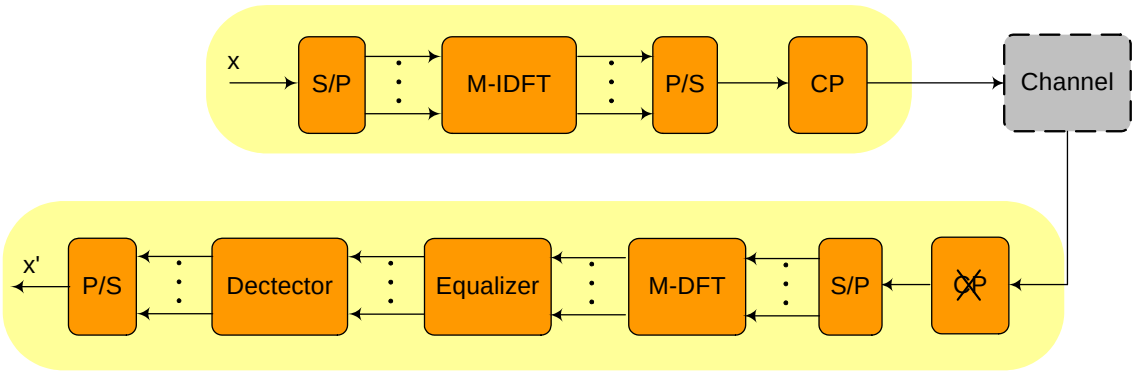

Figure 2.1: Transmitter and receiver for OFDM

2.3 Orthogonal Frequency Division Multiple Access

OFDMA is an OFDM-based multiple access scheme [Nee 00] that was first proposed for the return channel in Community Antenna Television (CATV) [Sari 96]. In OFDMA all the available sub-carriers are grouped into different sub-channels that are assigned to distinct users. It takes advantage of the orthogonality among sub-carriers to avoid interference between users, thereby achieving greater flexibility and efficiency in the allocation of system resources [Lawrey 97]. Each sub-channel may be compounded of adjacent localized sub-carriers (Localized FDMA, LFDMA) or by sub-carriers distributed across the total bandwidth (Distributed FDMA, DFDMA). A particular case of DFDMA is Interleaved FDMA (IFDMA) in which the sub-carriers are equally spaced over the entire system bandwidth.

In Fig. 2.2 four users are multiplexed following the localized scheme, thereby the entire system bandwidth is divided into four different sub-bands.

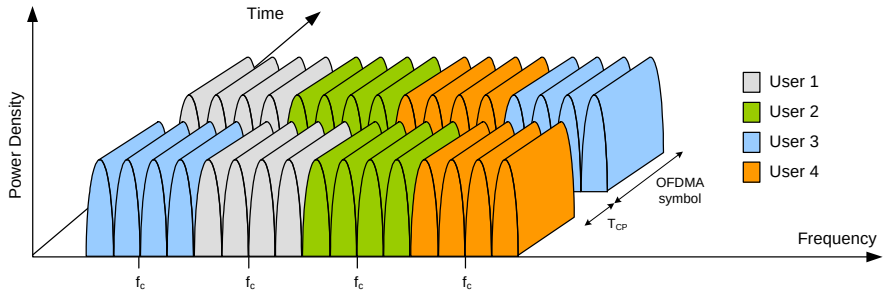

Figure 2.2: User allocation example in OFDMA (LFDMA)

Due to the fact that it combines scalability, multi-path robustness, and Multiple-Input Multiple-Output (MIMO) compatibility [Nee 00], OFDMA has been adopted in 802.16 (WiMAX) standards [IEEE 09] and in the Long Term Evolution (LTE) for the Universal Mobile Telecommunications System (UMTS) [3GPP 08] specifications. However, the OFDMA (and OFDM) waveform exhibits very pronounced

envelope fluctuations, resulting in a high PAPR [Myung 07]. Because of this drawback, OFDMA requires expensive linear power amplifiers, which in turn increases the cost of the terminal and reduces its autonomy, as the battery drains faster.

2.4 Single Carrier with Frequency Domain Equalization

Traditionally, for single carrier transmissions, equalization is performed in the time domain provided the channel impulse response in time domain is not too long. For broadband multipath channels, this condition is not fulfilled and subsequently, conventional time domain equalizers are impractical due to the high computational cost they imply. In this case, SC-FDE technique is used to fight the frequency-selective fading channel. It outperforms the conventional Time-Domain Equalization (TDE) as the former exhibits a lower complexity that grows with the number of symbols of dispersion. Thus, FDE is an effective technique for high-data-rate wireless communications systems suffering from very long ISI [Falconer 02].

Although the first study of the use of equalization in the frequency domain dates from 1973 [Walzman 73], the realization about the potential of this technique came after it was proposed as a low-complexity solution to digital terrestrial broadcasting [Sari 95]. The importance of this study lays on the fact that the striking similarities between the implementation of an OFDM system and that of a single carrier system with a FDE were first pointed out there [Pancaldi 08].

A SC-FDE system shares some common elements with OFDM as depicted in Fig. 2.3. These similarities allow the coexistence of SC-FDE and OFDM modems, that is, an equipment may be able to operate with any of these transmission techniques. In an SC-FDE system, information bits are grouped and mapped into a complex symbol belonging to a given complex constellation. The sequence of modulated symbols is divided into data blocks and transmitted sequentially. Each of those

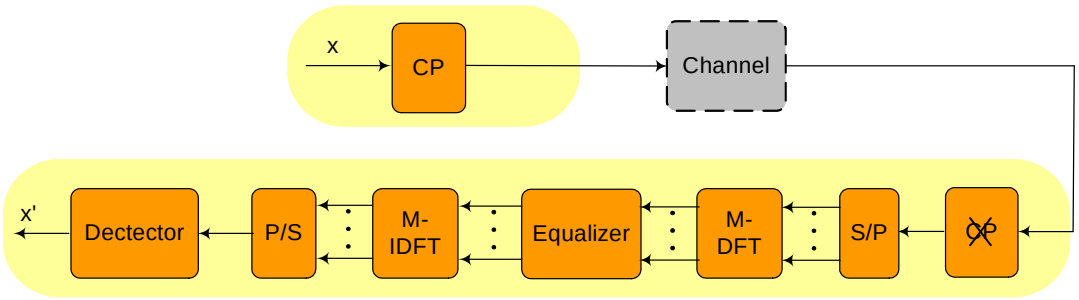

Figure 2.3: Transmitter and receiver for SC-FDE

data blocks is cyclically extended with a copy of the last part of the block (i.e., a CP), which is transmitted as a guard interval. The insertion of the CP has similar advantages to those already described in OFDM. First, if the length of the CP is longer than the length of the channel impulse response, then, Inter-Block Interference (IBI) due to multipath propagation is avoided. Second, the transmitted data propagating through the channel can be modeled as a circular convolution between the channel impulse response and the transmitted data block. This becomes a point-wise multiplication of the DFT samples in the frequency domain. Thus, channel distortion can be removed dividing the DFT of the received signal by the DFT of the channel impulse [Myung 06]. This frequency domain equalization is performed at the receiver after transforming the received signal to the frequency domain by applying a DFT. After the equalization, an IDFT transforms the single carrier signal back to the time domain. Unlike OFDM, where a separate detector is employed for each subcarrier, a single detector recovers the original modulation symbols in this case. In the overall, SC-FDE performance is similar to that of OFDM with essentially the same complexity, even for long channel delay. However, there are several advantages when it is compared to OFDM [Myung 07]:

- it is less sensitive to nonlinear distortion and hence, it allows the use of low-cost power amplifiers [Falconer 02],

- it offers a greater robustness against spectral nulls and,

- it is less sensitive to carrier frequency offset.

On the other hand, its main disadvantage with respect to OFDM is that neither channel-adaptive subcarrier bit nor power loading are possible with this transmission technique.

2.5 Single Carrier Frequency Division Multiple Access

SC-FDMA is an extension of SC-FDE that allows multiple access with a complexity similar to that of OFDMA. Both technologies use almost the same transceiver blocks, being the DFT pre-coding and inverse pre-coding stages, which are added in SC-FDMA at transmitter and receiver ends, the main difference between them (see Fig. 2.4). Thanks to those blocks, SC-FDMA has better capabilities in terms of envelope fluctuations of the transmitted signal and, therefore, its PAPR is lower (up to 2 dB) than in OFDMA [Myung 07]. That leads to greater efficiency in power consumption, a desirable feature in user equipments. In addition, SC-FDMA complexity focuses on the receiver-end, hence, it is an appropriate technology for uplink transmission since complexity at the base station is not an issue. Due to these features, SC-FDMA was chosen as the medium access technique for 3GPP LTE uplink [3GPP 08]. Note that the DFT operation in SC-FDMA spreads the energy of one sub-carrier over all allocated sub-carriers before the IFFT, which means that spectral nulls in the channel are reduced with averaging [Ergen 09]. After computing the DFT of the input data, the result is either distributed over the entire bandwidth (DFDMA) or placed in consecutive sub-carriers (LFDMA). In both cases, unoccupied carriers are set to zero. When the sub-carriers are equally spaced over the entire system bandwidth, it is called interleaved mode (IFDMA) [Myung 08]. Regardless of the manner in which the sub-carriers are mapped, the result is a sequence X_l ($l = 0, 1, 2, M-1$) of M complex amplitudes that is transformed by means of an M-IDFT

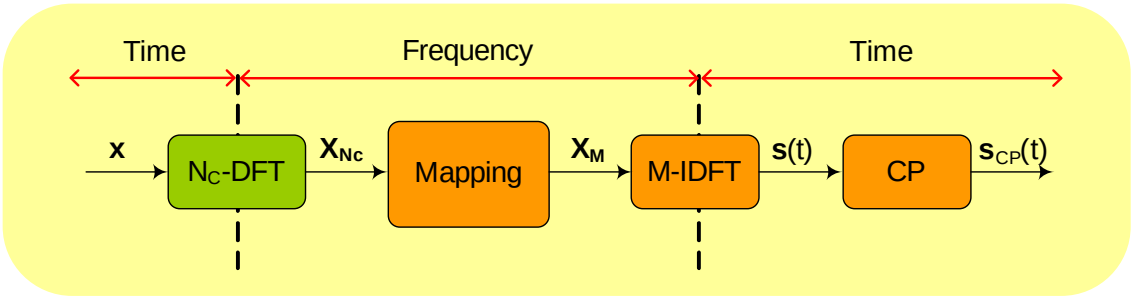

(a) SC-FDMA Transmitter

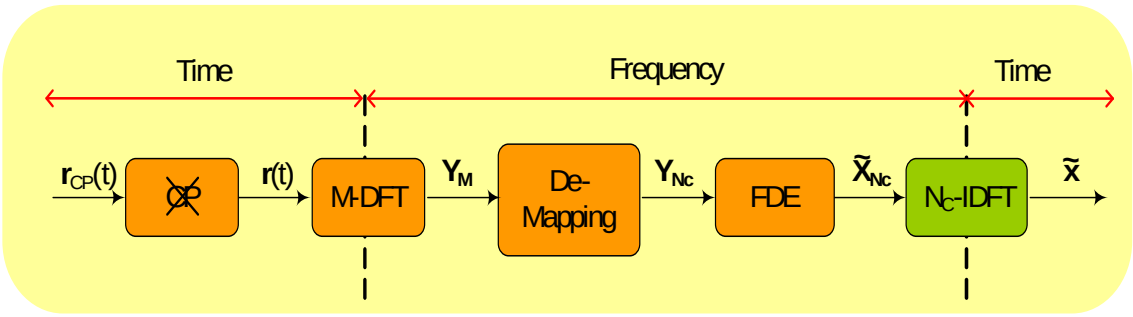

(b) SC-FDMA Receiver

Figure 2.4: SC-FDMA transmitter and receiver schemes

to a signal in the time domain which is transmitted sequentially. As in SC-FDE, a cyclic prefix is also added as a guard interval between blocks to avoid IBI caused by multi-path propagation and to make possible frequency domain equalization.

In Fig. 2.5 four users are multiplexed following the localized scheme, thereby the entire system bandwidth is used by the users in different instants. Note that, in OFDMA, each data symbol modulates a single sub-carrier whereas in SC-FDMA it modulates the whole allocated wideband carrier. Thus, the modulated symbols are transmitted sequentially over air and the final transmitted signal is a single carrier one unlike OFDMA where the final signal is compounded of the superposition of the allocated sub-carriers. Both techniques transmit the same amount of data symbols in the same time period using the same bandwidth. However SC-FDMA symbols are transmitted sequentially over a single carrier as opposed to the parallel transmission of OFDM/OFDMA over multiple carriers. Also, the users are orthogonally multiplexed and de-multiplexed in the frequency domain, which gives SC-FDMA

the aspect of FDMA [Myung 08].

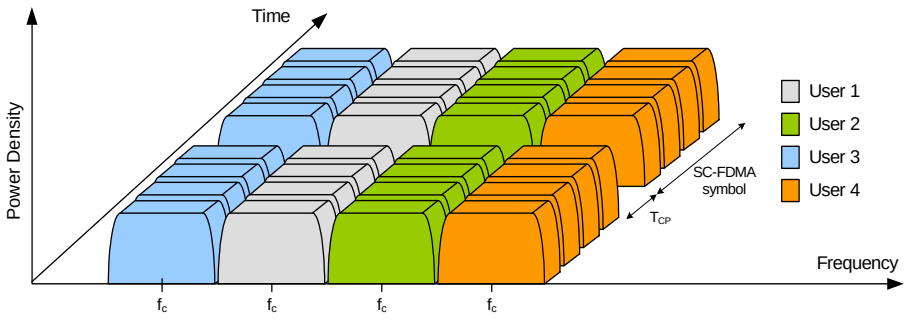

Figure 2.5: User allocation example in SC-FDMA (LFDMA)

2.6 Conclusions

In this chapter we introduce SC-FDMA, a multiple access technique that utilizes single carrier modulation, orthogonal frequency multiplexing, and frequency domain equalization. This promising technology was chosen for the uplink of new generation wireless communication systems. SC-FDMA was adopted because it simplifies the transmitter in the handsets and reduces the power consumption with lower PAPR feature. Those advantages come with the price of more complexity than OFDMA in the receiver structure. This drawback is not an issue since the receiver is in the base station, which does not have power or complexity limits [Ergen 09]. Because of its merits, SC-FDMA has been chosen as the uplink multiple access scheme in 3GPP LTE and is under consideration for LTE Advanced [Myung 08].

Chapter 3

Fundamentals of Random Variables

3.1 Introduction

In this chapter we present some basic concepts related to probability theory. It is not our intention to make a rigorous compilation but to revise the concepts that we use throughout the following chapters.

First, we briefly introduce the fundamentals of probability theory starting with the set of axioms on which this theory is founded and the concepts of probability density and distribution functions. Then, we pay special attention to the definition of the characteristic function which is intimately related to the inversion theorem. The transformation of random variables is addressed next including the calculation of the density function for some specific transformations to be used along this thesis (e.g., the ratio of two random variables). We provide several examples of these transformations that will be used in the following chapters.

We devote section 3.3 to the Gaussian distribution and some other related distributions such as the Rayleigh, Rice or Nakagami-μ. All of them depend on underlying Gaussian random variables. We also present, in section 3.4, two distribution families that have proven themselves as suitable candidates to model physical phenomena

for which observed data exhibit tails decay following a power law that cannot be modeled by the classical Gaussian distributions. These families are the elliptical and stable families of distributions.

This chapter concludes with the central limit theorem, which is closely related to the concept of characteristic function and the sum of independent random variables. First, the central limit theorem is defined for the sum of independent random variables with finite variance. Then, we address a generalization of this theorem that deals with those cases in which the variance diverges and that is connected with the definition of stable distributions.

3.2 Probability Theory Overview

Probability is the branch of mathematics that studies phenomena whose outcomes are not deterministic but rather subject to chance. There are several competing interpretations of the actual meaning of probabilities. The more conventional interpretation is held by frequentists that view probability simply as a measure of the frequency of outcomes. Bayesians treat probability more subjectively, as a statistical procedure which endeavors to estimate parameters of an underlying distribution based on the observed distribution [Weisstein 99].

The work described in this thesis and the results presented here are based on probability theory, which is historically motivated by the frequency interpretation of probability. Probability theory provides a framework based on a formal set of three axioms and the consequences thereof. Its roots can be found in the attempt to analyze the equitable division of stakes in games of chance that Blaise Pascal and Pierre de Fermat made through correspondence in 1654 [Seneta 06].

The first major treatise blending calculus with probability theory was *Théorie*

Analytique des Probabilités, written by Laplace in 1812. Initially, probability theory mainly considered discrete events, and its methods were mainly combinatorial. Eventually, analytical considerations compelled the incorporation of continuous variables into the theory. This culminated in modern probability theory whose foundations were laid by Kolmogorov with his axiom system for probability theory in 1933. There, he combined the notion of sample space, introduced by Richard von Mises, and measure theory. Fairly quickly, this became the undisputed axiomatic basis for modern probability theory [Heyde 06a]. The measure-theoretic formulation of these axioms is shown below.

Definition 3.1. *Let the sample space (i.e., the set of all possible events) be* Ω *and let* F *be the Borel* σ*-field of subsets of* Ω *such that*

- $A \in F$ *implies that* $\bar{A} \in F$ *and*
- $A_i \in F$, $1 \leq i < \infty$, *implies that* $\bigcup_{i=1}^{\infty} A_i \in F$,

that is, F *is a non-empty collection of subsets of* Ω *(including* Ω *itself) that is closed under complementation and countable unions of its members. Then, the probability* P *is a set function on* F *satisfying the following axioms:*

1. $P(A) \geq 0 \ \forall A \in F$,
2. *if* $A_i \in F$, $1 \leq i < \infty$ *and* $A_i \bigcap A_j = \emptyset, i \neq j$, *then* $P\left(\bigcup_{i=1}^{\infty} A_i\right) = \sum_{i=1}^{\infty} A_i$,
3. $P(\Omega) = 1$,

and the triplet (Ω, F, P) *is a probability space.*

A n-dimensional function $\mathbf{X}(\omega) = \{X_1(\omega), X_2(\omega), \ldots, X_n(\omega)\}$ defined on the probability space (Ω, F, P) $\forall$ $\omega \in \Omega$ is called a random variable if the set $\{\omega : X(\omega) \leq x\}$ belongs to F for every $\mathbf{x} = \{x_1, x_2, \ldots, x_n\} \in \mathbb{R}^n$ [Heyde 06a]. Random variables are categorized as discrete or continuous random variables depending on whether their sample spaces are countable or continuous. In this thesis we deal with continuous random variables unless stated otherwise.

3.2.1 Cumulative Distribution and Probability Density Functions

Given a random variable X, there exists an associated distribution function $F_X(s)$ that uniquely specifies the probability measure which X induces on the real line. This Cumulative Distribution Function (CDF) is denoted by $F_X(x)$ and determines the probability of the event $\{X \leq x\}$ where x is a real number, that is,

$$F_X(x) = P(X \leq x) \quad x \in \mathbb{R}. \tag{3.2.1}$$

The function $F_X(x)$ is nondecreasing, right continuous, and has at most a countable set of points of discontinuity [Heyde 06a]. The derivative of $F_X(x)$, if it exists, is called the Probability Density Function (PDF) of the random variable X and it is denoted $f_X(x)$ [Proakis 00], that is,

$$f_X(x) = \frac{dF_X(x)}{dx} \qquad x, t \in \mathbb{R}. \tag{3.2.2}$$

Equivalently, the CDF can be calculated as the cumulative value (integral for a continuous distribution or sum for a discrete distribution) of the PDF. In a more formal way

$$F_X(x) = P(X \leq x) = \int_{-\infty}^{x} f_X(t)dt \qquad x, t \in \mathbb{R}. \tag{3.2.3}$$

The PDF of a continuous random variable X is a properly normalized function $f_X(x)$ that assigns a probability density to each possible outcome within some interval. Hence, the probability of a random variable falling within an interval can be calculated as the integral of the PDF in this interval, that is,

$$P(a \leq x \leq b) = \int_{a}^{b} f_X(x)dx = F_X(b) - F_X(a) \qquad x \in \mathbb{R}. \tag{3.2.4}$$

Note that, by definition, $f_X(x) \geq 0$ and

$$\int_{-\infty}^{\infty} f_X(x)dx = 1 \qquad x \in \mathbb{R}. \tag{3.2.5}$$

These definitions can be extended to multiple random variables. For a set of random variables X_i $i = 1, 2, \ldots, n$, the corresponding joint CDF is defined [Proakis 00] as

$$F_{X_1,X_2,\ldots,X_n}(x_1, x_2, \ldots, x_n) = P(X_1 \leq x_1, X_2 \leq x_2, \ldots, X_n \leq x_n) = \int_{-\infty}^{x_1}\int_{-\infty}^{x_2}\cdots\int_{-\infty}^{x_n} f_{X_1,X_2,\ldots,X_n}(t_1, t_2, \ldots, t_n)dt_1dt_2\ldots dt_n$$

$$\{x_i, t_i\} \in \mathbb{R} \quad \forall i = 1, 2, \ldots, n, \tag{3.2.6}$$

where $f_{X_1,X_2,\ldots,X_n}(x_1, x_2, \ldots, x_n)$ is the joint PDF. Equivalently,

$$f_{X_1,X_2,\ldots,X_n}(x_1, x_2, \ldots, x_n) = \frac{\delta^n F_{X_1,X_2,\ldots,X_n}(x_1, x_2, \ldots, x_n)}{\partial x_1, \partial x_2, \ldots, \partial x_n} \quad x_i \in \mathbb{R} \quad \forall i = 1, 2, \ldots, n. \tag{3.2.7}$$

For a given random variable x_j it is possible to compute the marginal distribution $f_{X_j}(x_j)$ from the joint density as follows

$$f_{X_j}(x_j) = \int_{-\infty}^{\infty}\int_{-\infty}^{\infty}\cdots\int_{-\infty}^{\infty} f_{X_1,X_2,\ldots,X_n}(t_1, t_2, \ldots, t_n)dt_1dt_2\ldots dt_n \quad \{x_i, t_i\} \in \mathbb{R} \quad \forall i \neq j.$$

Given the occurrence of the value x_j of X_j, the conditional probability density function of the set of random variables X_i with $i \neq j$ can be expressed as

$$f_{X_1,X_2,\ldots,X_n}(x_1, x_2, \ldots, x_n/x_j) = \frac{f_{X_1,X_2,\ldots,X_n}(x_1, x_2, \ldots, x_n)}{f_{X_j}(x_j)} \quad x_i \in \mathbb{R} \quad \forall i \neq j. \tag{3.2.8}$$

3.2.2 Moments of Random Variables

The moments of a random variable play an important role in its characterization as they describe the nature of its distribution. Formally, the moments of a random variable X are defined as follows.

Definition 3.2. *Let X be a random variable with distribution $F_X(x)$. If the expected value of X^k,*

$$\mathrm{E}[X^k] = \int_{-\infty}^{\infty} x^k f_X(x)dx \quad k = 1, 2, \ldots \qquad x \in \mathbb{R} \tag{3.2.9}$$

exists, it is called the k-th moment of X.

Thus, the first moment, expected value or mean of a random variable X is defined as

$$m_X = \mathrm{E}[X] = \int_{-\infty}^{\infty} x f_X(x) dx \qquad x \in \mathbb{R}, \tag{3.2.10}$$

and it is used to define the central moments of X as

$$\mathrm{E}[(X - m_X)^k] = \int_{-\infty}^{\infty} (x - m_X)^k f_X(x) dx \quad k = 1, 2, \ldots \qquad x \in \mathbb{R}. \tag{3.2.11}$$

When $k = 2$, the central moment is called the variance of the random variable and provides a measure of its dispersion. It is usually denoted as σ_X^2 and can be calculated as

$$\sigma_X^2 = \mathrm{E}[(X - m_X)^2] = \int_{-\infty}^{\infty} (x - m_X)^2 f_X(x) dx \qquad x \in \mathbb{R}. \tag{3.2.12}$$

3.2.3 Moment-Generating and Characteristic Function

One of Laplace's greatest contributions for probability theory was the recognition of the mathematical power of transforms [Heyde 06a]. However, it was probably Cauchy the first to apply a name to the functions, using the French term *fonction auxiliaire*. The term characteristic function (originally *fonction caractéristique* also in French) was first used by Poincaré in his work *Calcul des probabilités* in 1912. Curiously enough, Poincaré applied this term to what is today called the moment-generating function [David 95]. Ten years later, Lévy, in his *Sur la determination des lois de probabilité par leurs fonctions caractéristique*, substituted Poincaré's characteristic function for the Fourier transform of the distribution function as we know it nowadays [Dugué 06]. The reason behind its name laid on the fact that, once it is known, it is possible to determined the distribution function as the probability distribution of a random variable, that is, $f_X(x)$ is completely defined by its characteristic function $\Psi(\omega)$. Both moment-generating and characteristic functions can be defined in a more formal way as follows.

Definition 3.3. *If X is a random variable and s is a parameter, real or complex, the function of s defined by*

$$M_X(s) = \mathrm{E}[exp(sX)] = \int_{-\infty}^{\infty} f_X(x) e^{s\omega x} dx \qquad x \in \mathbb{R} \text{ and } s \in \mathbb{C}, \tag{3.2.13}$$

is called the Moment-Generating Function (MGF) for X. If $s = \jmath\omega$, where $\jmath$ is the imaginary unit, the function $\Psi_X(\omega)$ defined as

$$\Psi_X(\omega) = M_X(\jmath\omega) = E[exp(\jmath\omega X)] = \int_{-\infty}^{\infty} f_X(x) e^{\jmath\omega x} dx \qquad x, \omega \in \mathbb{R}. \tag{3.2.14}$$

is called the Characteristic Function (CHF) for X.

As stated before, both functions are closely related to integral transforms: the integral in (3.2.13) corresponds to the Laplace transform of $f_X(x)$ whereas (3.2.14) corresponds to its Fourier transform.

Note that, although it always converges for $s = 0$ as $M_X(0) = 1$, the integral (3.2.13) may diverge for some values of s. Thus, the MGF can be used only for a narrow class of nonnegative integer-valued random variables for which the integral (3.2.13) always converges. On the contrary, the integral (3.2.14) always converges at least for all real values of ω provided $f_X(x)$ is a valid PDF. That is,

$$\left| \int_{-\infty}^{\infty} f_X(x) e^{\jmath\omega x} dx \right| \leq \int_{-\infty}^{\infty} |f_X(x) e^{\jmath\omega x}| \, dx = \int_{-\infty}^{\infty} f_X(x) dx = 1 \qquad x, \omega \in \mathbb{R}. \tag{3.2.15}$$

Hence, the corresponding characteristic function always exists when treated as a function of a real-valued argument even though the moment-generating function may not exist [Feller 71].

3.2.4 Inversion Theorem in Probabilistic Theory

There is a one-to-one correspondence between characteristic functions and density functions, thereby is possible to obtain one from the other by applying the transform

pair constituted by the Fourier transform and the inverse Fourier transform. The density function $f_X(x)$ of a random variable X can be calculated from its characteristic function $\Psi_X(\omega)$ as

$$f_X(x) = \frac{1}{2\pi} \int_{-\infty}^{\infty} \Psi_X(\omega) e^{-\jmath\omega x} d\omega \qquad x, \omega \in \mathbb{R}. \tag{3.2.16}$$

Despite it is always possible to obtain the characteristic function from the density distribution, its converse is not always true[1]. That is, if f is Lebesgue-integrable its Fourier transform is not necessarily Lebesgue-integrable too; it may be only conditionally integrable rather than Lebesgue-integrable, i.e., the integral of its absolute value may be infinite.

Lévy in his work *Calcul des probabilités* (1925) presented the most famous inversion formula, that is,

$$F_X(b) - F_X(a) = \frac{1}{2\pi} \lim_{T\to\infty} \int_{-T}^{T} \frac{e^{\jmath\omega a} - e^{-\jmath\omega b}}{\jmath\omega} \Psi_X(\omega)\, d\omega \qquad x \in \mathbb{R}. \tag{3.2.17}$$

Its practical use is limited to some special cases unless the random variable of interest is always strictly positive. In this thesis, we use an alternative version of the inversion theorem formula provided by Gil-Peláez [Gil-Peláez 51] that yields

$$F_X(x) = \frac{1}{2} + \frac{1}{2\pi} \int_{0}^{\infty} \frac{e^{\jmath x\omega}\Psi_X(-\omega) - e^{-\jmath x\omega}\Psi_X(\omega)}{\jmath\omega}\, d\omega \qquad x \in \mathbb{R}. \tag{3.2.18}$$

With this expression, it is possible to evaluate directly the CDF of a given distribution once its CHF is known. Several examples of the application of this formula can be found throughout the following chapters.

3.2.5 Transformations of Random Variables

In many practical cases, we are interested in the probability distributions or densities of functions of one or more random variables. That is, we have a set of random

[1] Stable distributions are a notable example of this as we show in section 3.4.2.

variables, $X_1, X_2, \ldots, X_n$ with a known joint probability and/or density function and we need to know the distribution of some function of these random variables.

The calculation of this distribution can be performed through the change of variable theorem of multivariate calculus. Probabilities in the continuous case are integrals, and an integral can be evaluated by changing the variables to a new set of coordinates and using the corresponding Jacobian term [DasGupta 10]. This idea can be expressed formally an the Multivariate Jacobian Formula which follows.

Let $\mathbf{X} = (X_1, X_2, \ldots, X_n)$ have the joint density function $f(x_1, x_2, \ldots, x_n)$, such that there is an open set $S \subseteq \mathbb{R}^{\times}$ with $P(\mathbf{X} \in S) = 1$. Suppose $u_i = g_i(x_1, x_2, \ldots, x_n)$, $1 \leq i \leq n$ are n real-valued functions of $x_1, x_2, \ldots, x_n$ such that:

- $(x_1, x_2, \ldots, x_n) \to (g_1(x_1, x_2, \ldots, x_n), \ldots, g_n(x_1, x_2, \ldots, x_n))$ is one-to-one function of $(x_1, x_2, \ldots, x_n)$ on S to $\mathbf{U} = (u_1, u_2, \ldots, u_n)$ on $T \subseteq \mathbb{R}^n$ with $P(\mathbf{U} \in T) = 1$;
- the inverse functions $x_i = h_i(u_1, u_2, \ldots, u_n)$, $1 \leq i \leq n$ are continuously differentiable on T with respect to each u_j; and
- the Jacobian determinant

$$\mathbf{J} = \begin{vmatrix} \frac{\partial x_1}{\partial u_1} & \frac{\partial x_1}{\partial u_2} & \cdots & \frac{\partial x_1}{\partial u_n} \\ \frac{\partial x_2}{\partial u_1} & \frac{\partial x_2}{\partial u_2} & \cdots & \frac{\partial x_2}{\partial u_n} \\ \vdots & \vdots & \ddots & \vdots \\ \frac{\partial x_n}{\partial u_1} & \frac{\partial x_n}{\partial u_2} & \cdots & \frac{\partial x_n}{\partial u_n} \end{vmatrix} \tag{3.2.19}$$

  is non-zero.

Then the joint density of $U_1, U_2, \ldots, U_n$ is given by

$$f_{U_1, U_2, \ldots, U_n}(\mathbf{u}) = f(h_1(\mathbf{u}), h_2(\mathbf{u}), \ldots, h_n(\mathbf{u}))\, |\mathbf{J}|$$

where $|\mathbf{J}|$ denotes the absolute value of the Jacobian determinant $\mathbf{J}$, $\mathbf{u} = u_1, u_2, \ldots, u_n$ and the notation f on the right-hand side means the original joint density of $X_1, X_2, \ldots, X_n$.

The specific choice of the transformation is dictated by the concrete problem to be solved. In the following chapters this theorem will be applied, in its uni and bi-dimensional versions, to compute the distributions of some new random variables.

Products and Ratios of Random Variables

The product distribution is a probability distribution constructed as the distribution of the product of random variables which have known distributions. In a similar fashion, the ratio or quotient distribution is the distribution of the ratio of random variables which have known distributions. Translated into densities, they can be defined as follows.

Let X and Y be continuous random variables with a joint density $f_{X,Y}(x, y)$. Let $U = XY$ and $V = X/Y$. Then the densities of U and V are given by

$$f_U(u) = \int_{-\infty}^{\infty} f_{X,Y}\left(x, \frac{u}{x}\right) \frac{1}{|x|} dx, \tag{3.2.20}$$

and

$$f_V(v) = \int_{-\infty}^{\infty} f_{X,Y}(vy, y)|y|dy, \tag{3.2.21}$$

Note that in both cases we first apply the transformation and then calculate the marginal distribution.

The ratio distribution appears in some basic problem in statistics and has attracted the interest of several researchers. For those cases in which the pair (X, Y) is a standard bivariate normal the problem is fairly easy to solve. Thus, the results are well known [Hayya 75] and have applications in applied statistics and operations research [Pham-Gia 06]. However, the general case is a more complex problem as can been seen in [Cedilnik 06]. Fortunately, for the analyses carried out in this thesis, the problem, although it is not trivial, is tractable. The Cauchy and the Student t distributions presented in section 3.4.1 are examples of ratio distributions.

Others Transformations of Random Variables

In this subsection we provide expressions to compute the densities of some other transformations of random variables that we use later.

Proposition 3.2.1. *Let X be a continuous, real and non-negative random variable with a density $f_X(x)$. Let $Z = X^2$. Then the density of Z is given by*

$$f_Z(z) = f_X\left(\sqrt{z}\right)\frac{1}{2\sqrt{z}}, \tag{3.2.22}$$

where Z is real and non-negative. If $X \in (-\infty, \infty)$ then

$$f_Z(z) = f_X\left(\sqrt{z}\right)\frac{1}{\sqrt{z}}, \tag{3.2.23}$$

where Z is also real and non-negative.

Proposition 3.2.2. *Let X be a continuous, real and non-negative random variable with a density $f_X(x)$. Let $Z = \sqrt{X}$. Then, the density of Z is given by*

$$f_Z(z) = f_X\left(z^2\right)2z, \tag{3.2.24}$$

where Z is real and non-negative.

Proposition 3.2.3. *Let X be a continuous random variable with a density $f_X(x)$. Let $Z = X^{-1}$. Then the density of Z is given by*

$$f_Z(z) = f_X\left(\frac{1}{z}\right)\frac{1}{z^2}. \tag{3.2.25}$$

Proposition 3.2.4. *Let X and Y be continuous random variables with a joint density $f_{X,Y}(x, y)$. Let $Z = X + Y$. Then the density of Z is given by*

$$f_Z(z) = \int_{-\infty}^{\infty} f_{X,Y}(x, z-x)dx = \int_{-\infty}^{\infty} f_{X,Y}(z-y, y)dy. \tag{3.2.26}$$

If X and Y are independent random variables, then

$$f_Z(z) = f_X(x) * f_Y(y) = \int_{-\infty}^{\infty} f_X(x)f_Y(z-x)dx = \int_{-\infty}^{\infty} f_X(z-y)f_Y(y)dy, \tag{3.2.27}$$

where $*$ is the convolution operation.

The convolution in eq. (3.2.27) can be extended to a n-dimensional integral for the sum of n independent random variables as follows:

Theorem 3.1. *Let* $\mathbf{X} = (X_1, X_2, \ldots, X_n)$ *be a vector of independent random variables. Then, the density function of their sum* $Z = \sum_{j=1}^{n} X_j$ *is the convolution of their individual densities and is given by*

$$f_Z(z) = f_{X_1}(x_1) * f_{X_2}(x_2) \cdots f_{X_n}(x_n). \tag{3.2.28}$$

The corresponding expression for the CHF of Z *yields*

$$\Psi_Z(\omega) = \prod_{j=1}^{n} \Psi_{X_i}(\omega), \tag{3.2.29}$$

that, in the case the variables are also identically distributed, can be reduced to

$$\Psi_Z(\omega) = \left(\Psi_X(\omega)\right)^n. \tag{3.2.30}$$

3.3 Gaussian and Related Distributions

The Gaussian or normal distribution was introduced by De Moivre in 1733 to approximate certain binomial distributions for large values of the parameter n, in the context of computing probabilities of winning in various games of chance [Read 06]. Laplace, in 1812, derived a more formal and general statement of this result and an early form of the central limit theorem. Gauss, in 1809, also obtained the normal law studying the distribution of errors in astronomical observations [Eisenhart 06]. Since then, it has been applied to many fields as physics or astronomy where random variables with unknown distributions are often assumed to be Gaussian.

The expression of the probability distribution of a Gaussian random variable yields

$$\mathcal{N}(\mu, \sigma) = \frac{1}{\sqrt{2\pi\sigma^2}} \exp\left(-\frac{(x-\mu)^2}{2\sigma^2}\right) \qquad x \in \mathbb{R}, \tag{3.3.1}$$

where μ is the mean and σ^2 the variance; for $\mu = 0$ and $\sigma^2 = 1$ it is denoted as standard normal.

Expression (3.3.1) can be extended to higher dimensions as

$$f_X(\mathbf{x}) = \frac{1}{(2\pi)^{k/2}|\boldsymbol{\Sigma}|^{1/2}} \exp\left(-\tfrac{1}{2}(\mathbf{x}-\boldsymbol{\mu})^T \boldsymbol{\Sigma}^{-1}(\mathbf{x}-\boldsymbol{\mu})\right), \qquad \mathbf{x} \in \mathbb{R}^n. \tag{3.3.2}$$

The n-multivariate distribution with mean vector $\boldsymbol{\mu}$ and covariance matrix $\boldsymbol{\Sigma}$ is denoted $\mathcal{N}(\boldsymbol{\mu}, \boldsymbol{\Sigma})$.

For multivariate Gaussian random variables, it is possible to define its envelope or amplitude distributions as the norm of the corresponding vector. In this case, the elements of the vector are the underlying Gaussian random variables of the amplitude. In a similar fashion, the power distribution can be defined as the square of the amplitude and, therefore, they share the same underlying Gaussian random variables. Along the next subsections, we introduce several envelope and power distributions that will be used in the following chapters to analyze the effects of frequency-domain equalization upon the received signal.

3.3.1 Rayleigh Distribution

The Rayleigh distribution is a particular case of an amplitude distribution that arises when studying the magnitude of a complex number whose real and imaginary parts both follow a zero-mean Gaussian distribution.

Definition 3.4. *Let X_1 and X_2 be two Gaussian random variables with zero mean and variance σ^2 and let R_{Ray} be the amplitude random variable defined as*

$$R_{Ray} = \sqrt{X_1^2 + X_2^2}. \tag{3.3.3}$$

Then the amplitude random variable R_{Ray} follows a Rayleigh distribution and its density can be expressed as

$$f_{R_{Ray}}(x) = \frac{x}{\sigma^2} e^{-\frac{x^2}{2\sigma^2}} \qquad x \in \mathbb{R} \text{ and } x \geq 0. \tag{3.3.4}$$

The parameter σ is related to the width of the density function but it cannot be interpreted as the variance of the Rayleigh random variable. In fact both the mean and the variance of Rayleigh random variable are proportional to σ since $E[R_{Ray}] = \sqrt{\frac{\pi}{2}}\sigma$ and $var(R_{Ray}) = \left(2 - \frac{\pi}{2}\right)\sigma^2$.

In telecommunications, this distribution arises often in the study of non-coherent

communication systems and also in the study of land mobile communication channels, where the phenomenon known as fading is often modeled using Rayleigh random variables.

3.3.2 Rice Distribution

The Rice distribution or Rician distribution is the probability distribution of the absolute value of a bivariate normal random variable with potentially non-zero mean.

Definition 3.5. *Let X_1 and X_2 be two Gaussian random variables with non-zero means (0 and α) and variance σ^2. Let R_{Rice} be the amplitude random variable defined as*

$$R_{Rice} = \sqrt{X_1^2 + X_2^2}. \tag{3.3.5}$$

Then the amplitude random variable R_{Rice} follows a Rice distribution and its density can be expressed as

$$p_{R_{Rice}}(x) = \frac{x}{\sigma^2} e^{-\frac{\alpha^2+x^2}{2\sigma^2}} I_0\left(\frac{x\alpha}{\sigma^2}\right) \qquad x, \alpha \in \mathbb{R} \text{ and } x \geq 0 \; \alpha \geq 0, \tag{3.3.6}$$

where $I_m(x)$ is the modified Bessel function of the first kind with order m.

The mean of a Rician random variable yields

$$E[R_{Rice}] = \sigma\sqrt{\frac{\pi}{2}} L_{\frac{1}{2}}\left(\frac{-\alpha^2}{2\sigma^2}\right), \tag{3.3.7}$$

and its variance

$$var(R_{Rice}) = \alpha^2 + 2\sigma^2 - \frac{1}{2}\pi\sigma^2 L_{\frac{1}{2}}^2\left[-\frac{\alpha^2}{2\sigma^2}\right], \tag{3.3.8}$$

where $L_{1/2}$ is the generalized Laguerre orthogonal polynomial with order $n = 1/2$ [Abramowitz 64]. This polynomial can be expressed also as a sum of Bessel function, that is,

$$L_{\frac{1}{2}}\left(-\frac{\alpha^2}{2\sigma^2}\right) = \frac{e^{-\frac{\alpha^2}{4\sigma^2}}}{2\sigma^2}\left(\alpha^2 I_1\left(\frac{\alpha^2}{4\sigma^2}\right) + \left(\alpha^2 + 2\sigma^2\right) I_0\left(\frac{\alpha^2}{4\sigma^2}\right)\right). \tag{3.3.9}$$

This distribution is often used to model propagation paths consisting of one strong direct LOS component and many random weaker components [Simon 05]. Note that for $\alpha = 0$ the expression (3.3.6) becomes the PDF of a Rayleigh random variable.

3.3.3 Nakagami-μ distribution

The Nakagami-μ distribution [Nakagami 58] is the probability distribution of the absolute value of a 2μ-dimensional normal random variable with zero mean and variance Ω.

Definition 3.6. *Let* $\mathbf{X}$ *be a centered* 2μ*-dimensional Gaussian random vector with zero mean and variance* Ω*. Let* R_{Naka} *be the amplitude magnitude defined as the norm of* $\mathbf{X}$*, that is,*

$$R_{Naka} = \|\mathbf{X}\| = \sqrt{X_1^2 + X_2^2 + \ldots + X_{2\mu}^2}. \tag{3.3.10}$$

Then, it is said that R_{Naka} *is a Nakagami-*μ *random variable and its distribution yields*

$$f_{R_{Naka}}(x) = \frac{2}{\Gamma(\mu)} \left(\frac{\mu}{\Omega}\right)^{\mu} x^{2\mu-1} e^{-\frac{x^2\mu}{\Omega}} \qquad x \in \mathbb{R} \text{ and } x \geq 0, \tag{3.3.11}$$

where the parameter μ *determines the shape whereas* Ω *controls the spread.*

The parameter Ω is the second order moment that can be calculated as

$$\Omega = E[R_{Naka}^2] = \int_{-\infty}^{\infty} x^2 f_{R_{Naka}}(x) dx. \tag{3.3.12}$$

Its mean and variance are

$$E[R_{Naka}] = \frac{\Gamma\left(\mu + \frac{1}{2}\right)}{\Gamma(\mu)} \sqrt{\frac{\Omega}{\mu}}, \tag{3.3.13}$$

and

$$var(R_{Naka}) = \Omega - \mu\Omega \left(\frac{\Gamma\left(\mu + \frac{1}{2}\right)}{\Gamma(\mu + 1)}\right)^2 \tag{3.3.14}$$

Note that this distribution includes Rayleigh distribution as a particular case ($\mu = 1$) and it approximates Rice distribution when $\mu \to \infty$. In communications systems it is used, for instance, to describe the amplitude of the received signal after maximum ratio diversity combining.

3.3.4 Chi-Square Distribution

The chi-square distribution with k degrees of freedom is the distribution of a sum of the squares of k independent standard normal random variables. Thus, it can be also described as a square Nakagami-μ distribution for which $\mu = k/2$.

Definition 3.7. *Let $\mathbf{X} = X_1, X_2, \ldots, X_k$ be a k-dimensional Gaussian random vector with zero-mean and unitary variance (i.e., standard normal). Let χ^2 be the square of the amplitude random variable defined as*

$$\chi^2 = X_1^2 + X_2^2 + \ldots + X_k^2. \tag{3.3.15}$$

Then χ^2 is a chi-square random variable and its density function yields

$$f_{\chi^2}(x) = \Gamma\left(\frac{k}{2}\right) 2^{-\frac{k}{2}} e^{-\frac{x}{2}} x^{\frac{k}{2}-1} \qquad x \in \mathbb{R} \text{ and } x \geq 0. \tag{3.3.16}$$

In a chi-square distribution the mean and the variance depend on the number of underlying standard normal random variables k, that is,

$$E[\chi^2] = k,$$

and

$$var(\chi^2) = 2k.$$

The power distribution of an OFDM signal transmitted over a Rayleigh fading channel distribution follows a chi-square distribution with two degrees of freedom [Nee 00].

3.3.5 Inverse-Chi-Square Distribution

Although the inverse-chi-square distribution is not an amplitude distribution, it is closely related to the chi-square distribution defined above and we deal with it through the following chapters.

Definition 3.8. *Let X be a random variable with a chi-square probability density. Then, the density corresponding to its multiplicative inverse (reciprocal) χ^{-2} calculated with (3.2.25) yields*

$$f_{\chi^{-2}}(x) = \Gamma\left(\frac{k}{2}\right) 2^{-\frac{k}{2}} e^{-\frac{1}{2x}} x^{-\frac{k}{2}-1}, \qquad x \in \mathbb{R} \text{ and } x \geq 0 \tag{3.3.17}$$

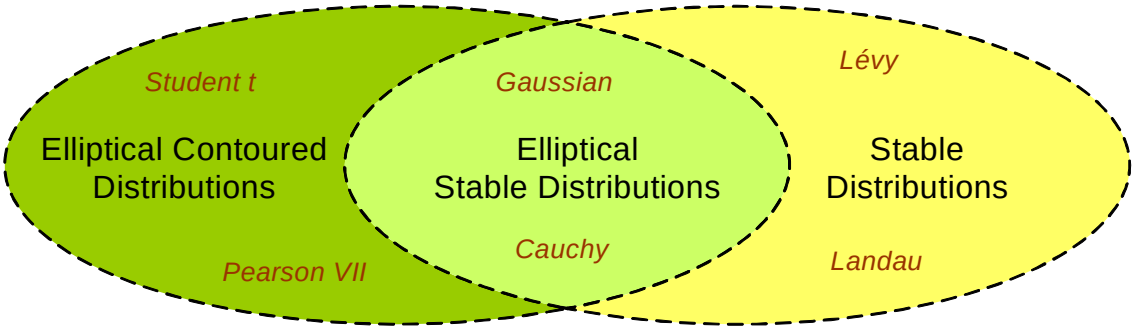

Figure 3.1: Distribution Families

and it is known as an inverse chi-square distribution.

Note that this distribution has no mean if $k \leq 2$ since $E[\chi^{-2}] = \dfrac{1}{k-2}$. In a similar fashion, if $k \leq 4$, it has no variance either as $var(\chi^{-2}) = \dfrac{1}{(k-2)^2(k-4)}$.

3.4 Non-Gaussian Distributions

The use of the normal distribution can be theoretically justified in situations where many small effects are added together into a variable that can be observed. However, there exist distributions of observed data in nature that exhibit tails decay following a power law that cannot be modeled by the classical Gaussian distribution. In many of these cases, elliptical and stable distributions can be useful for modeling this kind of data because they contain long-tailed and short-tailed distributions (relative to the normal). It must be noted that the Gaussian distribution is a particular case belonging to both families. Furthermore, elliptical distributions generalize the normal law, so they possess many properties parallel to those of this well known distribution. Many traditional methods in statistical data analysis can be directly applied to an elliptical population [Fang 06].

3.4.1 Elliptical Contoured Distributions

Elliptical Contoured Distributions (ECDs) may be seen as a natural generalization of the multivariate Gaussian that allows heavier tails as well as asymptotic tail dependence [Tsanakas 04]. The elliptical family includes, among others, Gaussian, Cauchy, logistic, Kotz and Pearson type II and type VII distributions. This family of distributions is closely related to the stable laws [Reiss 07] and it contains the subclass of elliptically contoured stable distributions which also includes known distributions, such as the multivariate normal and Cauchy distributions. The relations between theses classes of distributions appear depicted in Fig. 3.1.

The first formal introduction of elliptical distributions is traditionally attributed to Kelker [Kelker 70] although they appeared before in modern engineering literature (e.g., in information theory [McGraw 68]). In [Cambanis 81] they received a first systematic treatment although the most comprehensive and cited study on them can be found in [Fang 90b]. Interested reader can consult the early review and bibliography provided by [Chmielewski 81]. To complete the historical perspective, the introduction sections in [Tsanakas 04], [Balakrishnan 09] and [Fang 06] are also recommended. Lastly, Johnson [Johnson 87, Ch.6] provides thorough studies of those distributions.

In the remainder of this sub-section, we present the different definitions and properties of these distributions. We specifically describe the Pearson VII family and some related distributions that are used through the following chapters. We conclude this sub-section with a brief summary of some applications of these distributions in different fields. Elliptical distributions are a generalization of the family of spherically symmetric distributions whose definition follows.

Definition 3.9. *An $n \times 1$ random vector $\mathbf{x}$ is said to have a spherically symmetric distribution (or simply a spherical distribution) if there exists a function ϕ of a scalar*

variable such that

$$\Psi(\mathbf{t}) = \phi(\mathbf{t}^T\mathbf{t}), \tag{3.4.1}$$

where Ψ is the characteristic function of $\mathbf{x}$. We write $\mathbf{x} \sim S_n(\phi)$ and the function ϕ will be called the characteristic generator of the spherical distribution.

From the above definition, the characteristic function of a vector with a spherical distribution is constant on spheres and, as a natural consequence, the contours of equal value of its probability density function, provided it exists, have a spherical shape. Hence, these distributions are named spherical distributions. In the case of bidimensional spherical distributions, the term circular symmetry is used. Formally, a complex random variable Z is said to be circular if it is rotation invariant [Ollila 08], that is, if it preserves its probability distribution when it is multiplied by $e^{\jmath\alpha}$ for any given α [Picinbono 94].

In the same way in which multivariate normal distribution $\mathcal{N}(\boldsymbol{\mu}, \boldsymbol{\Sigma})$ is an extension of the standard multinormal distribution $\mathcal{N}(0, \mathbf{I_n})$, elliptical distributions are obtained applying affine transformations to vectors that follow spherical distributions as is stated in the following definition.

Definition 3.10. *An $n \times 1$ random vector $\mathbf{x}$ has an elliptically symmetric distribution (an elliptically contoured distribution or simply an elliptical distribution) with parameters $\boldsymbol{\mu}(n \times 1)$ and $\boldsymbol{\Sigma}(n \times n)$ if*

$$\mathbf{x} =^d \boldsymbol{\mu} + \mathbf{A^T y}, \tag{3.4.2}$$

where $=^d$ means equal in distribution, $\mathbf{y} \sim S_k(\phi)$ and $\mathbf{A^T} : n \times k$, $\mathbf{A^T A} = \boldsymbol{\Sigma}$ with $rank(\boldsymbol{\Sigma}) = k$.

We write $\mathbf{x} \sim \mathrm{EC_n}(\boldsymbol{\mu}, \boldsymbol{\Sigma}, \phi)$. Taking into account the properties of the characteristic function, the following assertion can be easily verified.

Definition 3.11. *If $\mathbf{x} \sim \mathrm{EC_n}(\boldsymbol{\mu}, \boldsymbol{\Sigma}, \phi)$ with $rank(\boldsymbol{\Sigma}) = k$, then the characteristic function of $\mathbf{x}$ is*

$$\Psi(\mathbf{t})_{EC} = E[e^{\jmath \mathbf{t}^T \mathbf{x}}] = exp(\jmath \mathbf{t}^T \boldsymbol{\mu}) \phi(\mathbf{t}^T \boldsymbol{\Sigma} \mathbf{t}). \tag{3.4.3}$$

A random vector $\mathbf{x} \sim \mathrm{EC_n}(\boldsymbol{\mu}, \boldsymbol{\Sigma}, \phi)$, in general does not necessary possess a density. But, if it exists (i.e., $rank(\boldsymbol{\Sigma}) = n$), it must be of the form

$$f_{\mathbf{x}}(\mathbf{x}; \boldsymbol{\Sigma}) = \frac{c_n}{|\boldsymbol{\Sigma}|^{1/2}} g_n\left((\mathbf{x}-\boldsymbol{\mu})^T \boldsymbol{\Sigma}^{-1} (\mathbf{x}-\boldsymbol{\mu})\right), \tag{3.4.4}$$

where $g_n(x)$ is a non-negative function, called density generator, such that

$$\int_0^\infty x^{n/2-1} g_n(x) dx < \infty. \tag{3.4.5}$$

and c_n is a corresponding normalizing constant

$$c_n = \frac{\Gamma(n/2)}{(2\pi)^{n/2} \int_0^\infty x^{n/2-1} g_n(x) dx}. \tag{3.4.6}$$

In that case notation $\mathrm{EC_n}(\boldsymbol{\mu}, \boldsymbol{\Sigma}, g_n)$ is used instead of $\mathrm{EC_n}(\boldsymbol{\mu}, \boldsymbol{\Sigma}, \phi)$.

Either the corresponding density generator $g_n(x)$ or the CHF for some of those distributions appears in Table 3.1 where

$$u = (\mathbf{x}-\boldsymbol{\mu})^T \boldsymbol{\Sigma}^{-1} (\mathbf{x}-\boldsymbol{\mu}). \tag{3.4.7}$$

Note that the square root of u is called the generating variable of the distribution and it is very important to simplify most of the calculations involving these distributions to a one-dimensional integral.

Equation (3.4.7) defines the contours of constant density for this family of distributions as ellipsoids which leads to the name elliptically contoured distributions (see examples in Figs. 3.2e and 3.2f). When $n = 1$, the class of elliptical distributions coincides with the class of one-dimensional symmetric distributions. Note that if the components of a random vector following an elliptical distribution are uncorrelated, then the distribution becomes spherical. Moreover, these components are independent only if, in addition of being uncorrelated, they are normally distributed as appears in Fig. 3.2d.

ECDs have many interesting properties. For instance, all marginal distributions of an elliptical distributed random vector are elliptical and have the same generator;

Table 3.1: Some sub-classes of n-dimensional ECDs

Sub-class	Density generator $g_n(u)$ or CHF $\Psi(\mathbf{t})$
Kotz	$g_n(u) = u^{m-1}\exp\left(-r\,u^s\right) \quad r, s > 0,\ 2p + n > 2$
Multinormal	$g_n(u) = \exp(-u/2)$
Pearson VII	$g_n(u) = (1 + u/s)^{-m}, m > n/2, s > 0$
Student t	$g_n(u) = (1 + u/s)^{-(n+m)/2}, m > 0$ an integer
Cauchy	$g_n(u) = (1 + u/s)^{-(n+1)/2}, s > 0$
Pearson II	$g_n(u) = (1 - u)^{-m}, m > 0$
Logistic	$g_n(u) = \dfrac{\exp(-u)}{(1 + \exp(-u))^2}$
Laplace	$g_n(u) = \exp(-\lvert u\rvert)$
Stable laws	$\Psi(\mathbf{t}) = \exp(r(\mathbf{t}^T\mathbf{t})^\alpha) \quad r > 0, 0 < \alpha \leq 2$
Scale Mixture of Normals	$\Psi(\mathbf{t}) = \int_0^\infty t^{-p/2}\mathcal{N}(\mu, \sigma^2 t) f\,(t)\,dt$ where $f(t)$ is a PDF.

all the conditional distributions are also elliptical and any linear combination of vectors following elliptical distribution is a vector that is also included in this class of distributions. As a particular case of this last property, the convolutions of spherical distributions are also spherical. In a similar fashion, the ratio of spherical random variables is also a spherical random variable [Fang 06].

Pearson type VII Distributions

The Pearson type VII family of distributions, which was originally introduced by Pearson in [Pearson 16], is part of the more general family of elliptical distributions.

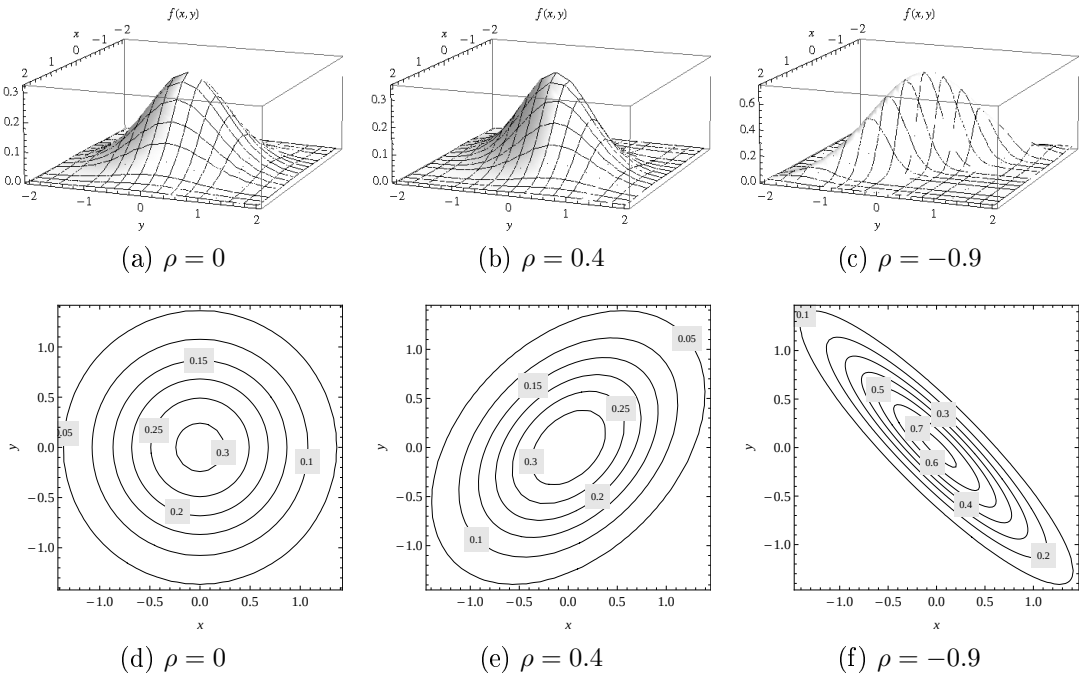

(a) $\rho = 0$ (b) $\rho = 0.4$ (c) $\rho = -0.9$

(d) $\rho = 0$ (e) $\rho = 0.4$ (f) $\rho = -0.9$

Figure 3.2: Circular and elliptical bivariate Laplace distributions with different correlation value ρ

The bivariate Pearson type VII distribution is a second-order distribution whose contours of probability densities are ellipses with constant eccentricity. The general expression for this family of distributions assuming a correlation coefficient of ρ, is given by

$$p_{\text{pearsonVII}}(x, y) = \frac{\Gamma(m)}{\Gamma(m-1)} \frac{a^2}{\pi\sqrt{1-\rho^2}} \left(1 - \frac{a^2\left(x^2 - 2xy\rho + y^2\right)}{\rho^2 - 1}\right)^{-m} \tag{3.4.8}$$

where $a \geq 0$ is the normalizing constant defined in (3.4.6), $m \geq 1/2$ and $\Gamma(m)$ is the Euler Gamma function [Abramowitz 64].

The absolute value of the correlation coefficient ρ coincides with the eccentricity value for the corresponding contour which is an ellipse. For an increasing linear relationship or decreasing linear relationship between the variables, the contour becomes a line with slope $\rho = 1$ or $\rho = -1$. In the specific case in which variables are uncorrelated, i.e., $\rho = 0$ in eq. (3.4.8), there is no linear dependency between the variables, the joint PDF is circularly symmetric and probability values depend only

on the radius of the circle on which they lie [Gubner 06]. Thanks to this property, its marginal PDFs are described by the same even function

$$p_{\text{pearsonVII}}(x) = \frac{\Gamma\left(m-\frac{1}{2}\right)}{\Gamma(m-1)}\frac{a}{\sqrt{\pi}}\left(1+a^2x^2\right)^{-(m-\frac{1}{2})}. \tag{3.4.9}$$

The general expression for a univariate Pearson type VII distribution presented in eq. (3.4.9) includes Cauchy and Student t distributions as particular cases [Fang 06]. If $m \leq 2$, the distribution has no finite variance or higher order statistics and, therefore, it does not have an MGF. Nonetheless, a general expression for its CHF is derived in Appendix A.1

$$\Psi(\omega) = \frac{1}{2^{m-2}\Gamma(m-1)}\left(\frac{|\omega|}{a}\right)^{m-1} K_{m-1}\left(\frac{|\omega|}{a}\right) \tag{3.4.10}$$

where $|\omega|$ is the absolute value of ω and K_m is the modified m-th order Bessel function of the second kind [Bocher 92].

Student t Distributions

In this section, we focus on the multivariate Student t distribution that will also appear in the following chapters. A random vector $\mathbf{t} = (t_1, \ldots, t_n)^T$ follows a n-dimensional Student t distribution with a $n \times 1$ location vector $\boldsymbol{\mu}$, a $n \times n$ positive definite scale matrix $\boldsymbol{\Sigma}$ and $\nu > 0$ degrees of freedom, if its joint PDF is given by

$$f(\mathbf{t}) = \frac{\Gamma\left(\frac{n+\nu}{2}\right)}{\Gamma(\frac{\nu}{2})\sqrt{\pi n}|\boldsymbol{\Sigma}|^{1/2}}\left(1+\frac{1}{\nu}(\mathbf{t}-\boldsymbol{\mu})^T\boldsymbol{\Sigma}^{-1}(\mathbf{t}-\boldsymbol{\mu})\right)^{-\frac{\nu+n}{2}} \qquad \mathbf{t}\in\mathbb{R}^n. \tag{3.4.11}$$

Then, it will be denoted as $\mathbf{t} \sim t_n(\boldsymbol{\mu}, \boldsymbol{\Sigma}, \nu)$.

Note that the Student t distribution is a particular case of the multivariate Pearson type VII distribution with $m = \frac{\nu+1}{2}$ and $a = \frac{1}{\sqrt{\nu}}$. Additionally, if $\nu = 1$, then (3.4.11) is the PDF of the n-variate Cauchy distribution.

The limiting form of (3.4.11) as $\nu \to \infty$ is the joint PDF of the n-variate normal distribution with mean vector $\boldsymbol{\mu}$ and covariance matrix $\boldsymbol{\Sigma}$.

As was explained in section 3.4.1, the multivariate Student t is an elliptical contoured distribution [Fang 90a], so its contours of equal density have an elliptical shape (spherical if $\boldsymbol{\Sigma}$ is proportional to the identity matrix). This is clearly illustrated in figure 3.3 which shows the PDFs and some of the contours of two bivariate Student t distributions.

The marginal distributions of a multivariate Student t are also Student t distributions. More precisely, if $\mathbf{t} \sim t_n(\boldsymbol{\mu}, \boldsymbol{\Sigma}, \nu)$ and the following partitions are considered,

$$\mathbf{t} = \begin{pmatrix} \mathbf{t}_1 \\ \mathbf{t}_2 \end{pmatrix}, \qquad \boldsymbol{\mu} = \begin{pmatrix} \boldsymbol{\mu_1} \\ \boldsymbol{\mu_2} \end{pmatrix}, \qquad \boldsymbol{\Sigma} = \begin{pmatrix} \boldsymbol{\Sigma_{11}} & \boldsymbol{\Sigma_{12}} \\ \boldsymbol{\Sigma_{21}} & \boldsymbol{\Sigma_{22}} \end{pmatrix},$$

where $\mathbf{t}_1$ is a $n_1 \times 1$ vector and $\boldsymbol{\Sigma}_{11}$ is a $n_1 \times n_1$ matrix; then $\mathbf{t}_1 \sim t_{n_1}(\boldsymbol{\mu}_1, \boldsymbol{\Sigma}_{11}, \nu)$ and $\mathbf{t}_2 \sim t_{n-n_1}(\boldsymbol{\mu}_2, \boldsymbol{\Sigma}_{22}, \nu)$.

Note that if $n = 1$, then (3.4.11) is

$$f(t) = \frac{\Gamma\left(\frac{1+\nu}{2}\right)}{\Gamma(\frac{\nu}{2})\sqrt{\pi\sigma^2}} \left(1 + \frac{1}{\nu\sigma^2}(t-\mu)^2\right)^{-\frac{\nu+1}{2}} \qquad t \in \mathbb{R}, \tag{3.4.12}$$

which is the expression of the PDF of a univariate Student t distribution with location parameter μ, scale parameter σ^2 and ν degrees of freedom. It is denoted by $t \sim t(\mu, \sigma^2, \nu)$.

The moments of first and second order of this distribution are

$$E(t) = \mu \quad \text{and} \quad var(t) = \frac{\nu}{\nu - 2}\sigma^2, \quad \nu > 2;$$

so, if the degrees of freedom are 2, this distribution does not possess a finite variance. The Student t distribution has increasingly heavy tails as ν decreases toward unity. With or without moments, the PDF becomes successively less peaked around 0 as $\nu \downarrow 1$.

An important characterization of this type of distributions is their representations as a scale mixture of normals when the mixing distribution is the inverted-gamma. Both the scale mixture of normals and the inverted-gamma are defined

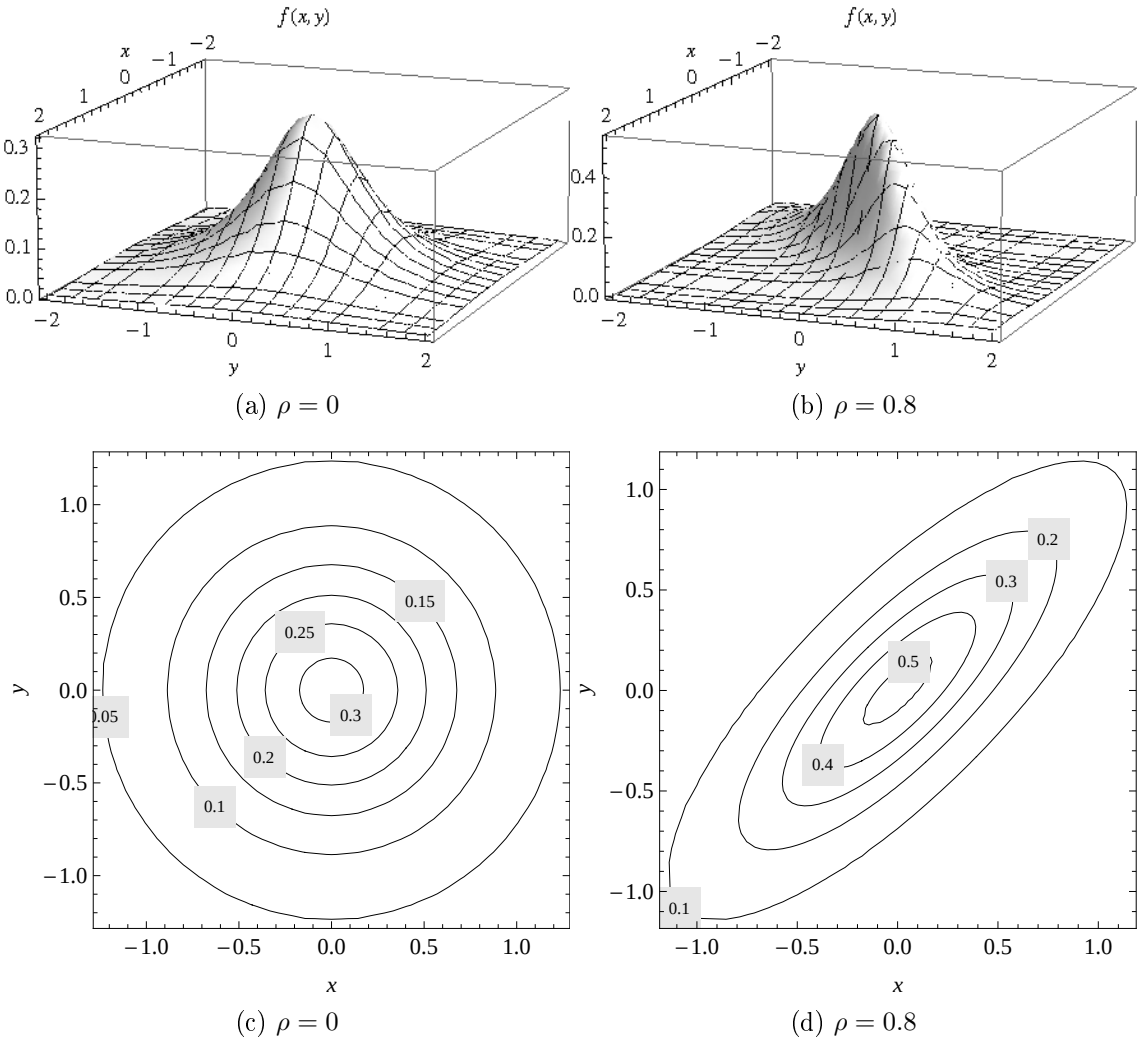

(a) $\rho = 0$ (b) $\rho = 0.8$

(c) $\rho = 0$ (d) $\rho = 0.8$

Figure 3.3: (a) and (b) show the PDFs for two different bivariate Student t distributions $t_2\left(\begin{pmatrix} 0 \\ 0 \end{pmatrix}, \begin{pmatrix} 1 & 0 \\ 0 & 1 \end{pmatrix}, 2\right)$ and $t_2\left(\begin{pmatrix} 0 \\ 0 \end{pmatrix}, \begin{pmatrix} 1 & 0.8 \\ 0.8 & 1 \end{pmatrix}, 2\right)$, respectively. In (c) and (d) are represented some contours of equal value of these densities

below.

Definition 3.12. *A random variable X defined on $\mathbb{R}$ has a scale mixture of normal distribution if the density of X can be written in the form*

$$f_X(x) = \int_0^\infty t^{-p/2}\mathcal{N}(\mu, \sigma^2 t) f\,(t)\, dt, \tag{3.4.13}$$

where $f(t)$ is a density funtion.

Definition 3.13. *A random variable X follows an inverted-gamma distribution with parameters $a > 0$ and $p > 0$, and will be denoted as $X \sim Ga^{-1}(a, p)$, if $1/X$ follows a gamma distribution $Ga(a, p)$, with shape parameter a and scale parameter p. Its density function is*

$$f(x) = \frac{a^p}{\Gamma(p)} e^{-a/x} x^{-(p+1)}, \qquad x > 0.$$

Considering the above definition, if $t \sim t(\mu, \sigma^2, \nu)$, then its distribution can be expressed as

$$t \sim \int_0^\infty \mathcal{N}(\mu, \sigma^2\lambda) f\left(\lambda | \frac{\nu}{2}, \frac{\nu}{2}\right) d\lambda. \tag{3.4.14}$$

Finally, note that [Kotz 04] presents an excellent monograph on multivariate Student t distributions in which many of the above properties are explained. The reading of [Johnson 95] it is also recommended for the univariate case.

Behrens-Fisher distributions

The standard Behrens-Fisher distribution with degrees of freedom $\nu_1, \nu_2 > 0$ and angle $\phi \in [0, \pi/2]$ is defined as

$$b_0 = t_1 \sin\phi - t_2 \cos\phi, \tag{3.4.15}$$

where t_1 and t_2 are independent random variables and $t_i \sim t(0, 1, \nu_i)$ for $i = 1, 2$, and it is denoted as $b_0 \sim$ Be-Fi(ν_1, ν_2, ϕ) [Box 73].

Both the following extension of this distribution to a location-scale family and the distribution of the convolutions of two arbitrary Student t distributions appear in [Girón 99].

A random variable b is said to be distributed as a Behrens-Fisher distribution with location parameter $\mu \in \mathbb{R}$, scale parameter $\sigma > 0$, degrees of freedom $\nu_1, \nu_2 > 0$ and angle $\phi \in [0, \pi/2]$, and will be denoted as $b \sim \text{Be-Fi}(\mu, \sigma^2, \nu_1, \nu_2, \phi)$, if

$$\frac{b-\mu}{\sigma} \sim \text{Be-Fi}(\nu_1, \nu_2, \phi)$$

Thus, if t_1 and t_2 are independent random variables such that $t_i \sim t(\mu_i, \sigma_i^2, \nu_i), i = 1, 2$, then

$$t_1 + t_2 \sim \text{Be-Fi}\left(\mu_1 + \mu_2, \sigma_1^2 + \sigma_2^2, \nu_1, \nu_2, \phi\right),$$

where $\phi \in [0, \pi/2]$ is such that $\tan^2 \phi = \sigma_1^2/\sigma_2^2$.

For the particular case that t_1 and t_2 are independent and identically distributed as $t(\mu, \sigma^2, \nu)$, then

$$t_1 + t_2 \sim \text{Be-Fi}(2\mu, 2\sigma^2, \nu, \nu, \pi/4). \tag{3.4.16}$$

The density function and the cumulative distribution of the Behrens-Fisher distribution can not be expressed in a simple explicit form, except for the cases $\nu_1 = \nu_2$, when these functions depend on a hypergeometric function, and for odd values of ν_1 and ν_2, for which the Behrens-Fisher distribution is a finite mixture of Student t distributions, as is established in [Girón 01]. For the rest of values of the degrees of freedom, the PDF and the CDF of the Behrens-Fisher distribution may be computed by numerical integration. The following expression, derived using (3.4.14), is useful to obtain those numerical values.

If $b \sim \text{Be-Fi}(\mu, \sigma^2, \nu_1, \nu_2, \phi)$, then

$$b \sim \int_0^\infty \int_0^\infty \mathcal{N}(\mu_1 + \mu_2, \lambda_1\sigma_1^2 + \lambda_2\sigma_2^2) f\left(\lambda_1 | \frac{\nu_1}{2}, \frac{\nu_1}{2}\right) f\left(\lambda_2 | \frac{\nu_2}{2}, \frac{\nu_2}{2}\right) d\lambda_1 d\lambda_2, \tag{3.4.17}$$

where $f(|,)$ is an inverted-gamma distribution as defined in eq. (3.4.14). The generalized Behrens-Fisher distribution is defined in [del Castillo 01] as the convolution of a finite number of Student t distributions. All the above results about the Behrens-Fisher distribution can be extended to the generalized case.

Definition 3.14. *A random vector* $\mathbf{X}$ *follows a standard generalized Behrens-Fisher distribution with parameters* $a_1, a_2, \ldots, a_p$ *and degrees of freedom* $\nu_1, \nu_2, \ldots, \nu_p$ *(where* $a_1, a_2, \ldots, a_p \in \mathbb{R}$, $a_1^2 + a_2^2 + \ldots + a_p^2 = 1$ *and* $\nu_1, \nu_2, \ldots, \nu_p > 0$*) if* $\mathbf{X} = a_1 t_1 + a_2 t_2 + \ldots + a_p t_p$ *where* $t_1, t_2, \ldots, t_p$ *are independent random variables and* $t_i \sim t(0, 1, \nu_i)$ *for* $i = 1, 2, \ldots, p$*, and it is denoted as* $\mathbf{X} \sim$ *Be-Fi*$(a_1, a_2, \ldots, a_p, \nu_1, \nu_2, \ldots, \nu_p)$.

If $\mathbf{Y} = \boldsymbol{\mu} + \sigma\mathbf{X}$ where $\mu \in \mathbb{R}$, $\sigma > 0$ and $\mathbf{X} \sim$ Be-Fi$(a_1, a_2, \ldots, a_p, \nu_1, \nu_2, \ldots, \nu_p)$, then $\mathbf{Y}$ is distributed according a generalized Behrens-Fisher distribution, and it will be denoted as $\mathbf{Y} \sim$ Be-Fi$(\boldsymbol{\mu}, \sigma^2, a_1, a_2, \ldots, a_p, \nu_1, \nu_2, \ldots, \nu_p)$.

It is easy to prove that if $\mathbf{X} = \sum_{i=1}^{p} t_i$, where t_i are independent random variables and $t_i \sim (\mu_i, \sigma_i^2, \nu_i)$ for $i = 1, \ldots, p$, then

$$\mathbf{X} \sim \text{Be} - \text{Fi}\left(\sum_{i=1}^{p}\mu_i, \sum_{i=1}^{p}\sigma_i^2, \left(\frac{\sigma_1}{\sum_{i=1}^{p}\sigma_i}\right)^{\frac{1}{2}}, \ldots, \left(\frac{\sigma_p}{\sum_{i=1}^{p}\sigma_i}\right)^{\frac{1}{2}}, \nu_1, \ldots, \nu_p\right).$$

Finally, for numerical calculations, the expression (3.4.17) can also be extended to a p-dimensional integral.

Sum of Independent Pearson type VII Distributions

As stated before, Pearson type VII distributions may not have a finite variance. In such cases, as we shall explain in Section 3.5.2, it is not possible to apply the Central Limit Theorem and the distribution of the sum cannot be assumed to tend in law to a Gaussian distribution. However, it is still possible to calculate the CHF of the sum of several independent random variables as the product of their respective CHFs [Grinstead 97]; its PDF can be calculated as the inverse Fourier transform of the resulting CHF. For a random variable ν resulting from the sum of random variables following a univariate Pearson type VII distribution the CHF expression yields

$$\Psi_\nu(\omega) = \prod_{k=1}^{N_c}\Psi(\omega) = \left(\frac{1}{2^{m-2}\Gamma(m-1)}\left(\frac{|\omega|}{a}\right)^{m-1}K_{m-1}\left(\frac{|\omega|}{a}\right)\right)^{N_c}, \qquad (3.4.18)$$

and the corresponding expression for the PDF may be written as

$$p_\nu(x) = \frac{1}{2\pi}\left(\frac{1}{2^{m-2}\Gamma(m-1)}\right)^{N_c}\int_{-\infty}^{\infty}\left(\left(\frac{|\omega|}{a}\right)^{m-1}K_{m-1}\left(\frac{|\omega|}{a}\right)\right)^{N_c}e^{-j\omega x}d\omega, \tag{3.4.19}$$

which is equivalent to the convolution of N_c univariate Pearson type VII densities and, to the best of the author's knowledge, has no analytical solution for $N_c > 2$. The analytical expression corresponding to the convolution of two univariate Pearson type VII densities is derived in Appendix B.

Applications of ECDs

Several examples of the use of elliptical distributions in engineering and economics can be found in the literature. Since the early work by Davenport [Davenport 52] on the probability distribution of speech signals in the time domain, the Laplace distribution has been successfully used to model those signals [Gazor 03]. This distribution is also suitable to model the distributions of the Discrete Cosine Transform (DCT) coefficients used in image compression algorithms [Lam 00]. In the field of patter recognition Pearson type II and type VII distributions are proposed [Cooper 62] to model statistical information extracted from the data. The family of elliptical distributions are shown admissible candidates for generalizing the theory of portfolio choice and equilibrium in capital asset markets, as well as attractive alternatives for use in empirical studies [Owen 83]. More recently, these distributions have been characterized and applied to signal processing algorithms [Ollila 11] and analysis of communication systems [Sánchez-Sánchez 09a].

3.4.2 Stable Laws

In this sub-section, we introduce the stable laws (stable distributions) and review some of their principal properties. The stable laws were discovered by Lévy in 1919

as a solution to an important subproblem of the central limit theorem [Lévy 24]. These distributions, as was explained with elliptical distributions, are a class of heavy tailed distributions that can be useful for modeling physical and financial data. Some of their physical applications are, for instance, the reflection of a rotating mirror, the gravitational field of stars or the fluctuations in the energy loss of a charged particle passing through a thin layer of matter which are satisfactorily described by means of Cauchy, Holtsmark and Landau distributions respectively; all of them belong to the stable distributions [Feller 71]. A more in depth study of this class of distributions appears in Samorodnitsky et al. [Samorodnitsky 94] and Nolan [Nolan 11].

Stable or α-stable distributions are fixed points (attractors) for the addition of independent and identically distributed (i.i.d.) random variables with finite or infinite variance [Heyde 06b].

There are several equivalent definitions of a stable distribution; three of them are presented below.

Definition 3.15. *A random variable X is said to have a stable distribution if for any positive numbers A and B, there is a positive number C and a real number D such that*

$$AX_1 + BX_2 =^d CX + D, \tag{3.4.20}$$

where X_1 and X_2 are independent copies of X, and where $=^d$ denotes equality in distribution[2]*. The distribution is said to be strictly stable if this holds with $D = 0$. Thus, a random variable X with a symmetric stable distribution, that is, X and $-X$ have the same distribution, is strictly stable.*

It is possible to conclude that the stable distributions are the only distributions that can be obtained as limits of normalized sums of i.i.d. random variables [Samorodnitsky 94] from the definition below.

Definition 3.16. *A random variable X is said to have a stable distribution if it has a domain of attraction, i.e., if there is a sequence of i.i.d. random variables*

[2]Note that, although a degenerate random variable X concentrated at one point is always stable, random variables with stable distribution are assumed to be non-degenerate unless stated otherwise.

$Y_1, Y_2, ...$ and sequences of positive d_n and real numbers a_n such that

$$\frac{Y_1 + Y_2 + \cdots + Y_n}{d_n} - a_n =^d X. \tag{3.4.21}$$

If the above holds with $a_n = 0$ for all n, then the distribution of X is stable in the strict sense. For every stable distribution it is possible to find $d_n = n^{1/\alpha}$ for some characteristic exponent α with $0 < \alpha \leq 2$. Determining what random variables are attracted to which limiting random variables with which choices of d_n, a_n constitutes the domain of attraction problem [Monrad 06]. If X is Gaussian and each random variable Y_i has a finite variance, eq. (3.4.21) becomes the ordinary Central Limit Theorem (CLT). The Generalized Central Limit Theorem (GCLT) introduced by Gnedenko and Kolmogorov [Gnedenko 54] extends the latter. These limit theorems will be addressed again in section 3.5.

Traditionally a stable distributions is defined in function of its characteristic function.

Definition 3.17. *A random variable X is stable if its characteristic function has the following form*

$$\Psi(\omega) = \exp\left(i\mu\omega - \sigma^\alpha |\omega|^\alpha [1 - i\beta sign(\omega)\Omega]\right) \qquad \omega \in \mathbb{R}, \tag{3.4.22}$$

where Ω is given by

$$\Omega = \begin{cases} \tan\frac{\pi\alpha}{2} & \alpha \neq 1 \\ \frac{-2}{\pi}\ln\omega & \alpha = 1 \end{cases} \tag{3.4.23}$$

and where $0 < \alpha \leq 2$, $-1 \leq \beta \leq 1$, $\sigma > 0$ and $\mu \in \mathbb{R}$.

The characteristic exponent α provides a measure of the thickness of the tails of the distribution and determines the existence of mean and variance (higher moments always diverge for those distributions). Only the Gaussian distribution (i.e., $\alpha = 2$) has a finite variance whereas any distribution with $\alpha < 2$ has an infinite variance. Similarly, distributions with $\alpha \leq 1$ have also an infinite mean. The skewness parameter β is a measure of asymmetry; when $\beta = 0$ there is symmetry around zero and the distribution is symmetric α stable (SαS). If distribution skewness implies that

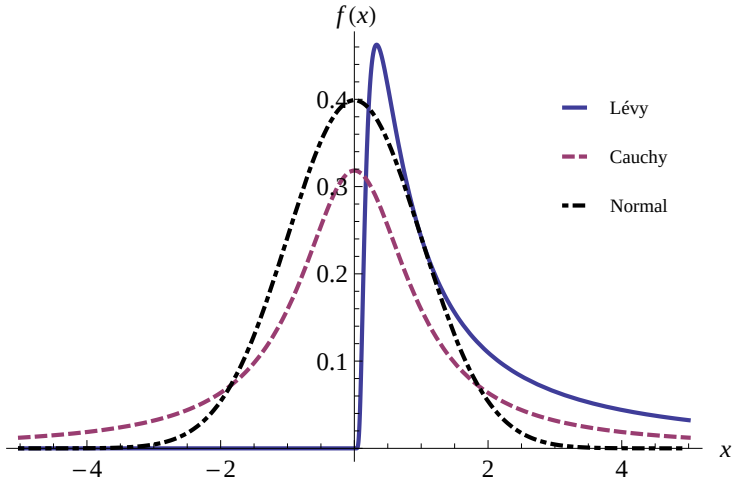

Figure 3.4: Examples of uni-dimensional stable distributions with known densities: Lévy, Cauchy and Normal distributions

only positive values are possible it becomes a positive α-stable (PαS) distribution. Equivalently, with negative α-stable (NαS) distribution possible values are always negative. The dispersion parameter σ is similar to the variance of the Gaussian distribution as it can provide an idea of how concentrated the random variable is around its mean if they both exist, whereas μ is a location parameter.

These parameters completely determine a stable distribution $S_\alpha(\sigma, \beta, \mu)$; a stable distribution is characterized by its CHF as closed formulas for densities and distribution functions only exist for a few stable laws [Monrad 06]. These are the Gaussian distribution ($\alpha = 2$), the Cauchy distribution ($\alpha = 1$) and the Lévy distribution ($\alpha = 1/2$). The expression of the density function for those distributions is shown in Table 3.2 and depicted in Fig 3.4.

It is worth noting that except for the normal distribution, all stable distributions have thick tails: the PDF is asymptotically proportional to $|x|^{-(1+\alpha)}$ and the CDF is asymptotically proportional to $|x|^{-\alpha}$ as $x \to \infty$.

The stable distributions have been widely used in many different fields, such as economics, physics, hydrology, biology or electrical engineering. For instance, the

Table 3.2: Stable distributions with PDF

Distribution	PDF
Gaussian	$\frac{1}{\sqrt{2\pi\sigma^2}}\exp\left(-\frac{(x-\mu)^2}{2\sigma^2}\right)$
Cauchy	$(1+x/c)^{-(n+1)/2}, c>0$
Lévy	$\sqrt{\frac{c}{2\pi}}\frac{1}{x^{3/2}}\exp\left(\frac{-c}{2x}\right)$

use of stable laws in economic modeling is discussed in Du Mouchel [DuMouchel 75] including Mandelbrot's work to model distributions of income [Mandelbrot 60]. On the other hand, Berger and Mandelbrot used stable stochastic processes to describe the patterns of error clustering in telephone circuits [Berger 63].

However, the most important application in signal processing and communications is impulsive noise modeling as stable distributions have been shown to successfully model noise over certain impulsive channels. One of the early works was [Rappaport 66] in which Rappaport and Kurst used Cauchy distribution to represent severe impulsive noise. In [Stuck 74] Stuck and Kleiner statistically characterized noise in telephone lines. This work was an attempt to understand how signal processing might be impacted if additive noise was perturbed away from a Gaussian probability distribution towards a close stable probability distribution: i.e., having a characteristic exponent less than two [Stuck 00]. In [Shao 93b] a stable model developed to characterize a general class of man-made and natural impulsive noises, including atmospheric noise, automotive ignition noise and noise observed over telephone lines, was applied to the detection of known signals in additive noise. Most of the literature related to this application is collected in [Shao 93a].

Additionally, α-stable distributions were also used to model the Radar Cross Section (RCS) of ships as well as sea clutters examples [Pierce 96]. The characteristics

for positive α-stable distributions and their application to model seismic activity, ocean wave variability, and radar sea clutter modulation are presented in [Pierce 97]. Stable distributions were also applied in the field of array signal processing to the direction-of-arrival estimation problem first in [Tsakalides 95] and later in [Brcic 02].

3.5 Central Limit Theorems

Historically known as the law of errors through the work of Laplace and Gauss, the term central limit theorem (CLT) is a generic name applied to any theorem giving convergence in distribution to the normal law for a sum of an increasing number of random variables [Heyde 06b].

De Moivre in 1718 and later Laplace in 1812 established the result for the case of Bernoulli trials, whereas Chebyshev (1887) and Liapunov (1900 and 1901) developed effective methods for the rigorous proof of limit theorems for sums of arbitrarily distributed random variables. The former used the method of moments and the latter characteristic functions. Nadarajah [Nadarajah 08] provides a review of the known results on sums of exponential, gamma, lognormal, Rayleigh and Weibull random variables.

In wireless communications, the sums of random variables arise naturally in many practical applications and the CLT usually serves to characterize the resulting random variables. However, in this work we deal with a less common situation in which the initial assumptions of this theorem are not fulfilled (i.e., variables in the sum have non-finite variance) and, hence, the CLT cannot be applied. In this case, a generalized version of this theorem, which is closely related to stable distributions, can be applied.

3.5.1 The Central Limit Theorem

The Lindeberg-Lévy central limit theorem is the most well known of these theorems. It refers to the convergence in distribution of a suitably standardized sum of i.i.d. random variables with finite variance, to a normal random variable with zero mean and unit variance [Wolfson 06]. Its formal statement is as follows.

Definition 3.18. *Let $x_1, x_2, \ldots, x_n$ be a sequence of i.i.d. random variables with $\mathrm{E}[x_k] = \mu$ and $var(x_k) = \sigma_k^2 < \infty$ for all k. Then*

$$Pr[\sum_{k=1}^{n}(x_k - \mu) \leq x] \rightarrow \frac{1}{\sqrt{2\pi}} \int_{-\infty}^{x} e^{-t^2/2} dt \quad \forall x \in \mathbb{R}, \tag{3.5.1}$$

as $n \rightarrow \infty$.

Usually, in practical applications, the central limit theorem can be applied in a loose manner as it is possible to relax the assumptions of identical distributions and independence. For instance, the random variables in the sum do not need to have the same distribution and they do not need to be independent either, as long as each random variable has only a small impact on the sum, and provided the correlation among them is not too high.

3.5.2 The Generalized Central Limit Theorem

In many practical applications, it is not possible to apply the CLT because the i.i.d. random variables in the sum have no finite variance. The GCLT, introduced by Gnedenko and Kolmogorov [Gnedenko 54], deals with these special cases. This theorem states that a sum of independent random variables from the same distribution, when properly centered and scaled, belongs to the domain of attraction of a stable distribution. Further, the only distributions that arise as limits from suitably scaled and centered sums of random variables are stable distributions [Brown 10].

Definition 3.19. *Let $x_1, x_2, \ldots, x_n$ be a set of n i.i.d. random variables which follow a distribution $p_{x_i}(x)$ $\forall$ $1 \leq j \leq n$ with heavy-tails such that*

$$p_{x_i}(x) = P(x) \simeq A|x|^{-(1+\alpha)} \qquad |x| \rightarrow \infty, \tag{3.5.2}$$

where α is an exponent describing how fast the distribution decays to 0, and all the moments $E[x^q] = \int_{-\infty}^{\infty} x^q P(x)dx$ such that $q \geq \alpha$ are divergent. Let T_n be the sum of $x_1, x_2, \ldots, x_n$ such that

$$T_n = \frac{\sum_{i=1}^{n} x_j}{n^{1/\alpha}}, \tag{3.5.3}$$

where α is a scaling exponent [Voit 05].

Then, for $\alpha > 2$, the variables in the sum have finite mean and variance and the usual form of the central limit theorem is valid. However, for $\alpha < 2$, the mean value and/or the variance diverge and the distribution of T_n is in the domain of attraction of a stable law as stated in definition 3.16.

A direct application of this theorem can be found in [Voit 05] where it is shown how the sum of many independent random variables, with power-law tail $p(x) \sim |x|^{-(1+\alpha)}$ where $0 < \alpha < 2$, is distributed according to a stable distribution with characteristic exponent α. The GCLT is also applied, for instance, to study the behavior of atomic and molecular samples cooled through the interaction with lasers [Bardou 02] or to define a thermodynamic framework in [Abe 00].

Note that the GCLT does not include the case in which $\alpha = 2$; to the best of our knowledge, in this case it is not possible to establish whether or not the sum of random variables converges in distribution.

Chapter 4

Analysis of Enhanced Noise in OFDM after FDE

4.1 Introduction

The purpose of this chapter is to study the statistical distribution of the enhanced noise after linear FDE in an OFDM system. In the following sections we find the density for the resulting noise term after equalization for Rayleigh, Rice and Nakagami-μ fast fading channels. Those densities will serve us to derive an expression for the BER in an OFDM uncoded transmission.

We focus on the Zero-Forcing (ZF) equalization method where the enhanced noise results from the ratio of two different complex random variables; its numerator is always the complex Gaussian random variable corresponding to the Additive White Gaussian Noise (AWGN), whereas its denominator depends on the fading channel considered. The Minimum Mean Square Error (MMSE) is not analyzed because the ZF equalizer in OFDM in general has the same performance that the MMSE equalizer in BER, although the latter offers lower MSE (see [Wang 04] and section 4.2.3 in [Wang 05] for a detailed justification).

To the best of our knowledge, there is very little literature in which a similar analysis is undertaken. Only in [Aghamohammadi 90], [Shayesteh 95] and [Wilson 99] a similar approach can be found in the way the density of linearly modulated signals in Rayleigh and Rice fading channels with imperfect channel estimation is derived. We show how the results presented here are consistent with those. Furthermore, we extend the analysis to the Nakagami-μ fading channel. It must be noted that, to the best of our knowledge, the literature regarding OFDM performance in Nakagami-μ fading channels is not abundant and it is mainly based on semi-analytical expressions (see [Count 01] and [Subotic 07]). The results obtained from these analyses serve us to derive a closed-form expression for the BER in an OFDM system.

4.2 System Model

The block diagram for a simple OFDM system compounded by transmitter and receiver-ends is depicted in Fig. 4.1. We showed in section 2.1 how the available bandwidth in OFDM is divided into orthogonal sub-carriers. Thus, a sequence of modulated complex symbols x is mapped in parallel into the allocated sub-carriers whereas the remaining sub-carriers are forced to zero. Thanks to the dual IDFT

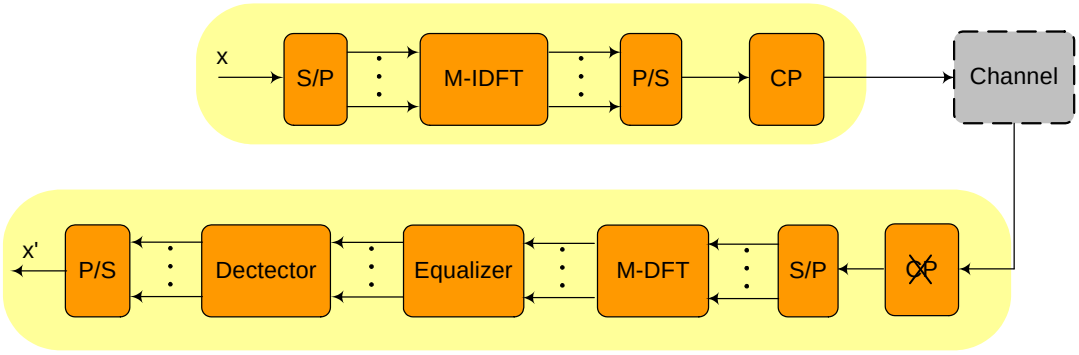

Figure 4.1: Transmitter and receiver for OFDM

and DFT operations at transmitter and receiver-ends, and to the addition of the cyclic prefix, the received signal in the frequency domain can be expressed as a

version of the transmitted one transformed by channel response and contaminated with thermal noise. In a more formal way,

$$\mathbf{r} = \mathbf{H}\mathbf{x} + \boldsymbol{\eta}, \tag{4.2.1}$$

where $\mathbf{H}$ is a $N \times N$ diagonal matrix whose elements h_k with $k = 1, \ldots, N$ are the channel frequency response at the sub-carriers; $\boldsymbol{\eta}$ is a vector with the complex AWGN component for each sub-carrier η_k. The complex random variable corresponding to the channel frequency response for a given sub-carrier k, h_k, is assumed to have zero mean and to be normalized in power, whereas each noise term has zero mean and variances N_0. Both η_k, and h_k are circularly symmetric random variables.

Throughout this dissertation, perfect synchronization and ideal estimation of the channel frequency response are assumed at the receiver end.

4.3 Channel Model

In the system under analysis, the received signal is the sum of the line-of-sight (LOS) paths and all resolvable multipath components. In our study we consider only the multipath fading due to the constructive and destructive combination of randomly delayed, reflected, scattered, and diffracted signal components. This type of fading is relatively fast and is, therefore, responsible for the short-term signal variations. In the following sections we analyze three different scenarios in which the fast fading follows different distributions, that is, Rayleigh, Rice and Nakagami-μ distributions.

The Rayleigh distribution is frequently used to model multipath fading with no direct LOS path, whereas Rice distribution is often used to model propagation paths consisting of one strong direct LOS component and many random weaker components [Simon 05]. These distributions are obtained by using mathematics to capture the underlying physical properties of the channel models. However, some experimental data does not fit well into either of these distributions. Thus, the more general

Nakagami-μ fading distribution was developed [Nakagami 58]; its parameters can be adjusted to fit a variety of empirical measurements [Goldsmith 05]. Thus, the Nakagami-μ distribution has been widely applied in the modeling of physical fading radio channels due to its good fit to empirical fading [Beaulieu 05]. Usually, Nakagami-μ fading occurs for multi-path scattering with relatively large delay-time spreads and with different clusters of reflected waves. The parameter μ allows modeling signal fading conditions that range from severe to moderate or light fading. Note that, in frequency-selective Nakagami-μ fading channels, the magnitude of the channel frequency response can be approximated with Nakagami-μ distributed random variables [Kang 03].

4.4 BER Analysis Techniques

There exist different approaches to calculate the BER from the expression for the received symbol after equalization eq. (4.2.1) in coherent digital communications. The classical one is based on averaging the conditional BER, which usually involves a Gaussian Q-function [Abramowitz 64], over the PDF of the instantaneous Signal to Noise Ratio (SNR) per bit $f_\gamma(\gamma)$, which is closely related to the fading statistics.

$$BER = \int_0^\infty Q(a\sqrt{\gamma}) f_\gamma(\gamma) d\gamma, \tag{4.4.1}$$

where a is a constant that depends on the specific modulation/detection combination [Simon 05]. The main drawback of this approach is that, usually, it does not result in finding a closed-form expression for the average BER,

Another elegant approach is using the MGF of the instantaneous SNR of the received signal conditioned to the channel response as proposed in [Simon 98b]. It exploits an alternate form of the Q-function [Simon 05] to obtain an integral representation of the conditional BER

$$BER = \frac{1}{\pi} \int_0^{\pi/2} M_\gamma \left(\frac{-a}{2 \sin^2 \theta} \right) d\theta, \tag{4.4.2}$$

where $M_\gamma()$ is the MGF of γ.

This approach leads to expressions of the average BER that involve a single finite-range integral whose integrand contains only elementary functions and which can therefore be easily computed numerically [Simon 98a]. However, in this dissertation we address some cases in which it is not possible to derive an expression for the MGF either for the instantaneous SNR or for the fading channel.

In this thesis, the BER analysis is performed by applying the framework proposed in [López-Martínez 10] that allows obtaining a closed-form expression for the BER for multilevel QAM (M-QAM). This approach is based in the assumption of independent bit-mapping for in-phase and quadrature components (e.g., Gray mapping). The resulting general expression can be simplified if the complex noise affecting the symbol before the decision stage, the enhanced noise, is circularly symmetric as then, only one of its marginal distributions is needed. In this case, we can use the following expression for the BER

$$BER = \sum_{n=1}^{L-1} w(n) I(n), \tag{4.4.3}$$

where $I(n)$ are the so-called Components of Error Probability (CEP), $w(n)$ are coefficients dependent on constellation mapping, $L = 2$ for BPSK, and $L = \sqrt{M}$ for M-QAM. The CEPs can be expressed in function of the CDF $F_{\eta_r}(\ )$ corresponding to the real part of the noise η affecting the symbol before the decision stage $\eta_r = \Re\{\eta\}$ as follows

$$I(n) = Pr\{\Re\{\eta\} > (2n-1)d\} = 1 - F_{\eta_r}((2n-1)d) \tag{4.4.4}$$

where d is the minimum distance between each symbol and the decision boundary, e.g., $d = \sqrt{E_s}$ for BPSK and $d = \sqrt{\dfrac{3E_s}{2\,(M-1)}}$ for M-QAM, and the coefficients $w(n)$ are directly computed as in [López-Martínez 10].

As stated before, the resulting closed-from expression is written as a function of the CDF of the real part of the noise affecting the symbol before the decision stage.

Thus, in the following, we study the stochastic nature of this complex noise and provide functions to perform the evaluation of this distribution required in (4.4.4) for different fading channels when FDE is applied. Note that, we only consider circularly symmetric enhanced noise and, therefore, we only need to obtain one of its marginal distributions in order to apply 4.4.4.

4.5 Noise Analysis for ZF-FDE

In OFDM based communications systems, zero-forcing FDE implies a ratio between two complex Gaussian random variables, one of them corresponding to the AWGN at the receiver and the other to the channel frequency response. This second random variable depends on the nature of the aforementioned multipath fading. Three different types are considered here: the Rayleigh, Rice and Nakagami-μ distributions already presented in section 3.3.

The channel frequency response for each system sub-carrier is represented by the $M \times M$ diagonal matrix $\mathbf{H}$ whose entries are assumed to be i.i.d. complex circularly symmetric random variables. In this point, we must keep in mind that the Fourier transform is a linear transformation and therefore, it preserves normality [Ghosh 69]. Thus, as the underlying random variables for the considered impulse response are Gaussian, the respective underlying random variables for the channel frequency response follow the same distribution. For instance, for Rayleigh fading channels, the channel frequency response has as underlying variables zero-mean and unitary-variance complex Gaussian [Ohno 04] whereas, for Ricean channels, these complex Gaussian have non-zero mean.

Kang et al. show in [Kang 03] how, for frequency-selective Nakagami-μ fading channels, the magnitudes of the channel frequency response can be also approximated as Nakagami-μ distributed random variables. Their fading and mean power parameters can be expressed as explicit functions of the fading and mean power

parameters of the channel impulse response.

In this section we derive the PDF for different random variables resulting for quotients of other random variables; those quotients are the Rayleigh/Rayleigh, the Rayleigh/Rice and the Rayleigh/Nakagami-μ ratios.

After applying zero-forcing equalization and under the assumption of ideal estimation of the channel frequency response, the expression for the received symbol can be derived from (4.2.1) as

$$\hat{\mathbf{x}} = \mathbf{x} + (\mathbf{H}^H\mathbf{H})^{-1}\mathbf{H}^H\eta \tag{4.5.1}$$

Thus, the expression for the k-th received symbol is

$$\hat{x}_k = x_k + \frac{\eta_k}{h_k} = x_k + \hat{\eta}_k, \tag{4.5.2}$$

where h_k is the channel frequency response at sub-carrier k.

The enhanced noise term $\hat{\eta}_k$ is the ratio of two i.i.d. complex circularly symmetric[1] random variables. In the following sections, for a given subcarrier, the k index will be suppressed for the sake of simplicity.

4.5.1 ZF Enhanced Noise for Rayleigh Fading Channels

In this case, the enhanced noise term $\hat{\eta}$ is the ratio of two i.i.d. circularly symmetric Gaussian random variables (i.e., the noise at the receiver and the channel frequency response for the considered sub-carrier). Both variables have zero-mean but different variances. Their ratio can be derived formally as follows.

Proposition 4.5.1. *Let X and Y be two complex Gaussian random variables with zero-mean and variance σ_X^2 and σ_Y^2 respectively. Let R_X and R_Y be the random variables for their respective modulus, both of them following a Rayleigh distribution, and let θ_X and θ_Y be random variables with a uniform distribution in $[0, 2\pi]$ for their respective phases. Let Z be the ratio X/Y and let R_Z be its modulus. Then,*

[1] It belongs to the class of the elliptical distributions presented in Chapter 3.

the density of R_Z is calculated, applying eq. (3.2.21) for quotient of two random variables, as

$$f_{R_Z}(r) = \frac{2\sigma_X^2\sigma_Y^2 r}{\left(\sigma_X^2 + \sigma_Y^2 r^2\right)^2} \qquad r \in \mathbb{R}\ ,\ r \geq 0. \tag{4.5.3}$$

Expression (4.5.11) is consistent with the one provided in [Simon 06]. As θ_Z is a uniform random variable defined in $[0, 2\pi]$ and R_Z and θ_Z are independent random variables[2], the density of the ratio $Z = X/Y$ yields

$$f_Z(r,\theta) = \frac{1}{2\pi}\frac{2\sigma_X^2\sigma_Y^2 r}{\left(\sigma_X^2 + \sigma_Y^2 r^2\right)^2} \qquad r \in \mathbb{R}\ ,\ r \geq 0. \tag{4.5.4}$$

In this case, as the channel frequency response is normalized $\sigma_X^2 = \sigma^2 = N_0/E_s$ and $\sigma_Y^2 = 1$ and hence, the distribution of the enhanced noise $\hat{\eta}$ can be written as

$$f_{\hat{\eta}}(r,\theta) = \frac{1}{\pi}\frac{\sigma^2 r}{\left(\sigma^2 + r^2\right)^2} \qquad r \in \mathbb{R}\ ,\ r \geq 0. \tag{4.5.5}$$

With a change of variables, eq. (4.5.5) can be transformed into the bivariate joint PDF for the real and imaginary components of the resulting complex random variable

$$f_{\hat{\eta}_r,\hat{\eta}_i}(x,y) = \frac{1}{\pi}\frac{\sigma^2}{\left(\sigma^2 + (x^2+y^2)\right)^2} \qquad x, y \in \mathbb{R}, \tag{4.5.6}$$

where $\hat{\eta}_r$ and $\hat{\eta}_i$ are the real and imaginary components of the enhanced noise term.

The expression in eq. (4.5.6) belongs to the Pearson type VII family of distributions, which were presented in section 3.4.1. In fact, it is the probability density function of a bivariate Student t distribution with 2 degrees of freedom, mean $(0,0)$, scale matrix $\frac{\sigma^2}{2}I_2$, where I_2 is the identity matrix of size 2.

As was explained in section 3.4.1, the marginal distributions of Student t distributions are also Student t, then it is obtained that

$$\hat{\eta}_R \overset{\mathrm{d}}{=} \hat{\eta}_I \sim t\left(0, \frac{\sigma^2}{2}, 2\right)$$

[2]The variables X and Y are circularly symmetric and they belong to the class of elliptical distributions introduced in section 3.4.1. Its ratio Z is also circularly symmetric and its modulus and phase are independent.

and the PDF of the real and the imaginary components are equal and given by

$$f_{\hat{\eta}_r}(x) = f_{\hat{\eta}_i}(x) = \frac{1}{2}\frac{\sigma^2}{(\sigma^2 + x^2)^{3/2}} \qquad x \in \mathbb{R}. \tag{4.5.7}$$

This density function appears in [Aghamohammadi 90] for linearly modulated signals transmitted over a Rayleigh fading channel and, more recently, in [Baxley 10] to obtain the Symbol Error Rate (SER) with imperfect channel knowledge for the same channel. It is a heavy-tailed distribution whose tails decay following a power law x^{-3} and it has no finite variance as was stated in section 3.4.1.

The CDF of $\hat{\eta}_r$ results in the following expression[3]

$$F_{\hat{\eta}_r}(x) = \frac{1}{2} + \frac{x}{2\sqrt{x^2 + \sigma^2}} \qquad x \in \mathbb{R}. \tag{4.5.8}$$

In appendix A.1 we provide the derivation for the corresponding CHF that results

$$\Psi_{\hat{\eta}_r}(\omega) = \sigma|\omega| K_1(\sigma|\omega|) \qquad \omega \in \mathbb{R}, \tag{4.5.10}$$

where $|\omega|$ means the absolute value of ω and $K_1(\,)$ is the modified first order Bessel function of the second kind [Bocher 92]. The fact that $\Psi_{\tilde{\eta}_r}(\omega)$ is a symmetric, exponentially decaying function with a decay rate that depends on the argument of K_1 will serve us in the following chapter to simplify the numerical computation.

4.5.2 ZF Enhanced Noise for Rice Fading Channels

In the case in which there exists a LOS component, the complex Gaussian random variable corresponding to the channel frequency response has a certain mean α, unitary variance and, consequently, its modulus follows a Rice distribution. As in

[3]Note that from eq. (4.5.8) with $\sigma^2 = \frac{N_0}{E_s}$ it is possible to derive the same analytical expression of BER for BPSK in OFDM over a Rayleigh fading channel provided by Proakis in [Proakis 00].

$$p_e = F_{\hat{\eta}_r}(-1) = \frac{1}{2}\left(1 - \sqrt{\frac{E_s}{E_s + N_0}}\right). \tag{4.5.9}$$

the previous section, the noise at the receiver is a complex circularly symmetric Gaussian random variable with zero-mean and variance σ^2.

Proposition 4.5.2. *Let X and Y be two complex Gaussian random variables with different means ($E[X] = 0$ and $E[Y] = \alpha$) and variances (σ_X^2 and σ_Y^2). Let R_X and R_Y be the random variables for their respective modulus. The former follows a Rayleigh distribution (eq. (3.3.4)) whereas the latter has a Rice distribution (eq. (3.3.6)). Let Z be the ratio X/Y and let R_Z be its modulus. Then, the density of R_Z is calculated, applying eq. (3.2.21) for quotient of two random variables, as*[4]

$$f_{R_Z}(r) = \frac{r\sigma_X^2\left(\alpha^2\sigma_X^2 + 2\sigma_Y^2\left(\sigma_X^2 + r^2\sigma_Y^2\right)\right)}{\left(\sigma_X^2 + r^2\sigma_Y^2\right)^3} e^{-\frac{\alpha^2 r^2}{2\left(\sigma_X^2 + r^2\sigma_Y^2\right)}} \qquad r \in \mathbb{R}\ ,\ r \geq 0. \quad (4.5.11)$$

As the numerator X is a complex circular random variable, it is rotation invariant [Picinbono 94]. Due to this property, it preserves the circular symmetry when it is multiplied by $e^{\jmath\alpha}$ for any given α. Thus, the variable Z has also circular symmetry and, consequently, its phase follows a uniform phase distribution between 0 and 2π and is independent from its modulus [Fang 06]. Hence, the density function of Z yields

$$f_Z(r,\theta) = \frac{1}{2\pi}\frac{r\sigma_X^2\left(\alpha^2\sigma_X^2 + 2\sigma_Y^2\left(\sigma_X^2 + r^2\sigma_Y^2\right)\right)}{\left(\sigma_X^2 + r^2\sigma_Y^2\right)^3} e^{-\frac{\alpha^2 r^2}{2\left(\sigma_X^2 + r^2\sigma_Y^2\right)}} \qquad r \in \mathbb{R}\ ,\ r \geq 0. \quad (4.5.12)$$

In this case the density of the enhanced noise $\hat{\eta}$ yields

$$f_{\hat{\eta}}(r,\theta) = \frac{r\sigma\left(\alpha^2\sigma + 2\left(\sigma + r^2\right)\right)}{2\pi\left(\sigma + r^2\right)^3} e^{-\frac{\alpha^2 r^2}{2(\sigma + r^2)}} \qquad r \in \mathbb{R}\ ,\ r \geq 0. \quad (4.5.13)$$

as $\sigma_X^2 = \sigma^2 = \dfrac{N_0}{E_s}$ and $\sigma_Y^2 = 1$. Note that for $\alpha = 0$ we obtain the same result presented in the previous section.

With a change of variable to cartesian coordinates we obtain the expression of the joint PDF as a function of the real and imaginary components of the enhanced

[4] This expression can be also derived applying eq. (3.2.25) to the expression provided in [Simon 06] for the ratio between independent Rice and Rayleigh distributed random variables.

noise term (i.e., $\hat{\eta}_r$ and $\hat{\eta}_i$)

$$f_{\hat{\eta}_r,\hat{\eta}_i}(x,y) = \frac{(x^2+y^2)\alpha^2\sigma + 2\left((x^2+y^2)\sigma+1\right)}{2\pi\left((x^2+y^2)\sigma+1\right)^3}\sigma e^{-\frac{\alpha^2}{2((x^2+y^2)\sigma+1)}} \qquad x,y \in \mathbb{R}. \tag{4.5.14}$$

As in the previous case, the resulting variable is a circularly symmetric random variable (see Fig. 4.2b). However, in this case and to the best of our knowledge, it is not possible to find a closed-form expression for the function corresponding to the two identical marginal distributions. Nevertheless, it is possible to use numerical integration to evaluate the corresponding CDF, that is,

$$F_{\hat{\eta}_r}(t) = F_{\hat{\eta}_i}(t) = \int_{-\infty}^{t}\int_{-\infty}^{\infty} f_{\hat{\eta}_r,\hat{\eta}_i}(x,y)dydx \qquad x,y \in \mathbb{R}. \tag{4.5.15}$$

This approach to the solution is similar to the one proposed in [Shayesteh 95] for the density function of linearly modulated signals transmitted over a Ricean fading channel. However, we consider that, due to the double numerical integration implied in expression (4.5.15), the alternative approach proposed in this dissertation for BER analysis is impractical for Rice selective fading channels.

4.5.3 ZF Enhanced Noise for Nakagami-μ fading channels

In this case we assume that the modulus of the complex random variable corresponding to the channel frequency response follows a Nakagami-μ distribution [Kang 03].

Proposition 4.5.3. *Let X be a complex Gaussian random variables with zero-mean and variance σ^2. Let Y be a n-dimensional Gaussian random vector with zero-mean and variance Ω. Let R_X and R_Y be the random variables for their respective modulus. The former follows a Rayleigh distribution eq. (3.3.4) whereas the latter has a Nakagami-μ distribution eq. (3.3.11) where $\mu = n/2$. Let Z be the ratio X/Y and let R_Z be its modulus. Then, the random variable R_Z is the ratio of R_X and R_Y and its density is calculated using eq. (3.2.21) and applying the integral formula 3.326-2 in [Gradshteyn 07] as*

$$f_{R_Z}(r) = \frac{\mu}{\sigma^2}\left(\frac{\mu}{\Omega}\right)^{\mu} r\left(\frac{r^2}{2\sigma^2}+\frac{\mu}{\Omega}\right)^{-1-\mu} \qquad r \in \mathbb{R} \text{ and } r \geq 0. \tag{4.5.16}$$

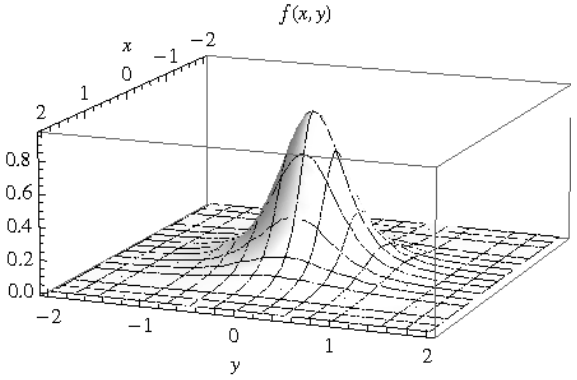

(a) 3D Plot

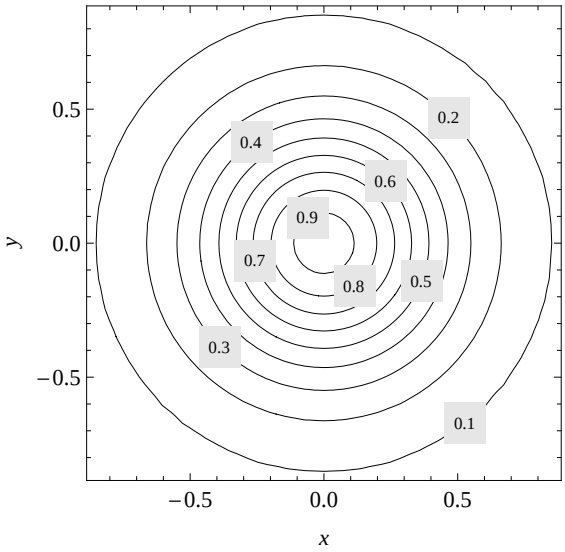

(b) Contour plot

Figure 4.2: Example of density of the Rayleigh/Rice ratio

As in the previous analysis, the numerator X is a complex circular random variable, thereby rotation invariant [Picinbono 94]. Again that means it preserves the circular symmetry when it is multiplied by $e^{\jmath\alpha}$ for any given α. That implies that the resulting random variable Z is also a circularly symmetric random variable and, consequently, its phase Φ_Z follows a uniform phase distribution between 0 and 2π and is independent from the modulus [Fang 06].

$$f_{R_Z,\Phi_Z}(r,\phi) = \frac{1}{2\pi}\frac{\mu}{\sigma^2}\left(\frac{\mu}{\Omega}\right)^{\mu} r\left(\frac{r^2}{2\sigma^2}+\frac{\mu}{\Omega}\right)^{\mu-1} \qquad r \in \mathbb{R}\ and\ r \geq 0. \tag{4.5.17}$$

Assuming that the channel is normalized in power, i.e., $\Omega = 1$, expression (4.5.17)

can be particularized to obtain the density of the enhanced noise $\hat{\eta}$. Its joint distribution in polar coordinates yields

$$f_{R_{\hat{\eta}},\Phi_{\hat{\eta}}}(r,\phi) = \frac{1}{2\pi}\frac{\mu^{\mu+1}}{\sigma^2} r \left(\frac{r^2}{2\sigma^2}+\mu\right)^{-1-\mu} \qquad r \in \mathbb{R}\ and\ r \geq 0, \tag{4.5.18}$$

where $\sigma = \dfrac{N_0}{E_s}$.

For $\mu = 1$ the Nakagami-μ distribution becomes a Rayleigh distribution and the density is the same obtained in section 4.5.1.

The joint PDF in Cartesian coordinates is

$$f_{\hat{\eta}_r,\hat{\eta}_i}(x,y) = \frac{\mu^{\mu+1}}{2\pi\sigma^2}\left(\frac{x^2+y^2}{2\sigma^2}+\mu\right)^{-1-\mu} \qquad x,y \in \mathbb{R}, \tag{4.5.19}$$

where $\hat{\eta}_r$ and $\hat{\eta}_i$ are the real and imaginary components of the enhanced noise. The resulting random variable follows a bivariate Pearson type VII distribution whose PDF (3.4.8) is particularized with $m = \mu + 1$ and $a = \frac{1}{2\mu}$. An example of this circularly symmetric density is provided in Fig. 4.3.

In this case it is possible to compute each corresponding marginal PDF

$$f_{\hat{\eta}_r}(x) = f_{\hat{\eta}_i}(x) = \sqrt{\frac{1}{\pi}}\frac{\Gamma\left(\mu+\frac{1}{2}\right)2^{\mu}\mu^{\mu}\sigma^{2\mu}}{\Gamma(\mu)\left(2\mu\sigma^2+x^2\right)^{\mu-\frac{1}{2}}} \qquad x \in \mathbb{R}, \tag{4.5.20}$$

where $\Gamma(n)$ is the Gamma function [Abramowitz 64].

For this marginal PDF the mean is zero and the variance yields $\sigma^2_{\hat{\eta}_r} = \dfrac{\mu\sigma^2}{\mu-1}$ provided $\mu > 1$. For $\mu \leq 1$ it has neither a finite variance nor higher order statistics and, therefore, has no MGF. Nonetheless, there is no restriction regarding the CHF which is derived in appendix A.1. Changing $n = \mu$ and $a = \frac{1}{\sqrt{2\mu}}$ in (A.1.5) we obtain

$$\Psi_{\hat{\eta}_r}(\omega) = \frac{\sigma^{\mu}|\omega|^{\mu}}{2^{\mu/2-1}\Gamma(\mu)}\mu^{\mu/2}K_{\mu}\left(\sigma\sqrt{2\mu}|\omega|\right) \qquad \omega \in \mathbb{R}, \tag{4.5.21}$$

where $|\omega|$ is the absolute value of ω and $K_{\mu}(\ )$ is the modified μ-th order Bessel function of the second kind [Bocher 92].

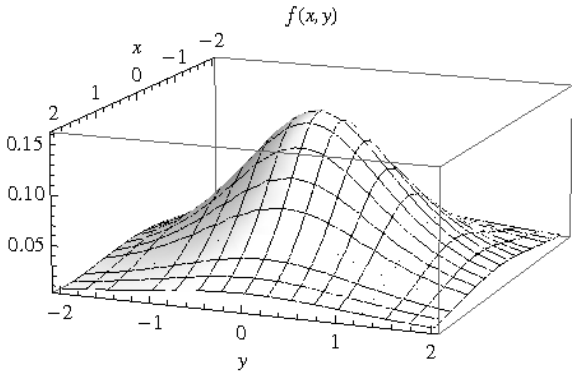

(a) 3D Plot

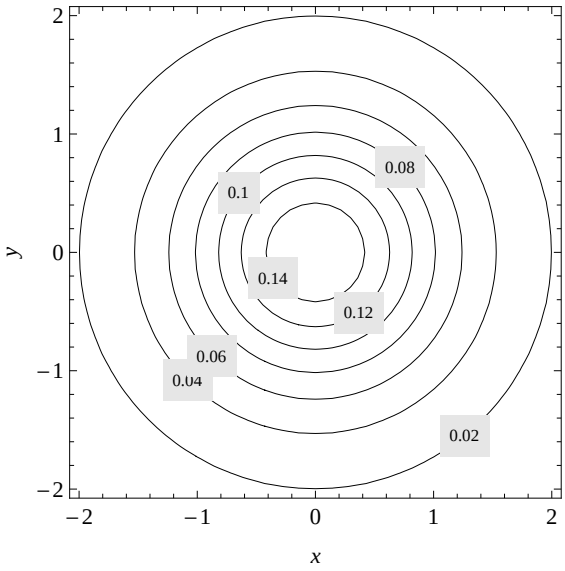

(b) Contour plot

Figure 4.3: Example of density of the Rayleigh/Nakagami-μ ratio

The corresponding CDF of $\hat{\eta}_r$ results in the following expression

$$F_{\hat{\eta}_r}(x) = \frac{(-1)^{-\mu}\Gamma\left(\mu+\frac{1}{2}\right)}{2\sqrt{\pi}\Gamma(\mu)} B_{-\frac{2\mu\sigma^2}{x^2}}\left(\mu, \frac{1}{2}-\mu\right) \qquad x \in \mathbb{R}, \tag{4.5.22}$$

where B is the incomplete Beta function [Abramowitz 64].

4.6 OFDM BER Analysis

As described in section 4.4, the expressions of the CDF for the enhanced noise after equalization, that is, of the noise term in the detection stage, allow us to compute

the BER for the different channels considered. More specifically, as the enhanced noise considered is circularly symmetric in all the cases, we only need it marginal CDF, $F_{\hat{\eta}_r}(\,)$. Thus, plugging equation (4.5.8) into expression (4.4.4) we can compute the CEPs for the Rayleigh fading channel as follows

$$BER = \sum_{n=1}^{L-1} w(n) \left(\frac{1}{2} - \frac{(2n-1)d}{2\sqrt{(2n-1)d)^2 + \sigma^2}} \right). \tag{4.6.1}$$

In a similar fashion, it is possible to derive the expression for Nakagami-μ fading channels using equation (4.5.22). The resulting BER expression is given by

$$BER = \sum_{n=1}^{L-1} w(n) \left(1 - \frac{(-1)^{-\mu}\Gamma\left(\mu + \frac{1}{2}\right)}{2\sqrt{\pi}\Gamma(\mu)} B_{-\frac{2\mu\sigma^2}{((2n-1)d)^2}} \left(\mu, \frac{1}{2} - \mu \right) \right). \tag{4.6.2}$$

Note that the BER analysis for Rice fading channels is omitted because, in this case, it is not possible to obtain an analytical expression either for the PDF or the CDF of the enhanced noise after ZF-FDE.

4.7 Simulations and Numerical Results

In this section, we validate the results obtained for the considered fading channels. With this purpose, BER values are obtained for SNR values ranging from 0 to 30 dB and compared with values obtained by means of simulations. In order to simplify the validation process in the case of Nakagami fading channels, we directly generate channel frequency response whose magnitudes are distributed according to a Nakagami-μ distribution with some integers and half-integer values of μ. In Fig. D.2 we show the numerical evaluation of the BER for a BPSK transmission for different values of μ. Note that for $\mu = 1$ the channel has a Rayleigh fading. If $\mu < 1$ BER values worsen (i.e., it is worse than Rayleigh scenario) whereas for $\mu > 1$ we obtain lower values of BER. A similar behavior can be observed in Fig. D.3 and D.4 where results for 4QAM and 16QAM are shown.

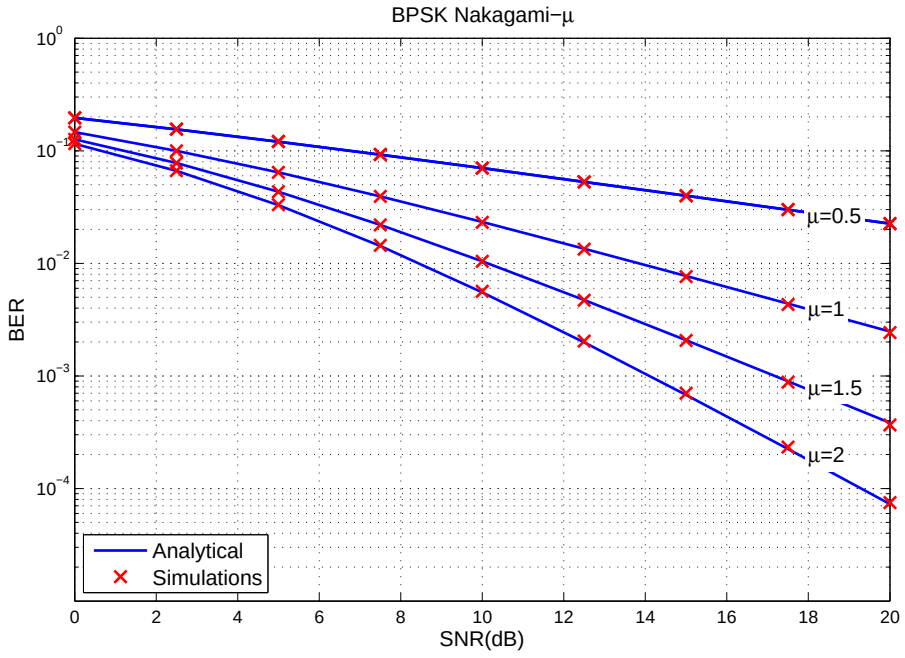

Figure 4.4: BER values for several Nakagami-μ fading channels, including Rayleigh ($\mu = 1$), with BPSK

4.8 Conclusions

In this chapter we study the enhanced noise after ZF-FDE for an OFDM signal transmitted over different fading channels (i.e., Rayleigh, Rice and Nakagami-μ). For these channels, due to the fact that Fourier transform is a linear transformation, the values of the complex channel frequency response follow the same distribution that the channel impulse response. This property is widely used in the literature for Rayleigh distributed random variables [Ohno 04] and even references can be found when the random variables follow a Nakagami-μ distribution [Kang 03]. Taking advantage of this property, we characterize the enhanced noise after equalization and apply derived expressions for the CDF to compute analytically the BER for Rayleigh and Nakagami-μ fading channels. In the case of Rice fading channels, we show that the proposed approach for BER analysis, although feasible, it is impractical due to the additional numerical computation required. Interested reader is referred to appendix B where all the expression derived through this chapter for the different

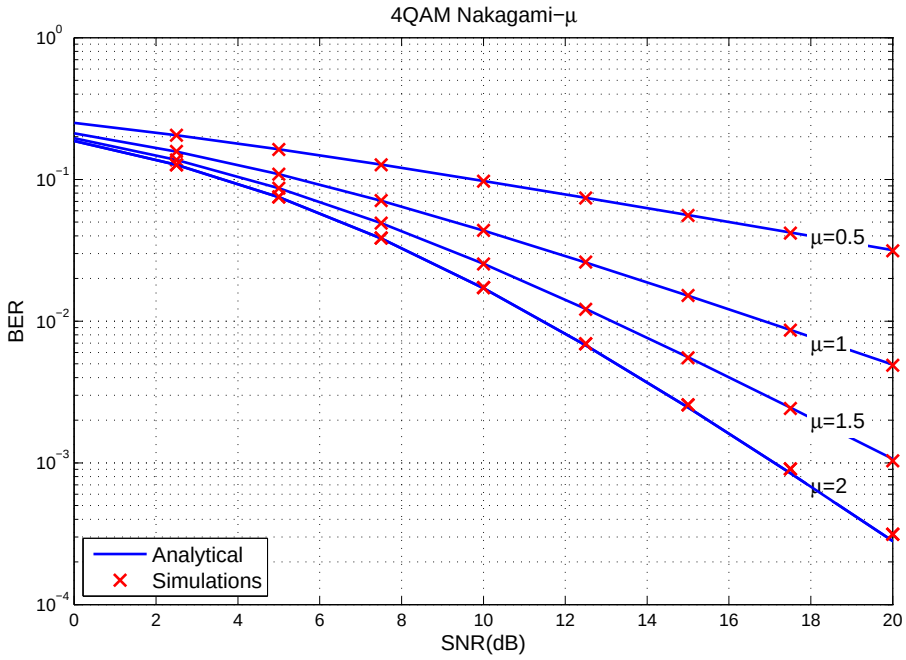

Figure 4.5: BER values for several Nakagami-μ fading channels, including Rayleigh ($\mu = 1$), with 4QAM

ratio random variables are gathered as a quick reference. These expressions are used in the next chapter to extend the BER analysis to SC-FDMA.

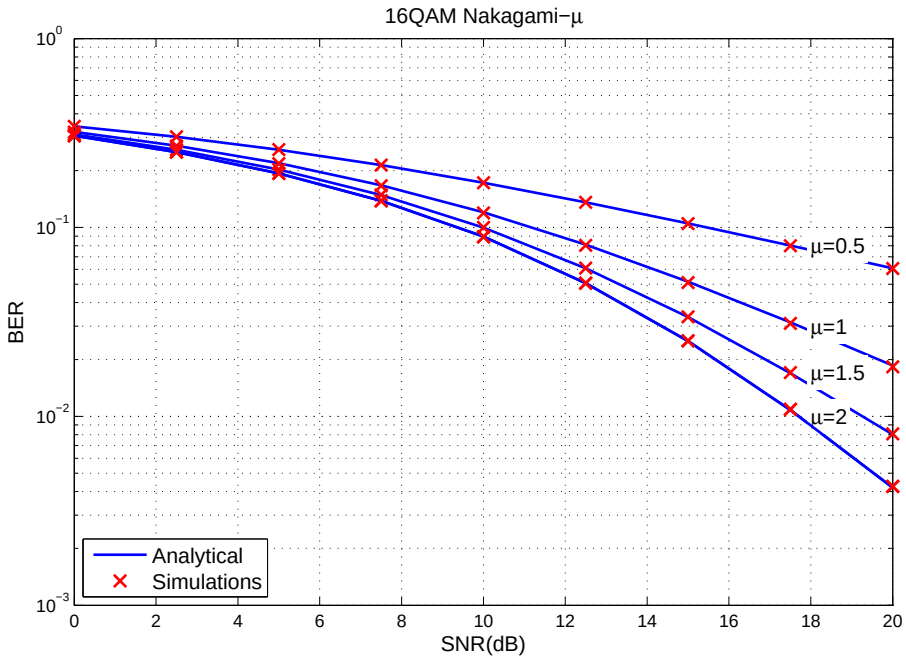

Figure 4.6: BER values for several Nakagami-μ fading channels, including Rayleigh ($\mu = 1$), with 16QAM

Chapter 5

BER Performance for M-QAM SC-FDMA over Nakagami-μ and Rayleigh Fading Channels

5.1 Introduction

This chapter is devoted to analyze the performance of a SC-FDMA transmission over Nakagami-μ fading channels. Obtained results can be particularized in order to include transmission over a Rayleigh fading channel as particular case. We first consider the case in which ZF equalization in the frequency domain is applied to compensate the effects of the channel on the received signal. The analysis is focused on the effects of equalization on the noise term before the decision stage in a similar fashion to the study for OFDMA presented in the previous chapter; some results obtained there for Nakagami-μ fading channels are used in this chapter. Then, we extend the study to a more realistic scenario in which MMSE equalization is performed; in this case the analysis is based on the application of the CLT.

These analyses, which are derived under the assumption of independence among the frequency responses for the allocated sub-carriers, allow us to obtain approximate closed-form BER expressions, which are validated through simulations, for the

two scenarios under study. Their suitability for approximating actual BER values is evaluated for different Rayleigh fading channels proposed by the ITU [ITU-R 97] and the 3GPP [3GPP 10]. In [Sánchez-Sánchez 11] we present the results for ZF-FDE with a generic Nakagami-μ fading channel; the extension for MMSE-FDE, a far more complex mathematical problem, is also addressed in this chapter.

Presented results are similar to those provided in [Wang 08] where the CDF of the Signal to Interference plus Noise Ratio (SINR) for FDE schemes is computed numerically under the same assumption of independence among allocated sub-carriers. However, our final expressions have a lesser computational cost. In fact, for ZF-FDE, we calculate BER values for BPSK and M-QAM modulations with a single numerical computation and without making any approximation.

5.2 System Model

The transmission process in SC-FDMA is similar to that in OFDMA and is depicted in Fig. 5.1. For a given user, a sequence of transmitted bits is mapped into a constellation of complex symbols (e.g., BPSK or M-QAM). The resulting complex sequence $\mathbf{x}$ of length N_c is pre-coded by means of a Discrete Fourier Transform (DFT) operation before being mapped onto the subset of N_c allocated sub-carriers. For a transmitted complex information vector of N_c symbols $\mathbf{x}$, the pre-coded complex symbol $\mathbf{X_{N_c}}$ is obtained by multiplying by the unitary Fourier matrix $\mathbf{F}$ to perform the aforementioned N_c-DFT operation. Each element in $\mathbf{F}$ is defined as $F_{j,k} = exp\{\frac{2\pi \mathrm{i}}{N_c} jk\}/\sqrt{N_c}$ and, therefore, $\mathbf{F}\mathbf{F}^H = \mathbf{I}$.

This step represents the main difference between SC-FDMA and OFDMA, as complex symbols are now transmitted sequentially rather than in parallel. The pre-coded sequence, represented by the column vector $\mathbf{X_{N_c}}$, is then mapped onto a different subset of allocated sub-carriers per user, i.e., N_c out of the M sub-carriers in which the total system bandwidth is divided. The subset may consist of a group

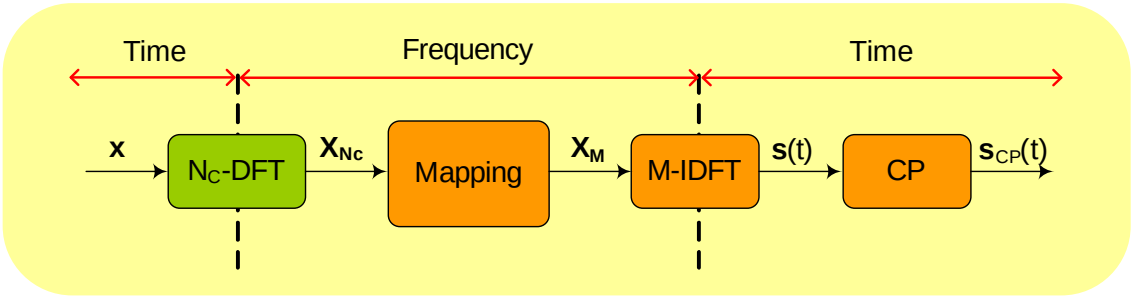

(a) SC-FDMA Transmitter

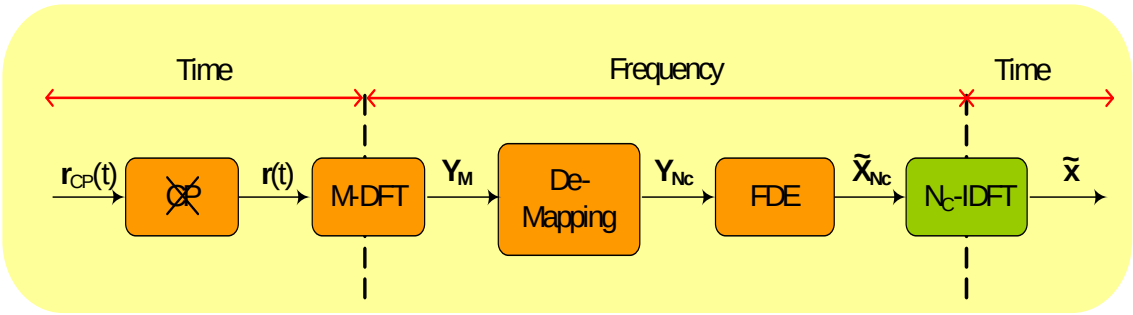

(b) SC-FDMA Receiver

Figure 5.1: SC-FDMA transmitter and receiver schemes

of adjacent (LFDMA) or interleaved sub-carriers (IFDMA) [Myung 06] and it is determined by the $M \times N_c$ mapping matrix $\mathbf{L}$ for which $L_{i,j} = 1$ if the pre-coded symbol j is transmitted over the sub-carrier i and zero otherwise.

The frequency-domain symbol is defined as $\mathbf{X_M} = \mathbf{L}\mathbf{X_{N_c}}$ and, consequently, non-allocated sub-carriers are forced to zero. From this point on, transmission is similar to that of OFDMA: an M-IDFT operation converts each frequency-domain symbol $\mathbf{X_M}$ into a time-domain symbol and a cyclic prefix, whose length must be greater than the channel impulse response, is added in order to avoid ISI.

In this study, we assume a frequency-selective Nakagami-μ channel, in which the magnitudes of the taps of the channel impulse response $|h(n)|$, $n = 1, \ldots, L-1$, can be modeled as i.i.d. Nakagami-μ random variables whose distribution yields

$$f_{|h(n)|}(x) = \frac{2}{\Gamma(\mu_n)} \left(\frac{\mu_n}{\Omega_n}\right)^{\mu_n} x^{2\mu_n - 1} e^{-\frac{x^2 \mu_n}{\Omega_n}} \qquad x \in \mathbb{R} \; and \; x \geq 0, \tag{5.2.1}$$

where $\mu_n > 1/2$ is the fading parameter and Ω_n the power of the n-th tap. In

the following we assume an exponential multipath intensity profile with an average power decay rate δ (i.e., $\Omega_n = \Omega_t e^{-\delta n}$) and equal fading parameter μ_t for all the taps.

At the receiver (see Fig. 5.1b), perfect channel estimation and synchronization are assumed, thereby avoiding interference from other users. The cyclic prefix is suppressed and an M-DFT operation converts each time-domain symbol into a frequency-domain symbol $\mathbf{Y_M}$. After applying $\mathbf{L}^H$ for de-mapping, the N_c allocated sub-carriers $\mathbf{Y_{N_c}}$ can be expressed as

$$\mathbf{Y_{N_c}} = \mathbf{L}^H \mathbf{H_M} \mathbf{L} \mathbf{F} \mathbf{x} + \mathbf{L}^H \boldsymbol{\eta_M}, \tag{5.2.2}$$

where $\boldsymbol{\eta_M}$ is the noise vector whose entries are i.i.d. complex Gaussian $\mathcal{CN}(0, N_0)$ and the channel frequency response for each sub-carrier is represented by the $M \times M$ diagonal matrix $\mathbf{H_M}$ whose entries are complex circularly symmetric random variables [Kang 03]. The magnitude of the frequency response can be well approximated with a Nakagami-μ random variables with new parameters μ and Ω, which, in generally, are different from their counterparts in the time-domain [Nakagami 58]. In fact, for a flat fading channel $\mu = \mu_t$, whereas if $\mu_t \geq 1$ then $1 \leq \mu < \mu_t$, and if $1/2 \leq \mu_t < 1$ then $1 > \mu > \mu_t$ [Kang 03]. Although this approximation was found to have limitations for channels with two taps in [Du 06], it can be considered valid for more general cases and it is an usual assumption [Wang 07]. In fact, for a Rayleigh fading channel (i.e., $\mu = 1$), it is exact for any value of L.

The expression for the recovered symbol in frequency after FDE $\widetilde{\mathbf{X}}_{\mathbf{N_c}}$ yields

$$\widetilde{\mathbf{X}}_{\mathbf{N_c}} = \mathbf{W} \mathbf{Y_{N_c}} = \mathbf{W} \mathbf{H} \mathbf{F} \mathbf{x} + \mathbf{W} \mathbf{L}^H \boldsymbol{\eta_M}, \tag{5.2.3}$$

where $\mathbf{H} = \mathbf{L}^H \mathbf{H_M} \mathbf{L}$ is a $N_c \times N_c$ diagonal matrix whose entries $\mathbf{h} = diag(\mathbf{H})$ are the channel frequency responses for each allocated sub-carrier and $\boldsymbol{\eta} = \mathbf{L}^H \boldsymbol{\eta_M}$ is a vector whose elements are the corresponding complex noise values. The elements of $\mathbf{h}$ are assumed to be i.i.d. random variables; this working assumption makes sense when the spacing between consecutive allocated sub-carriers is bigger than the coherence

bandwidth of the considered fading channel. The $N_c \times N_c$ equalization matrix $\mathbf{W}$ is defined for ZF-FDE as

$$\mathbf{W}_{ZF} = (\mathbf{H}^H\mathbf{H})^{-1}\mathbf{H}^H, \tag{5.2.4}$$

whereas under the MMSE criterion the definition is

$$\mathbf{W}_{MMSE} = \left(\frac{N_0}{E_S}\mathbf{I} + \mathbf{H}^H\mathbf{H}\right)^{-1}\mathbf{H}^H, \tag{5.2.5}$$

where E_S and N_0 are the signal and noise powers respectively.

Before detection, an inverse pre-coding is performed by means of an N_c-IDFT. Thus, for ZF the equalized symbol in time domain $\widetilde{\mathbf{x}}$ yields

$$\widetilde{\mathbf{x}} = \underbrace{\mathbf{F}^H}_{\text{Inv. Precoding}}\underbrace{(\mathbf{H}^H\mathbf{H})^{-1}\mathbf{H}^H}_{\text{FDE}}\mathbf{H}\mathbf{F}\mathbf{x} + \underbrace{\mathbf{F}^H}_{\text{Inv. Precoding}}\underbrace{(\mathbf{H}^H\mathbf{H})^{-1}\mathbf{H}^H}_{\text{FDE}}\boldsymbol{\eta}, \tag{5.2.6}$$

whereas for MMSE the expression yields

$$\widetilde{\mathbf{x}} = \underbrace{\mathbf{F}^H}_{\text{Inv. Precoding}}\underbrace{\left(\frac{N_0}{E_S}\mathbf{I} + \mathbf{H}^H\mathbf{H}\right)^{-1}\mathbf{H}^H}_{\text{FDE}}\mathbf{H}\mathbf{F}\mathbf{x} + \underbrace{\mathbf{F}^H}_{\text{Inv. Precoding}}\underbrace{\left(\frac{N_0}{E_S}\mathbf{I} + \mathbf{H}^H\mathbf{H}\right)^{-1}\mathbf{H}^H}_{\text{FDE}}\boldsymbol{\eta}. \tag{5.2.7}$$

Hence, the expression for the k-th received symbol after ZF-FDE is given by

$$\widetilde{x}_k = x_k + \sum_{j=1}^{N_c}\frac{F_{j,k}^*}{h_j}\eta_j = x_k + \sum_{j=1}^{N_c}\hat{\eta}_{j,k} = x_k + \tilde{\eta}_k \tag{5.2.8}$$

where $\hat{\eta}_{j,k} = \dfrac{F_{j,k}^*\eta_j}{h_j}$.

As it can been seen, each received symbol is the result of adding an effective noise term $\tilde{\eta}_k$ to the original transmitted symbol (eq. (5.2.8)). Hence, when ZF-FDE is applied, the effective noise is the result of adding an elementary noise term $\hat{\eta}_{j,k}$ (enhanced noise) for each allocated sub-carrier. Each elementary noise term is equivalent to the enhanced noise in OFDM reception with ZF-FDE.

For MMSE-FDE, the expression for the k-th received symbol after equalization yields

$$\widetilde{x}_k = x_k T_{k,k} + \sum_{\substack{l \neq k \\ l=1}}^{N_c} x_l T_{k,l} + \sum_{j=1}^{N_c} \frac{F_{j,k}^* h_j^*}{|h_j|^2 + N_0/E_S} \eta_j \tag{5.2.9}$$

where the elements of $\mathbf{T} = \mathbf{F}^H \mathbf{W}_{MMSE} \mathbf{H} \mathbf{F}$ are expressed as

$$T_{k,l} = \frac{1}{N_c} \sum_{j=1}^{N_c} \frac{F_{k,j}^* F_{l,j} |h_j|^2}{|h_j|^2 + N_0/E_S}. \tag{5.2.10}$$

The main difference between this expression and (5.2.8) is that for MMSE-FDE there exists, in addition to the term corresponding to the noise, a component of interference due to the other symbols. Note that the receiver symbol after FDE is attenuated by the term $T_{k,k}$. When the channel frequency response is such that $\frac{N_0}{E_S} \ll |h_j|^2$, the effect of the interference term decreases and the noise term tends to that of (5.2.8). After compensating the received symbol, we obtain the transmitted symbol contaminated by equivalent noise $\tilde{\eta}_k$ and interference δ_k terms, that is,

$$\hat{x}_k = x_k + \underbrace{T_{k,k}^{-1} \sum_{\substack{l \neq k \\ l=1}}^{N_c} x_l T_{k,l}}_{\text{Effective Interference}} + \underbrace{T_{k,k}^{-1} \sum_{j=1}^{N_c} \frac{F_{j,k}^* h_j^*}{|h_j|^2 + N_0/E_S} \eta_j}_{\text{Effective Noise}} = x_k + \delta_k + \tilde{\eta}_k = x_k + \xi_k, \tag{5.2.11}$$

where the term ξ_k gathers the effects of noise and interference that are inherently independent [Nisar 07].

5.3 Noise Characterization for ZF-FDE

In order to derive a mathematical model for the effective noise in SC-FDMA after ZF-FDE, we must first consider the elementary noise. Any given elementary noise term $\hat{\eta}_{j,k}$ is a random variable resulting from the ratio of two complex circularly symmetric random variables. In the remainder of the dissertation, indexes are dropped when possible for the sake of readability. Each complex random variable $\hat{\eta}$

has a Pearson type VII distribution and the expression in Cartesian coordinates of its PDF (4.5.19) was derived in section 4.5.1 as

$$f_{\hat{\eta}_r,\hat{\eta}_i}(x,y) = \frac{\mu^{\mu+1}}{2\pi\sigma^2}\left(\frac{x^2+y^2}{2\sigma^2}+\mu\right)^{-1-\mu} \qquad x,y \in \mathbb{R}, \tag{5.3.1}$$

where $\hat{\eta}_r$ and $\hat{\eta}_i$ are the real and imaginary components of the elementary noise term and $\sigma = \dfrac{N_0}{N_c E_S}$.

The effective noise is the sum of N_c elementary noise random variables as described in eq. (5.2.8). As all the terms in the sum are circularly symmetric random variables, the effective noise has also circular symmetry and its marginal distributions are described by the same even function. Thus, effective noise is also a circularly symmetric random variable and just one of its marginal distributions is needed to characterize it. This marginal distribution can be found in e.q. (4.5.20) but, for the sake of clarity, we repeat this equation in the following.

$$f_{\hat{\eta}_r}(x) = f_{\hat{\eta}_i}(x) = \sqrt{\frac{1}{\pi}}\frac{\Gamma\left(\mu+\frac{1}{2}\right)2^{\mu}\mu^{\mu}\sigma^{2\mu}}{\Gamma(\mu)\left(2\mu\sigma^2+x^2\right)^{\mu-\frac{1}{2}}} \qquad x \in \mathbb{R}, \tag{5.3.2}$$

5.3.1 Effective Noise Characterization for ZF-FDE

As stated before, effective noise after ZF-FDE is the sum of several elementary complex noise terms that follow a bivariate Pearson type VII distribution. In section 3.4.1, we obtained an expression (3.4.19) to calculate the PDF of a sum of independent Pearson type VII random variables. The density function in this case is given by

$$f_{\tilde{\eta}_r}(x) = \frac{1}{2\pi}\int_{-\infty}^{\infty}\left(\frac{\sigma^{\mu}|\omega|^{\mu}}{2^{1-\mu/2}\Gamma(\mu)}\mu^{\mu/2}K_{\mu}\left(\sigma\sqrt{2\mu}|\omega|\right)\right)^{N_c}e^{-j\omega x}d\omega. \tag{5.3.3}$$

It is possible to obtain an analytical result of (5.3.3) for its evaluation with $N_c = 2$

$$p_{\tilde{\eta}_r}(x) = \frac{2^{-2\mu-\frac{1}{2}}\Gamma\left(\mu+\frac{1}{2}\right)\Gamma\left(2\mu+\frac{1}{2}\right)}{\sigma\Gamma(\mu)^2\Gamma(\mu+1)}\sqrt{\frac{1}{\mu}}\,{}_2F_1\left(\mu+\frac{1}{2},2\mu+\frac{1}{2};\mu+1;-\frac{x^2 1}{8\mu\sigma^2}\right), \tag{5.3.4}$$

where ${}_2F_1(\ )$ is the Gauss hypergeometric function (see 15.1.1 in [Abramowitz 64]).

Additionally, it is also possible to calculate the associated CDF

$$F_{\tilde{\eta}_r}(x) = \frac{1}{2} + \frac{x\Gamma\left(\mu+\frac{1}{2}\right)\Gamma\left(2\mu+\frac{1}{2}\right)\sqrt{\frac{1}{\mu}}}{2^{2\mu+\frac{1}{2}}\sigma\Gamma(\mu)^2\Gamma(\mu+1)}\,{}_3F_2\left(\frac{1}{2},\mu+\frac{1}{2},2\mu+\frac{1}{2};\frac{3}{2},\mu+1;\frac{-x^2 1}{8\mu\sigma^2}\right), \tag{5.3.5}$$

where ${}_3F_2(\ )$ is a particularization of the generalized hypergeometric function ${}_pF_q$ [Daalhuis 10].

Although there is no analytical expression for the CDF of the effective noise $F_{\tilde{\eta}_r}(x)$ for $N_c \geq 2$, it is possible to use the inversion theorem as proposed by Gil-Peláez (see section 3.2.4) to evaluate it as

$$F_{\tilde{\eta}_r}(x) = \frac{1}{2} + \frac{1}{2\pi}\int_0^\infty \frac{e^{\jmath x\omega}\Psi_{\tilde{\eta}_r}(-\omega) - e^{-\jmath x\omega}\Psi_{\tilde{\eta}_r}(\omega)}{\jmath\,\omega}\,d\omega \tag{5.3.6}$$

where $\Psi_{\tilde{\eta}_r}(\omega)$ corresponds here to the CHF as was obtained in eq. (4.5.21).

For a Rayleigh fading channel, we have to particularize that expression using the CHF for a univariate Student t (4.5.10); the resulting expression follows

$$f_{\tilde{\eta}_r}(x) = \frac{1}{2\pi}\int_{-\infty}^{\infty} \left(\sigma|\omega|K_1(\sigma|\omega|)\right)^{N_c} e^{-\jmath\,\omega x} d\omega. \tag{5.3.7}$$

In general terms, the evaluation of eq. (5.3.7) requires numerical integration. Nevertheless, it is possible to use the results in Appendix B to obtain an analytical result for the evaluation for $N_c = 2$

$$f_{\tilde{\eta}_r}(x) = \frac{3\pi}{16\sqrt{2}\sigma}\,{}_2F_1\left(\frac{3}{2},\frac{5}{2};2;-\frac{x^2}{2\sigma^2}\right). \tag{5.3.8}$$

This is a Behrens-Fisher distribution introduced in section 3.4.1 and has also zero mean and infinite variance. Additionally, it is also possible to calculate the associated CDF

$$F_{\tilde{\eta}_r}(x) = \frac{1}{2} + \frac{3\pi x}{16\sqrt{2}\sigma}\,{}_2F_1\left(\frac{1}{2},\frac{5}{2},2,-\frac{x^2}{2\sigma^2}\right). \tag{5.3.9}$$

Figures 5.2a and 5.2b show the PDFs and the CHFs when powers of 10 are used as N_c values. Note that the PDF curves flatten and widen as the number of terms in the convolution increases, i.e., when the number of independent random variables in the sum increases. This behavior corresponds to a narrowing in the CHF curves as depicted in Fig. 5.2b. This flattening of the PDF curves causes slower decays for the their tails which implies that there is a greater area under the tails in the interval $(-\infty, -1]$, that is, a greater value of $F_{\tilde{\eta}_r}(-1)$. In the next section we shall show that this implies increasing values of BER.

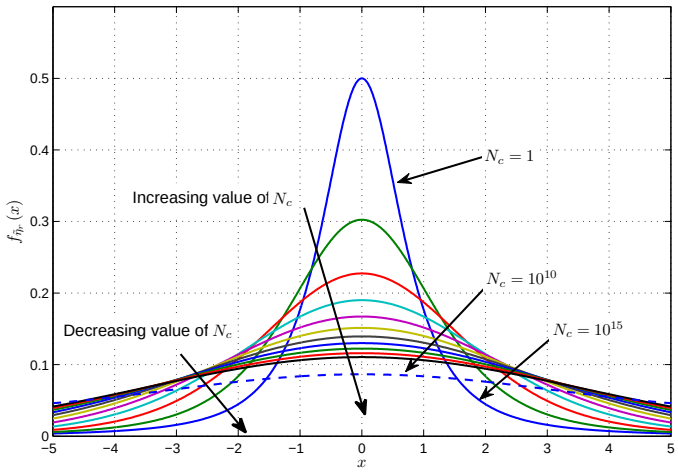

(a) $f_{\tilde{\eta}_r}(x)$

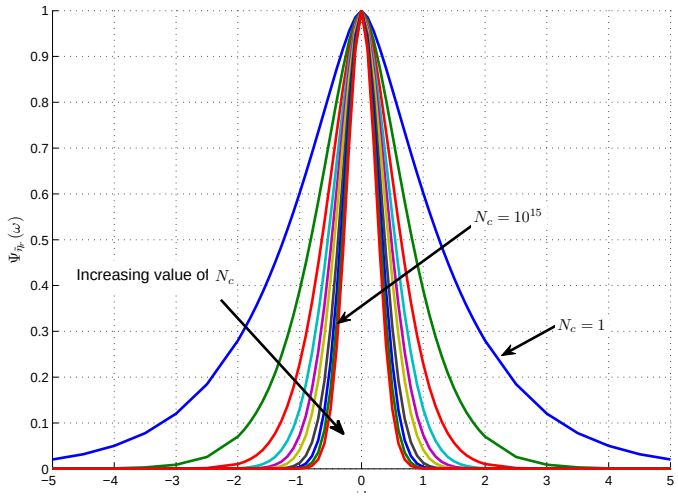

(b) $\Psi_{\tilde{\eta}_r}(x)$

Figure 5.2: Behavior of $f_{\tilde{\eta}_r}(x)$ and $\Psi_{\tilde{\eta}_r}(x)$ for N_c values from 1 to 10^{10} and 10^{15}

It could be thought that, as the effective noise after ZF-FDE is the sum of several independent random variables, it would be possible to apply the CLT (see section 3.5.1). However, we discover that, in Rayleigh fading channels (e.g., $\mu = 1$) for which the noise terms follow a Student t distribution that does not have a finite variance, it is not possible to apply the CLT to approximate the PDF of the effective noise.

We also tried to apply the GCLT and, with this purpose, we studied the tail of the distribution to find the exponent that determines the distribution decay. In this case, that decay exponent can be obtained as

$$f_{\hat{\eta}_r}(x) = \frac{1}{2}\frac{\sigma^2}{(\sigma^2 + x^2)^{3/2}} \simeq A|x|^{-(3)} \qquad |x| \to \infty, \tag{5.3.10}$$

and, therefore, the characteristic exponent results $\alpha = 2$.

We showed in section 3.5.2 that for $\alpha < 2$, the mean value and/or the variance diverge and the distribution of the sum is in the domain of attraction of a stable law as stated in definition. However, to the best of our knowledge, it is not possible to determine the distribution for the case under study, that is, for $\alpha = 2$.

5.3.2 Effective Conditioned SNR in ZF-FDE

If we conditioned the effective noise $\tilde{\eta}$ in eq. 5.2.8 to the channel frequency response $\mathbf{h} = [h_1 \dots h_{N_c}]$, we see it follows a complex normal distribution with zero-mean and variance $\frac{N_0}{E_S}\beta^{ZF}$

$$\tilde{\eta}|\mathbf{h} \sim \mathcal{CN}\left(0, \frac{N_0}{E_S}\beta^{ZF}\right) \tag{5.3.11}$$

where β, in the same way as in [Nisar 07], is

$$\beta^{ZF} = \frac{1}{N_c}\sum_{k=1}^{N_c}\frac{1}{|h_k|^2}. \tag{5.3.12}$$

Then, the expression for the instantaneous SNR yields

$$\gamma = \frac{E_S}{N_0\beta^{ZF}} = \frac{E_S}{N_0}\frac{N_c}{\sum_{k=1}^{N_c}\frac{1}{|h_k|^2}}. \tag{5.3.13}$$

Note that this SNR expression is, except for a constant, the harmonic mean of a set of random variables [Wang 08] and the computation of its MGF is, in general a complex problem. Even with $\mu = 1$ (i.e., Rayleigh fading channel), when each $|h_k|^2$ becomes a chi-squared random variable, there is not a closed-form expression for its MGF beyond two variables [Hasna 03]. Hence, to the best of our knowledge, it is not possible to compute the BER using the MGF of the instantaneous SNR and eq. (4.4.2) as proposed in [Simon 98b].

The enhancement factor β^{ZF} is the sum of random variables with positive values, any of which may serve as a lower bound of β^{ZF}. Specifically, the maximum of such possible lower bounds is

$$\beta^{ZF} > \frac{1}{N_c \left|h_{min}\right|^2}, \tag{5.3.14}$$

which implies that the instantaneous SNR γ has an upper bound

$$\gamma < N_c \left|h_{min}\right|^2 \frac{E_S}{N_0}. \tag{5.3.15}$$

In the case of a Rayleigh fading channel, we show in Appendix C that, for a set of independent h_k, the variable $Z = N_c \left|h_{min}\right|^2$ follows the same chi-square distribution as that of the enhancing factor $|h_0|^{-2}$ in OFDM. This implies that, in the case of ZF-FDE, for an SC-FDMA transmission with $N_c > 1$ over a fading channel with a selective channel frequency response, the value of γ is always lesser than that of OFDMA. Thus, the effective SNR after ZF-FDE for SC-FDMA is always below that of OFDMA; that causes a rate loss in the former as shown in [Wu 09] since, for a Rayleigh fading channel, BER values for SC-FDMA with ZF-FDE are always above the BER curve for OFDM.

5.4 Noise and Interference Characterization for MMSE-FDE

In this section characterized the effective noise after MMSE-FDE. To the best of our knowledge, it is not possible to derive an analytical expression for its density

function. However, under the assumption of independence between noise and interference, to approximate its variance in function of a random variable β^M whose PDF can be approximated as Gaussian density function by means of the CLT.

From (5.2.11) we know that the recovered symbol before detection results

$$\hat{x} = x + \delta + \tilde{\eta} = x + \xi, \tag{5.4.1}$$

where the effects of noise $\tilde{\eta}$ and interference δ are gathered in the effective noise term ξ. The density of the noise $\tilde{\eta}$ conditioned to the channel frequency response $\mathbf{h} = [h_1 \dots h_{N_c}]$ can be expressed as

$$p\left(\tilde{\eta}/\mathbf{h}\right) \sim \mathcal{CN}\left(0, \sigma_{\tilde{\eta}}^2\right), \tag{5.4.2}$$

where $\sigma_{\tilde{\eta}}^2$ is defined as

$$\sigma_{\tilde{\eta}}^2 = N_0 \frac{\frac{1}{N_c}\sum_{j=1}^{N_c}\left(\frac{|h_j|}{|h_j|^2+N_0/E_S}\right)^2}{\left(\frac{1}{N_c}\sum_{j=1}^{N_c}\frac{|h_j|^2}{|h_j|^2+N_0/E_S}\right)^2}. \tag{5.4.3}$$

In a similar fashion and as in [Nisar 07], the interference component conditioned to the channel frequency response can be assumed to follow a complex circularly symmetric Gaussian distribution with zero-mean and variance σ_δ^2 given by

$$\sigma_\delta^2 = E_S \frac{\frac{1}{N_c}\sum_{j=1}^{N_c}\left(\frac{|h_j|^2}{|h_j|^2+N_0/E_S}\right)^2 - \left(\frac{1}{N_c}\sum_{j=1}^{N_c}\frac{|h_j|^2}{|h_j|^2+N_0/E_S}\right)^2}{\left(\frac{1}{N_c}\sum_{j=1}^{N_c}\frac{|h_j|^2}{|h_j|^2+N_0/E_S}\right)^2}. \tag{5.4.4}$$

As noise and interference components are independent random variables, their sum can be modeled with another zero-mean complex circularly symmetric Gaussian

random variable whose variance results[1]

$$\sigma_\xi^2 = \frac{\frac{N_0}{N_c}\sum_{j=1}^{N_c}\left(\frac{|h_j|}{|h_j|^2+N_0/E_S}\right)^2 + \frac{E_S}{N_c}\sum_{j=1}^{N_c}\left(\frac{|h_j|^2}{|h_j|^2+N_0/E_S}\right)^2 - E_S\left(\frac{1}{N_c}\sum_{j=1}^{N_c}\frac{|h_j|^2}{|h_j|^2+N_0/E_S}\right)^2}{\left(\frac{1}{N_c}\sum_{j=1}^{N_c}\frac{|h_j|^2}{|h_j|^2+N_0/E_S}\right)^2}$$

$$= \frac{\frac{E_S}{N_c}\sum_{j=1}^{N_c}\frac{|h_j|^2}{|h_j|^2+N_0/E_S} - E_S\left(\frac{1}{N_c}\sum_{j=1}^{N_c}\frac{|h_j|^2}{|h_j|^2+N_0/E_S}\right)^2}{\left(\frac{1}{N_c}\sum_{j=1}^{N_c}\frac{|h_j|^2}{|h_j|^2+N_0/E_S}\right)^2} = E_S\frac{\frac{N_0}{E_S}\beta^M}{1-\frac{N_0}{E_S}\beta^M}, \tag{5.4.5}$$

with

$$\beta^M = \frac{1}{N_c}\sum_{j=1}^{N_c}\frac{1}{|h_j|^2+N_0/E_S}. \tag{5.4.6}$$

The j-th term in the sum (5.4.7) results

$$Z_j = \frac{1}{|h_j|^2+N_0/E_S}. \tag{5.4.7}$$

and it is the inverse of a chi-square random variable shifted by the constant N_0. Its density can be derived using (eq 3.2.21) as

$$f_{Z_j}(z) = f_{|h_j|^2}\left(\frac{1-z\frac{E_S}{N_0}}{z}\right)\frac{1}{z^2} = \frac{1}{z^2\Gamma(\mu)}\left(\frac{\mu}{\Omega}\right)^\mu\left(\frac{1}{z}-\frac{E_S}{N_0}\right)^{\mu-1}e^{\frac{\mu\left(\frac{E_S}{N_0}z-1\right)}{\Omega z}}. \tag{5.4.8}$$

It is possible to obtain analytical expressions for the mean and variance of Z_j for arbitrary values of Ω provided μ is an integer. In other cases, it would be still possible to use numerical integration to make the computation. Once those parameters are computed, the application of the CLT to approximate the density function of β^M is straightforward. This approximation can be used then to computed the BER for arbitrary Nakagami-μ fading channels.

[1]Note that

$$\frac{1}{N_c}\sum_{j=1}^{N_c}\frac{|h_j|^2}{|h_j|^2+N_0/E_S} = 1-\frac{1}{N_c}\sum_{j=1}^{N_c}\frac{N_0/E_S}{|h_j|^2+N_0/E_S}$$

Once we have characterized Z_j, we can rewrite expression (5.4.5) in a more elegant way

$$\sigma_\xi^2 = \sigma_{\tilde{\eta}}^2 + \sigma_\delta^2 = E_S \frac{\frac{N_0}{E_S}\beta^M}{1 - \frac{N_0}{E_S}\beta^M}, \tag{5.4.9}$$

and the density of the term ξ conditioned to the frequency channel yields

$$f\left(\xi/\mathbf{h}\right) = f\left(\xi/\beta^M\right) \sim \mathcal{CN}\left(0, \sigma_\xi^2\right). \tag{5.4.10}$$

As we assume independent bit-mapping and the variable is circularly symmetric, it is possible to work only with the marginal distribution corresponding to its real component

$$f(\xi_r/\mathbf{h}) = p(\xi_r/\beta^M) \sim \mathcal{N}\left(0, \sigma_{\xi_r}^2/2\right) \tag{5.4.11}$$

Thus, the density of the effective noise term in MMSE can be expressed as[2]

$$f_{\xi_r}(x) = \int_0^{E_S/N_0} \sqrt{\frac{\frac{1}{E_S}\left(\frac{E_S}{\beta^M N_0} - 1\right)}{\pi}}\, e^{-x^2 \frac{E_S}{\beta^M N_0} - 1} p_{\beta^M}(\beta^M) d\beta^M. \tag{5.4.12}$$

In the cases in which Z_j has a finite variance and under the assumption of independence among terms in the sum (5.4.7), it is possible to apply the CLT (see section 3.5.1). Thus, as (5.4.7) is the average of a sequence of N_c i.i.d. random variables each having finite values of expectation $\overline{Z}$ and variance $\sigma_Z^2 > 0$, the density of β^M can be approximated by the following Gaussian distribution

$$f_{\beta^M}(\beta^M) \approx \hat{f}_{\beta^M}(\beta^M) = \frac{1}{\sqrt{2\pi\sigma_Z^2/N_c}}\, e^{-\frac{\left(\beta^M - \overline{Z_j}\right)^2}{2\sigma_Z^2/N_c}}, \tag{5.4.13}$$

with mean $\overline{Z_j}$ and variance $\sigma_{Z_j}^2/N_c$.

[2]Note that

$$f_{\xi_r}(x) = \int_{-\infty}^{\infty} \frac{e^{-\frac{x^2}{2\sigma_{\xi_r}^2}}}{\sqrt{2\pi\sigma_{\xi_r}^2}} p_{\sigma_{\xi_r}^2}(\sigma_{\xi_r}^2) d\sigma_{\xi_r}^2 = \int_0^{E_S/N_0} \sqrt{\frac{\frac{1}{E_S}\left(\frac{E_S}{\beta^M N_0} - 1\right)}{\pi}} e^{-x^2\left(\frac{E_S}{\beta^M N_0} - 1\right)} p_{\beta^M}(\beta^M) d\beta^M.$$

There is an additional restriction that must not be neglected: the variable β^M is limited by definition to the interval $[0, E_S/N_0]$. In order to apply this restriction, the density is now approximated by a bounded version of (5.4.13), that is,

$$f_{\beta^M}(\beta^M) \approx p_{\beta^M}(\beta^M) = \frac{1}{\hat{F}(\frac{E_S}{N_0}) - \hat{F}(0)} \frac{1}{\sqrt{2\pi\sigma_Z^2/N_c}} e^{-\frac{\left(\beta^M - \bar{Z}\right)^2}{2\sigma_Z^2/N_c}} \quad \beta^M \in [0, E_S/N_0], \tag{5.4.14}$$

where $\hat{F}(x)$ is the CDF obtained through integration from (5.4.13).

In the following, we obtain analytical expressions for the case in which the magnitude of the channel frequency response follows a Rayleigh distribution (i.e., $\mu = 1$) and it is normalized, that is, $\Omega = 1$. For this value, the density function can be reduced to

$$f_{Z_j}(z) = \frac{e^{\frac{E_S}{N_0} - \frac{1}{z}}}{z^2} \quad \forall z \in [0, E_S/N_0]. \tag{5.4.15}$$

The corresponding expression for the mean yields

$$\overline{Z_j} = e^{\frac{E_S}{N_0}} \Gamma(0, 1), \tag{5.4.16}$$

where $\Gamma(z, x)$ is the incomplete Gamma function defined as [Abramowitz 64]

$$\Gamma(z, x) = \int_x^\infty t^{z-1} e^{-t} dt. \tag{5.4.17}$$

The variance is given by

$$\sigma_{Z_j}^2 = \frac{E_S}{N_0} - e^{\frac{E_S}{N_0}} \Gamma\left(0, \frac{E_S}{N_0}\right) - e^{2N_0} \Gamma\left(0, \frac{E_S}{N_0}\right)^2. \tag{5.4.18}$$

5.4.1 Effective Noise Characterization for MMSE-FDE

The expression for the CDF of the effective noise after MMSE-FDE can be derived from expression (5.4.12) through integration as follows

$$\begin{aligned} F_{\xi_r}(x) &= \int_{-\infty}^{x} \left(\int_0^{E_S/N_0} \sqrt{\frac{\frac{1}{E_S}\left(\frac{E_S}{\beta^M N_0}-1\right)}{\pi}} e^{-x^2 \frac{1}{E_S}\left(\frac{E_S}{\beta^M N_0}-1\right)} p_{\beta^M}(\beta^M) d\beta^M \right) dt \\ &= \int_0^{E_S/N_0} p_{\beta^M}(\beta^M) \left(\int_{-\infty}^{x} \sqrt{\frac{\frac{1}{E_S}\left(\frac{E_S}{\beta^M N_0}-1\right)}{\pi}} e^{-x^2 \frac{1}{E_S}\left(\frac{E_S}{\beta^M N_0}-1\right)} dt \right) d\beta^M. \end{aligned} \tag{5.4.19}$$

The inner integral can be rewritten using the $Q(\,)$ function

$$\int_{-\infty}^{x} \sqrt{\frac{\frac{1}{E_S}\left(\frac{E_S}{\beta^M N_0}-1\right)}{\pi}} e^{-x^2 \frac{1}{E_S}\left(1/\beta^M \frac{N_0}{E_S}-1\right)} dt = \left\{ \begin{array}{l} u = \sqrt{\frac{2}{E_S}\left(\frac{E_S}{\beta^M N_0}-1\right)}t \\ du = \sqrt{\frac{2}{E_S}\left(\frac{E_S}{\beta^M N_0}-1\right)}dt \end{array} \right\}$$

$$= \frac{1}{\sqrt{2\pi}} \int_{-\infty}^{xA} e^{-\frac{u^2}{2}} du = \frac{1}{\sqrt{2\pi}} \int_{-xA}^{\infty} e^{-\frac{u^2}{2}} du = Q\left(-xA\right) = 1 - Q\left(xA\right),$$

with

$$A = \sqrt{\frac{2}{E_S}\left(\frac{E_S}{\beta^M N_0}-1\right)}.$$

Hence, the CDF of the effective noise after MMSE-FDE can be expressed as

$$F_{\xi_r}(x) = 1 - \int_0^{E_S/N_0} p_{\beta^M}(\beta^M) Q\left(x\sqrt{\frac{2}{E_S}\left(\frac{E_S}{\beta^M N_0}-1\right)}\right) d\beta^M. \tag{5.4.20}$$

5.4.2 Conditioned Effective SNR in MMSE-FDE

We showed above that, for MMSE-FDE, the effective noise $\tilde{\xi}$ conditioned to the channel frequency response $\mathbf{h} = [h_1 \ldots h_{N_c}]$ follows a complex normal distribution with zero-mean and variance σ_ξ^2, that is,

$$\xi|\mathbf{h} \sim \mathcal{CN}\left(0, \sigma_\xi^2\right) \tag{5.4.21}$$

where σ_ξ^2 is defined in eq. (5.4.5).

In this case, the expression for the instantaneous SNR yields

$$\gamma = \frac{E_S}{\beta^M N_0} - 1, \tag{5.4.22}$$

with β^M being the random variable

$$\beta^M = \frac{1}{N_c} \sum_{j=1}^{N_c} \frac{1}{|h_j|^2 + N_0/E_S}, \tag{5.4.23}$$

for which we derived above an approximation of its PDF (eq. (5.4.14)).

5.5 SC-FDMA BER Analysis

The BER analysis presented in this subsection follows the same premises that the one performed in section 4.6: we consider square M-QAM with independent bit-mapping for in-phase and quadrature components, e.g., Gray mapping. As before, the effective noise term $\bar{\eta}$ (i.e., $\tilde{\eta}$ or ξ) is circularly symmetric and the BER can be expressed as a sum of CEPs (see eq. (4.4.3)) which depend on the CDF of the effective noise.

In the case of ZF-FDE, the integral in (5.3.6) can be accurately solved in a quite simple manner by means of the composite trapezoidal rule. Thus, the CDF can be calculated as

$$F_{\tilde{\eta}_r}(x) \approx \frac{1}{2} + \frac{1}{2\pi} \left(\frac{\omega_{\max} - \omega_{\min}}{n} \left[\frac{\Upsilon(x, \omega_{\min}) + \Upsilon(x, \omega_{\max})}{2} + \sum_{k=1}^{n-1} \Upsilon\left(x, \omega_{\min} + k\frac{\omega_{\max} - \omega_{\min}}{n}\right) \right] \right), \tag{5.5.1}$$

where the auxiliary function $\Upsilon(x, \omega)$ is defined as

$$\Upsilon(x, \omega) = \frac{e^{\jmath x\omega} \Psi_{\tilde{\eta}_r}(-\omega) - e^{-\jmath x\omega} \Psi_{\tilde{\eta}_r}(\omega)}{\jmath\, \omega}, \tag{5.5.2}$$

and $\Psi_{\tilde{\eta}_r}$ depends on the fading channel considered.

In eq. (5.5.1) the minimum value in the integration interval is $\omega_{\min}$, which is set to zero, whereas $\omega_{\max}$ should be suitably chosen as a function of the shape of the corresponding CHF. The number of points to evaluate inside the interval is denoted as n. For a Rayleigh fading channel, as shown in section 4.5.1, $\Psi_{\tilde{\eta}_r}(\omega)$ is a symmetric, exponentially decaying functions with a decay rate that depends on the argument of $K_1(\,)$. In fact, its decay is inversely proportional to the values of SNR and directly proportional to the values of N_c values. By making a reasonable choice for the value of $\omega_{\max}$, one can achieve a sufficient accuracy at low computational cost. By keeping this in mind and using eq. (5.5.1), it is possible to obtain an approximate closed-form expression for the BER

$$BER_{ZF} = \sum_{n=1}^{L-1} w(n) \left(\frac{1}{2} - \frac{\omega_{\max}}{2\pi n} \left(\frac{1 + \Upsilon\left((2n-1)d, \omega_{\max}\right)}{2} + \sum_{k=1}^{n-1} \Upsilon\left((2n-1)d, k\frac{\omega_{\max}}{n}\right) \right) \right), \tag{5.5.3}$$

where $\Upsilon(\,)$ is defined in 5.5.2.

In the case of MMSE-FDE the CEPs are computed directly using eq. (5.4.20) to calculate the CEPs and plugging those into the sum (4.4.3) we can compute BER values as follows

$$BER_M = \sum_{n=1}^{L-1} w(n) \int_0^{E_S/N_0} p_{\beta^M}(\beta^M)\, Q\left((2n-1)d \sqrt{\frac{2}{E_S}\left(\frac{E_S}{\beta^M N_0} - 1\right)} \right) d\beta^M. \tag{5.5.4}$$

BER values can be numerically computed using different numerical integration methods. Results presented in the following section are calculated by means of the double exponential integration [Mori 01].

5.6 Simulation and Numerical Results

In the following, we validate the expressions (5.5.3) and (5.5.4) through simulations. First, we consider the ideal scenario for which those expressions were derived: an SC-FDMA transmission with independent channel frequency responses among allocated sub-carriers. Then, a more realistic scenario based on channel models defined by ITU and 3GPP is considered. Our aim is to determine in which situations the provided analytical expressions can be used as an approximation for BER values in actual selective Rayleigh fading channels. In both cases, we use a semi-analytical model based on [Nisar 07] in which complex channel frequency responses, generated for the different allocated sub-carriers, are used to calculate the conditional probability for ZF (5.4.21) and MMSE (5.4.12).

5.6.1 Validation of Closed-form Expressions

In order to validate the closed-form expressions presented in the previous section, results from the evaluation of equations (5.5.3) and (5.5.4) for different numbers of sub-carriers are compared to values obtained from simulations. A channel model, in which the channel frequency response for the N_c allocated sub-carriers are modeled as i.i.d. random variables which follow a Nakagami-μ distribution. Two different Nakagami-μ fading channels are considered with μ values of 1 and 2, respectively. BER results for each channel are shown for BPSK and 16QAM modulations in Fig. 5.3 and 5.4.

In the first case, in which we consider the expression for ZF-FDE, the Nakagami-μ fading channel with $\mu = 1$ is equivalent to a Rayleigh fading channel and obtained results presented in Fig. 5.3 are consistent with those presented in [Sánchez-Sánchez 09b]. For low SNR values, BER curves are above the OFDM curve with a difference that increases with the number of allocated sub-carriers. In this case, the probability of having values close to zero for the channel frequency response can not be neglected.

When the number of terms in the sum N_c increases, the probability of having a term close to zero increments, the term becomes dominant and the BER worsens.

However, as SNR values increase, all the curves converge to the OFDM curve independently of N_c. This behavior is a direct consequence of the expansion in the ω axis of the characteristic function as explained in section 5.5: as SNR increases, all CHFs tend to converge to a common shape and, subsequently, their corresponding PDFs and BER values also converge. These results are consistent with the fact that, for ZF-FDE, OFDM determines the lower bound for SC-FDMA BER values, as noted in subsection 5.3.

For greater values of μ (e.g., $\mu = 2$), effective noise has a finite variance and BER curves for SC-FDMA have a significatively different behavior (see Fig. 5.4). For low values of SNR, SC-FDMA BER curves are very close to those for OFDM but, as the SNR increases, SC-FDMA seems to perform better that OFDM. In this case, the magnitude of the channel frequency responses have a non-zero minimum and, therefore, there is not nulls, thus the effective SNR always increases with the number of allocated sub-carriers N_c.

For Figs. 5.5 to 5.7, we consider the expression (5.5.4) for BER when MMSE-FDE is applied to compensate the effects of a Rayleigh fading channel; values obtained for BPSK, 4QAM and 16QAM are compared to those obtained through simulations for different values of N_c. By a simple inspection, it can be concluded that the validity of the provided expression depends highly on the number of sub-carriers and on the value of the power density N_0. For small values of SNR the values obtained with the aforementioned expression are consistent with those obtained through simulation. For higher values of SNR the expression values diverge with the smallest values of N_c considered. However, the approximation is still valid for greater values of N_c (e.g., 64 or greater) that are closer to practical values for a real system.

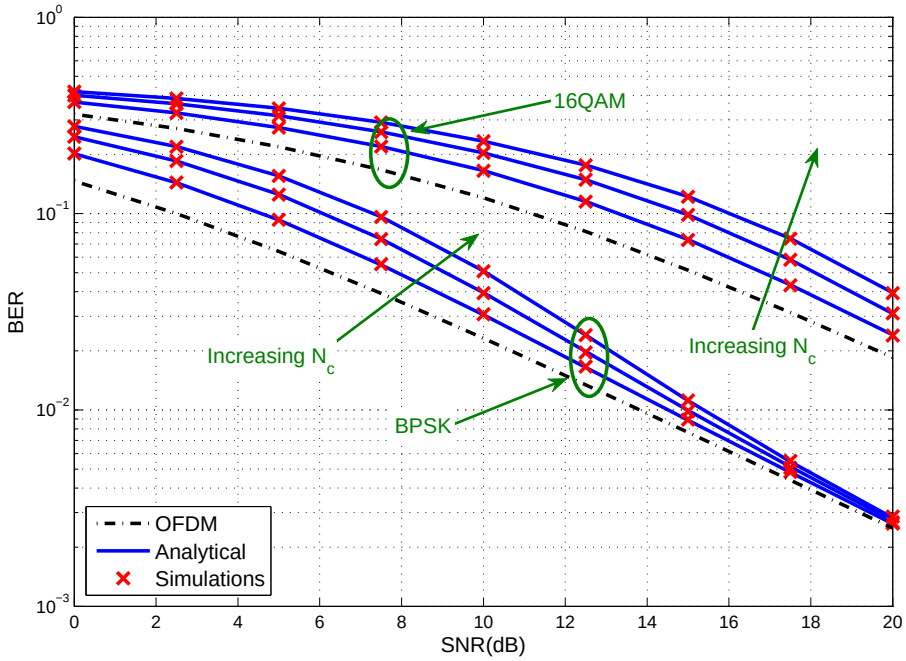

Figure 5.3: Analytical vs. Simulation BER values for Nakagami-μ channel ($\mu = 1$) with $N_c = 4, 16$ and 64

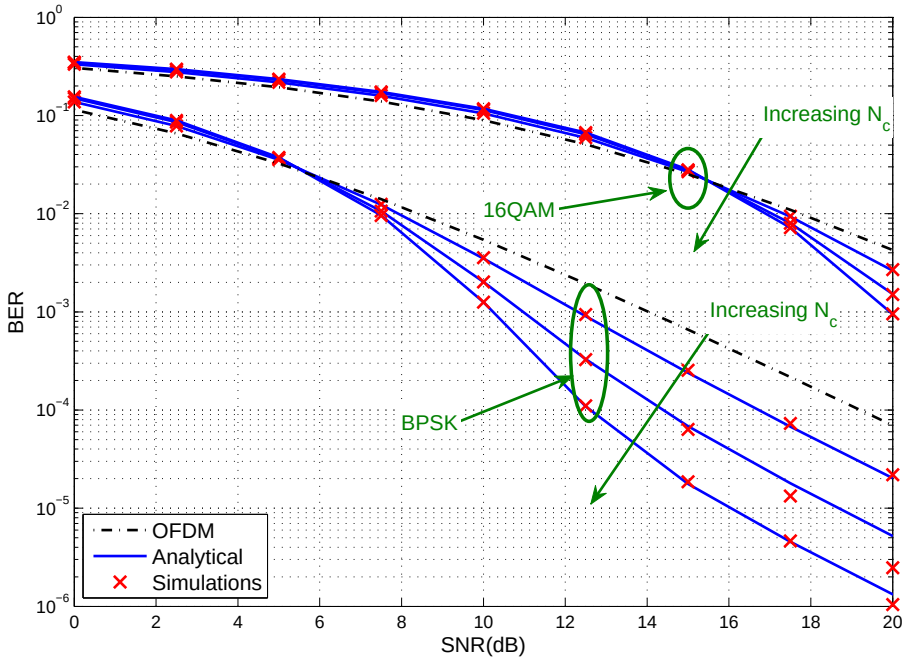

Figure 5.4: Analytical vs. Simulation BER values for Nakagami-μ channel ($\mu = 2$) with $N_c = 4, 16$ and 64

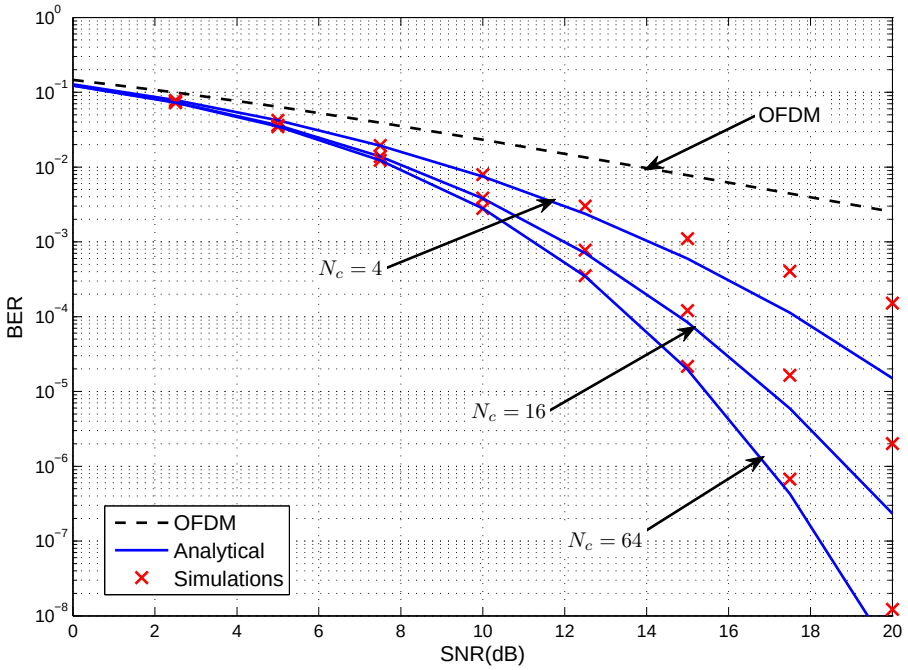

Figure 5.5: Analytical vs. simulation results for independent sub-carriers (BPSK) MMSE-FDE

5.6.2 Application to Realistic Scenarios

The analytical expressions for the BER presented in the previous section were derived under the assumption of independence among allocated sub-carriers. This assumption makes sense when coherence bandwidth of selective Rayleigh channels is sufficiently small in comparison to the distance between assigned sub-carriers. Here we analyze the circumstances under which the analytical expression may be used as an approximation for BER values in actual selective fading channels. The scenario under study is an SC-FDMA transmission with BPSK over some of the channel impulse response models proposed by the ITU in [ITU-R 97] and by the 3GPP [3GPP 10] for several terrestrial test environments. Representative simulations parameters are shown in Table 5.1 for the channel models under consideration. Channel models are implemented as a tapped-delay line characterized by the number of taps, the time delay relative to the first tap, the average power relative to the strongest tap and the Doppler spectrum of each tap (see Table 5.2). In this case

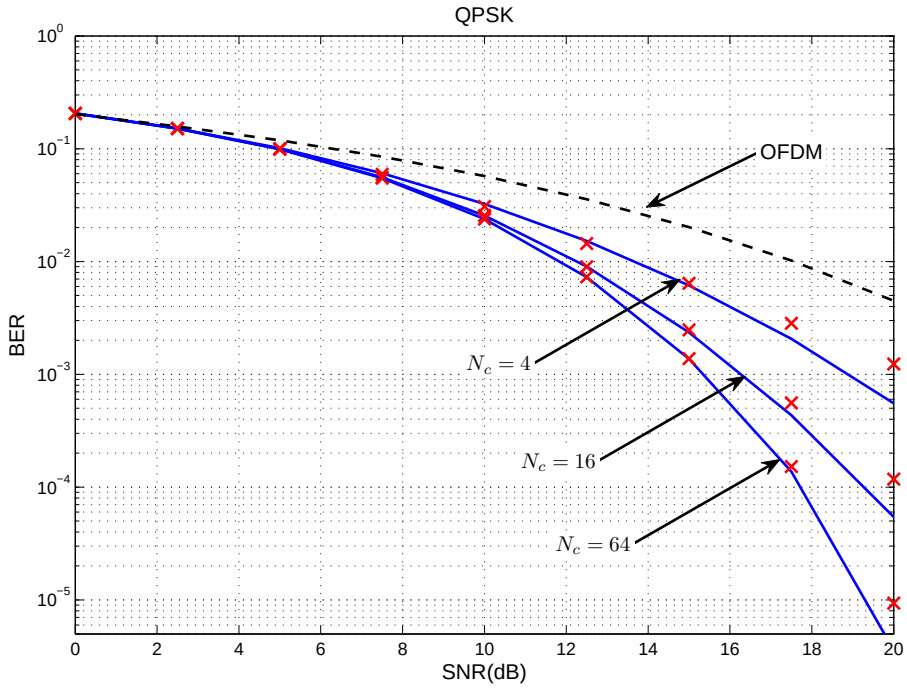

Figure 5.6: Analytical vs. simulation results for independent sub-carriers (4QAM) MMSE-FDE

we consider a selective Rayleigh fading channels, thereby the coefficients for the multipath fading model taps are assumed to be mutually independent zero-mean complex-valued Gaussian random variables. As a consequence, the real and imaginary parts of those random variables are also independent. The channel Power Delay Profile (PDP) is normalized in power, that is, the total power is unitary. The delay spread and 50% coherence bandwidth for each test environment is presented in Table 5.3. Within an ITU test environment, channel A and channel B are the low delay spread and the median delay spread cases respectively.

The Coherence Ratio (CR), defined as the ratio between Coherence Bandwidth (CB) and frequency spacing between consecutive allocated sub-carriers (ΔF), is also provided in Table 5.3, first, for localized sub-carriers spaced 15 KHz apart and then, for 16 sub-carriers interleaved over a total of 2048, that is, for a 1.92 MHz spacing between two consecutive allocated sub-carriers. These ratios provide information about the similarity between channel responses for consecutive allocated

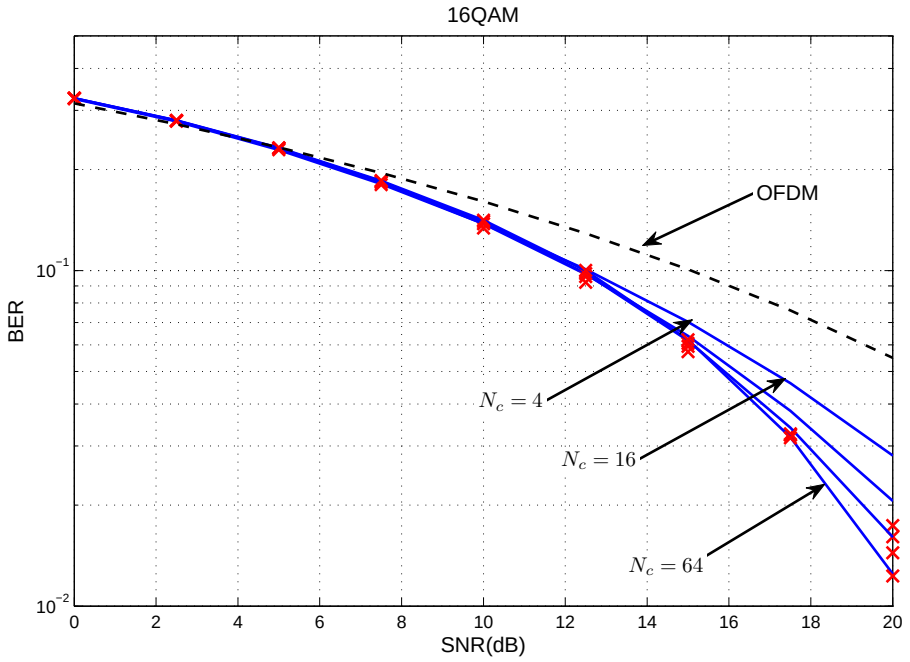

Figure 5.7: Analytical vs. simulation results for independent sub-carriers (16QAM) MMSE-FDE

sub-carriers: specifically, the higher its value, the more similar their channel responses are.

Usually, interleaved transmission yields small coherence ratio values, that is, CR ≤ 1. In such cases, the provided analytical BER expressions serve as an approximation of actual values for interleaved SC-FDMA with ZF-FDE and MMSE-FDE. However, for greater values of CR (e.g., in the Pedestrian A (PA) channel) BER results obtained from simulations are far from the values obtained using the proposed analytical expressions as depicted in Fig.5.8a. Nonetheless, expressions (5.5.3) and (5.5.4) provide values of BER that come closer to the values obtained through simulation when CR decreases. This behavior can be observed in results depicted in Figs.5.9a to 5.11a with the remarkable exception of those corresponding to the Vehicular B (VB) channel with MMSE-FDE. In this case, the approximation is not as close to the simulation curve as its CB and CR values would suggest. We think that the reason behind this strange behavior lies in its peculiar channel impulse response (see Table 5.2).

Note that localized transmissions present greater values of coherence bandwidth as the sub-carrier spacing is minimum, thereby the assumption of independence no longer holds and BER values cannot be approximated using the proposed expressions.

Two additional insights can be obtained by inspection of the simulation results. First, ZF-FDE OFDM determines the lower bound for SC-FDMA for Rayleigh fading channels, as can be inferred from BER values as shown in subsection 5.3. Second, both BER values obtained with expression (5.5.4) and simulation results for MMSE-FDE are below those of OFDM. That is consistent with the results provided in [Ciochina 07] and means that ZF-OFDM BER values can be considered as an upper bound in this case. In fact, BER values for MMSE-FDE are bounded between those of OFDM and the ones obtained with expression (5.5.4) under the assumption of independence.

Table 5.1: Simulation Parameters

Parameter	Value
Carrier Frequency	2.5GHz
System Bandwidth	20MHz
Sampling Frequency	30.72MHz
Sub-carrier Spacing ($\leq \Delta F$)	15KHz
FFT Size	2048
Data Carriers	16 & 64

5.7 Conclusions

The study of the stochastic nature of noise in SC-FDMA systems with ZF and MMSE-FDE has been addressed in this chapter. For ZF-FDE we show how, for SC-FDMA transmissions over a Nakagami-μ fading channel and under the assumption of independent sub-carriers, the effective noise is related to the Pearson type VII family of distributions. For MMSE we derive an approximation for the density of

Table 5.2: Tapped delay line parameters for considered channel models

PA		VB		ETU		EVA	
dB	ns	dB	ns	dB	ns	dB	ns
0	0	-2.5	0	-1	0	0	0
-9.7	110	0	300	-1	50	-1.5	30
-19.2	190	-12.8	8900	-1	120	-1.4	150
-22.8	4100	-10	12900	0	200	-3.6	310
-	-	-25.2	17100	0	230	-0.6	370
-	-	-16	20000	0	500	-9.1	710
-	-	-	-	-3	1600	-7	1090
-	-	-	-	-5	2300	-12	1730
-	-	-	-	-7	5000	-16.9	2510

Table 5.3: Delay Spread, Coherence Bandwidth and Coherence Ratio for considered channels

Channel Model	Delay Spread (rms)	Coherence BW (50%)	CR Localized	CR Interleaved 16/2048	CR Interleaved 64/2048
PA	46ns	4.35MHz	290	2.264	9.06
VB	4001ns	50KHz	3.33	0.026	0.104
ETU	990.93ns	160.6KHz	13.45	0.105	0.420
EVA	356.65ns	560.8KHz	37.8	0.292	1.168

the effective noise applying the CLT. In both cases, closed-form expressions for BER values in SC-FDMA transmissions over a Nakagami-μ fading channel with BPSK and M-QAM modulations were presented and validated by means of simulations. Additionally, the conditions under which they provide accurate approximations to actual BER values are determined. With this purpose SC-FDMA transmission over a Nakagami-μ fading channel with $\mu = 1$ (i.e., Rayleigh fading channel) was considered. It was shown how their suitability as approximations depends on the ratio between coherence bandwidth and frequency spacing among consecutive allocated sub-carriers. It was concluded that for small values of this ratio, close to or smaller than 1, provided expressions can safely be used to approximate BER values both for interleaved SC-FDMA. Additionally, it was shown that OFDM BER curves serve as

lower bounds for BER values in SC-FDMA with different constellations when ZF-FDE is applied whereas, according to simulations results, they are an upper bound for those obtained with MMSE-FDE. That is, for ZF-FDE, OFDM BER curves serve as lower bounds for BER values in SC-FDMA whereas, for MMSE-FDE, those same curves serve as upper bound for obtained BER values.

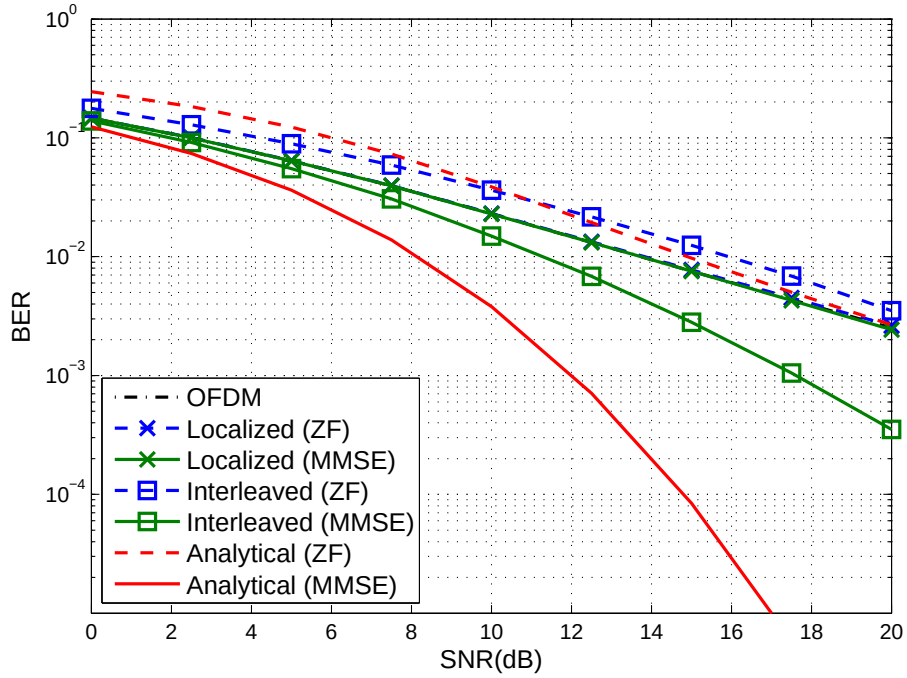

(a) $N_c = 16$

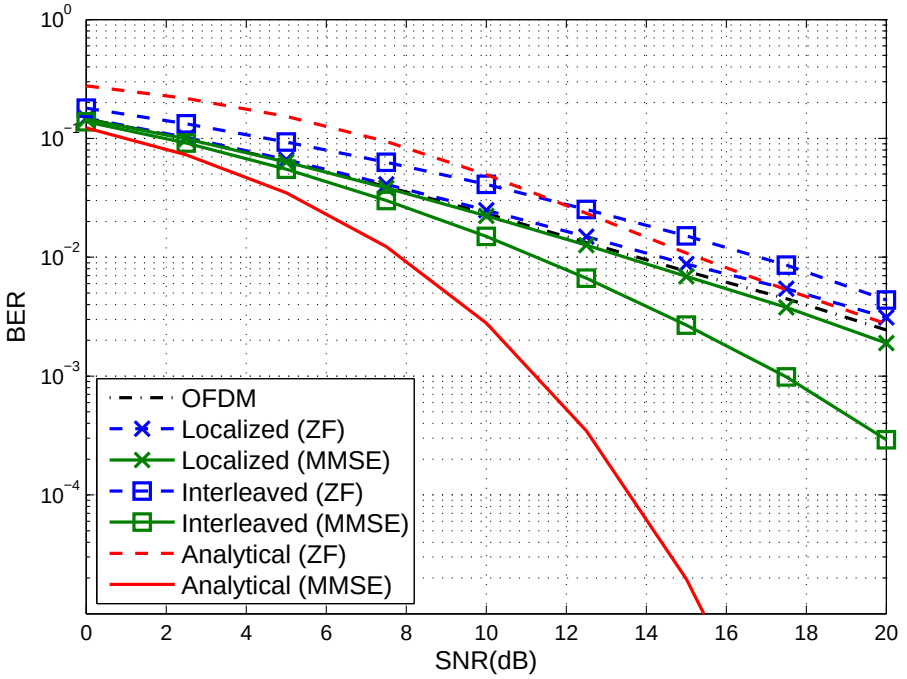

(b) $N_c = 64$

Figure 5.8: BER for Pedestrian A channel (BPSK)

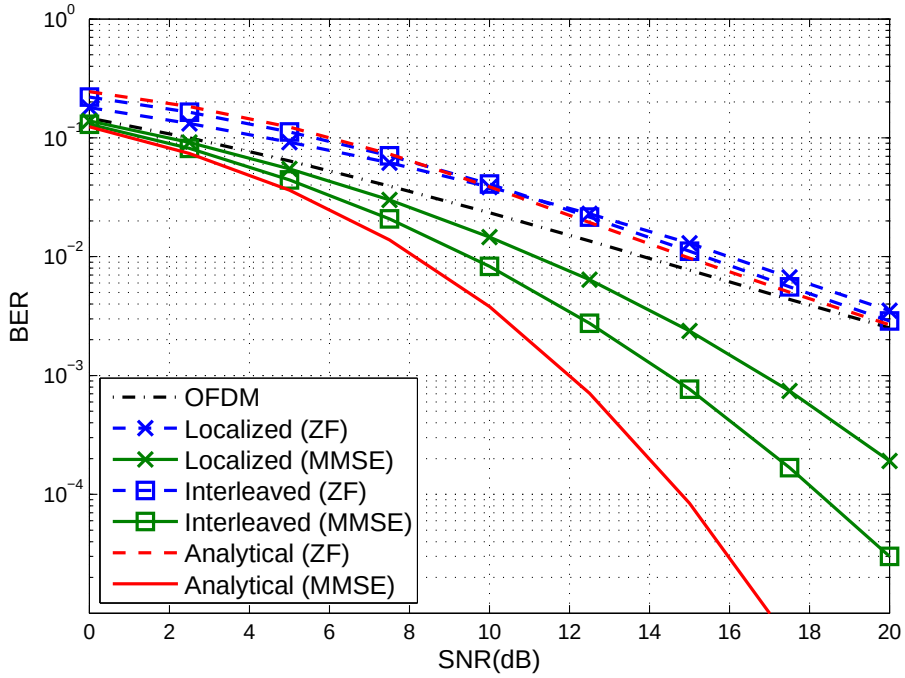

(a) $N_c = 16$

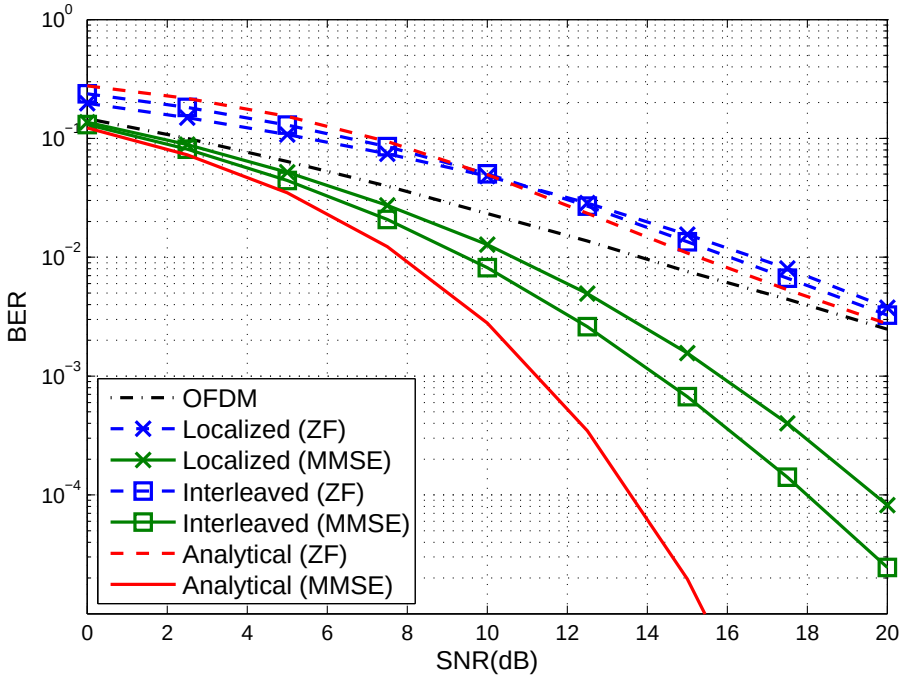

(b) $N_c = 64$

Figure 5.9: BER for Vehicular B channel (BPSK)

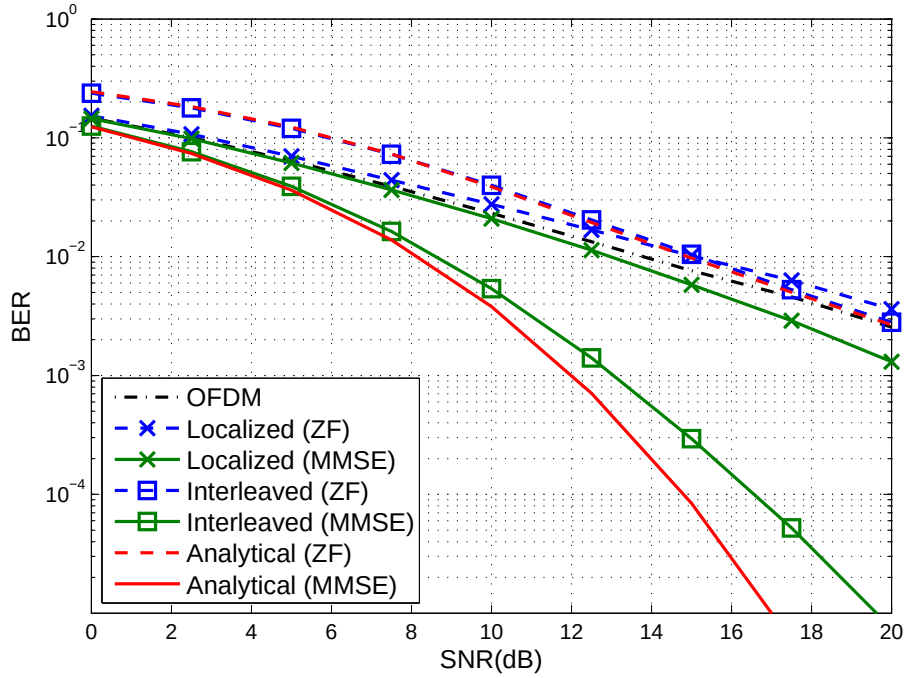

(a) $N_c = 16$

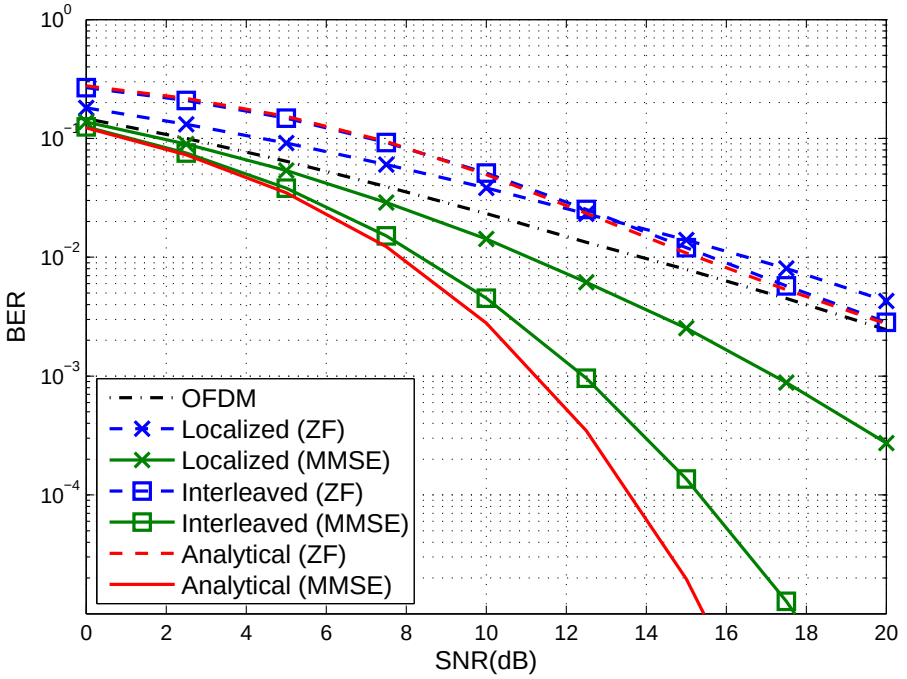

(b) $N_c = 64$

Figure 5.10: BER for Extended VA channel (BPSK)

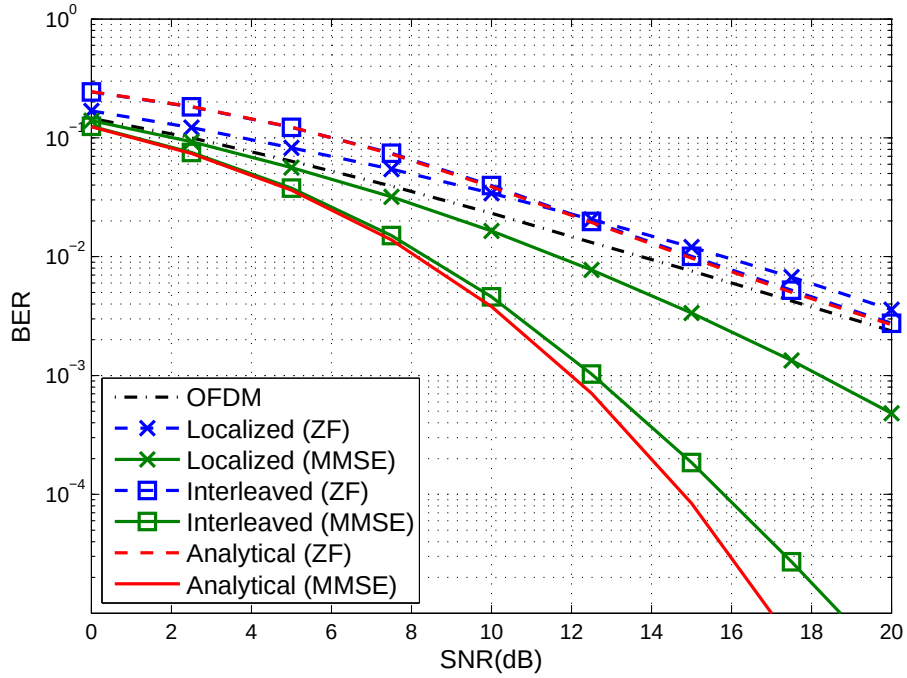

(a) $N_c = 16$

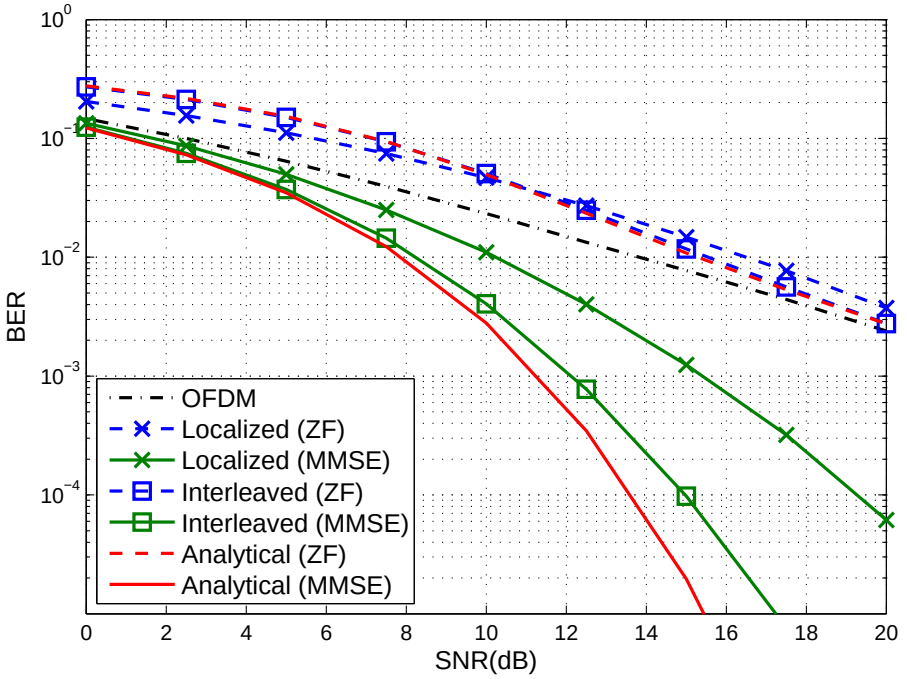

(b) $N_c = 64$

Figure 5.11: BER for Extended TU channel (BPSK)

Chapter 6

Spectral Efficiency for Adaptive SC-FDMA over Rayleigh Fading Channels

6.1 Introduction

The quality of the received signal in cellular communication systems depends on several factors such as the path loss exponent, the log-normal shadowing or the short term Rayleigh fading and noise. The use of Adaptive Modulation (AM) makes possible to improve the robustness and spectral efficiency of a transmitted signal suffering these impairments. In order to achieved that, the signal transmitted to or by a particular user is modified to account for the signal quality variation according to the estimated channel response at the receiver. Hence, by means of AM, it is possible to match the modulation scheme to the average channel conditions for each user. Thus, users with benign channel conditions are typically assigned higher order modulation (e.g., 64 QAM) whereas the modulation order decreases for users facing worse channel conditions.

In this chapter, we focus on the spectral efficiency for uncoded SC-FDMA transmission over a Rayleigh fading channel to perform an analytical study of the spectral

efficiency for ZF-FDE and MMSE-FDE. With this purpose, spectral efficiency values are derived for both OFDM and SC-FDMA when the same AM scheme is applied to track variations in the quality of the received signal due to the transmission over a fading channel. These values are derived for SC-FDMA assuming independence among allocated sub-carriers and compared to those obtained through simulations for localized and interleaved transmission over actual ITU and 3GPP channels.

6.2 Adaptive Modulation Schemes for SC-FDMA

6.2.1 Adaptive Modulation Overview

As it is a well known transmission technique, there is plenty of literature about AM; for instance, [Goldsmith 05] provides detailed descriptions of the AM system model. In this section, we briefly describe the adaptive modulation scheme used to evaluate spectral efficiency.

In this thesis, the transmit power is considered to be constant, thus the instantaneous SNR at the entrance of the detector γ is completely characterized by the channel model and the transmission technique employed. For a given value of γ, L consecutive and not overlapping fading regions $\{\Re_i \doteq [\gamma_i, \gamma_{i+1}]\}_{i=0,1,..,L-1}$ are considered with $\gamma_L \doteq \infty$. Within the fading region $\Re_i$, a certain QAM constellation with M_i bits/symbol is employed. The sets of switching thresholds $\{\gamma_i\}_{i=0,1,..,N-1}$ are designed to maximize the spectral efficiency under instantaneous BER constraints BER_T. The result is qualitatively depicted in Fig. 6.1: BER curves for different modulation schemes M_i $i = 1, \ldots, L-1$ over AWGN channel are intersected by the desired BER_T value and the crossing points determine the decision SNR thresholds. Additionally, for SNR values below a minimum threshold (i.e., in very poor channel conditions), there is an outage state in which there is no data transmission. To perform adaptation, γ is estimated at the receiver to determine the current fading region $\Re_i$, which is fed back to the transmitter.

Thus, L different constellations which includes BPSK and square QAM constellations of $R_r = 4^{r+1}$ $\{r = 0, .., M-1\}$ symbols are employed. The probability of falling in the fading region $\Re_i$ is

$$p_i \doteq \int_{\gamma_i}^{\gamma_{i+1}} p_\gamma(\gamma)\, d\gamma \tag{6.2.1}$$

where $p_\gamma(\gamma)$ is the PDF of the normalized instantaneous SNR fading.

The average spectral efficiency $\frac{R}{B}$ is simply given by

$$\frac{R}{B} = E[R(\gamma)] = \sum_{i=0}^{L-1} R_i p_i \tag{6.2.2}$$

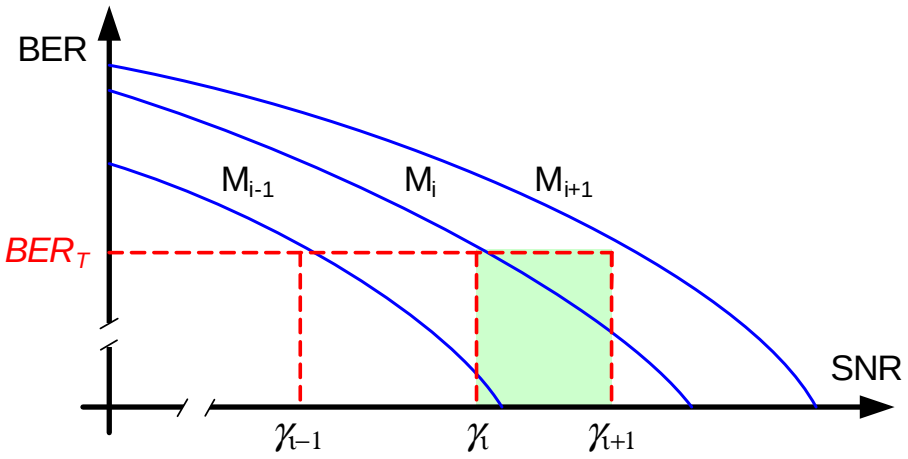

Figure 6.1: Example of adaptive modulation regions

6.2.2 Adaptive OFDMA and SC-FDMA

The use of adaptive modulation over OFDMA has been extensively addressed in the literature. Whereas interested reader is referred to [Simon 05] and [Goldsmith 05] for an in depth review on the matter, in the following we focus on its fundamental aspects. In OFDMA, the SNR at the entrance of the receiver at subcarrier k can be described for OFDM ZF equalization (from 4.5.2) as:

$$\gamma_{ZF}^{OFDMA} = \frac{E_S}{N_0} \frac{1}{\frac{1}{|h_k|^2}} = \frac{E_S}{N_0} |h_k|^2 , \tag{6.2.3}$$

where h_k is the frequency channel response at subcarrier k. Similarly for OFDMA MMSE the expression for the SNR yields

$$\gamma_{MMSE}^{OFDMA} = \frac{E_S}{N_0} \frac{1}{\left(\frac{|h_k|}{|h_k|^2+N_0}\right)^2}, \tag{6.2.4}$$

where $\sigma_s^2 = E_s = 1$ and $\sigma_\eta^2 = N_0$.

As OFDMA can be seen as a group of M parallel channels, Adaptive OFDMA simply employs the previously described adaptive modulation scheme over each sub-carrier, by selecting the constellation to be employed at each subcarrier comparing the thresholds to γ as described by eq. (6.2.3) or eq. (6.2.4) for ZF and MMSE respectively.

In the specific case of SC-FDMA, the study of the spectral efficiency is based on the system model presented in section 5.2. As described there, a sequence $\mathbf{x}$ is transmitted onto the subset of N_c allocated sub-carriers. In Chapter 5 the noise at the entrance of the detector was evaluated conditioned to the frequency channel response $\mathbf{h}$ and it was shown to be a combination of the channel response at the set of allocated sub-carriers. Thus, the SNR for ZF-FDE in SC-FDMA is given by

$$\gamma_{ZF} = \frac{E_S}{\beta^{ZF} N_0}, \tag{6.2.5}$$

with given by eq. (5.3.12), that is,

$$\beta^{ZF} = \frac{1}{N_c} \sum_{k=1}^{N_c} \frac{1}{|h_k|^2}. \tag{6.2.6}$$

For MMSE-FDE in SC-FDMA the instantaneous SNR is expressed as eq. (5.4.22), that is,

$$\gamma_{MMSE} = \frac{1}{E_S} \frac{E_S}{\beta^M N_0} - 1, \tag{6.2.7}$$

where

$$\beta^M = \frac{1}{N_c} \sum_{j=1}^{N_c} \frac{1}{|h_j|^2 + N_0/E_S}. \tag{6.2.8}$$

Please, note that the SNR is the same for the whole sequence $\mathbf{x}$, thereby forcing the use of the same constellation for all of individual symbols in the sequence. That means that the signalling necessary for SC-FDMA is N_c lower than those of OFDM for the same number of sub-carriers. This also implies that, in opposition to what happen in OFDMA, is not possible to perform a fine adaptation, in a per sub-carrier basis, in SC-FDMA.

Next sections analyze separately spectral efficiency results for ZF and MMSE equalization in SC-FDMA. Note that these results become those of OFDMA when $N_c = 1$. The working assumptions considered in chapter 5, such as ideal estimation of the channel frequency response or perfect synchronization, are also considered in the following. Moreover, the feedback of the SNR used to adapt the transmission rate is assumed to be ideal (i.e., instantaneous and error-free).

6.3 Spectral Efficiency Analysis for ZF-FDE

In this section we employ some expression derived in the previous chapter. For the sake of clarity, we repeat these expression when necessary. From the previous chapter, we know that, for SC-FDMA with ZF-FDE, the value of the instantaneous SNR at the receiver is determined by $\frac{E_S}{\beta^{ZF} N_0}$, where β^{ZF} is defined as

$$\beta^{ZF} = \frac{1}{N_c} \sum_{j=1}^{N_c} \frac{1}{|h_j|^2}. \tag{6.3.1}$$

The constellation corresponding to the i-th region is applied when the SNR is between the corresponding boundaries, that is,

$$\gamma_i < \frac{E_S}{\beta^{ZF} N_0} < \gamma_{i+1}. \tag{6.3.2}$$

We can rewrite this inequality and redefine the L regions to discretize the values of β^{ZF} as

$$\beta_{i+1}^{ZF} = \frac{1}{\gamma_{i+1}} \frac{E_S}{N_0} < \beta^{ZF} < \frac{1}{\gamma_i} \frac{E_S}{N_0} = \beta_i^{ZF}, \tag{6.3.3}$$

where β_i^{ZF} and β_{i+1}^{ZF} are the modified thresholds that depend on the SNR.

The average spectral efficiency can be calculated as

$$\frac{R}{B} = \sum_{i=1}^{L-1} \log_2(M_i)\, p_{\beta^{ZF}}\left(\beta_{i+1}^{ZF} < \beta^{ZF} < \beta_i^{ZF}\right) = \sum_{i=1}^{L-1} \log_2(M_i)\left[F_{\beta^{ZF}}\left(\beta_i^{ZF}\right) - F_{\beta^{ZF}}\left(\beta_{i+1}^{ZF}\right)\right]. \tag{6.3.4}$$

where L is the number of regions. This expression also requires $F_{\beta^{ZF}}(\beta^{ZF})$ that, for a selective Rayleigh fading channel, is the CDF of the sum of N_c identical weighted inverse-chi-square random variables (6.3.1), each of them with the following PDF

$$f_X(x) = \frac{e^{-\frac{1}{xN_c}}}{x^2 N_c}. \tag{6.3.5}$$

From this expression, the CHF is straightforwardly obtained (using (3.471.9) in [Grinstead 97]) as

$$\Phi_X(\omega) = 2\sqrt{\frac{-\omega}{N_c}\jmath}K_1\left(2\sqrt{\frac{-\omega}{N_c}\jmath}\right), \tag{6.3.6}$$

where $|\omega|$ is the absolute value of ω and K_1 is the modified first order Bessel function of the second kind [Bocher 92].

As the channel response for each sub-carrier is assumed to be independent, the CHF of β^{ZF} yields

$$\Phi_{\beta^{ZF}}(\omega) = \left(2\sqrt{\frac{-\omega}{N_c}\jmath}K_1\left(2\sqrt{\frac{-\omega}{N_c}\jmath}\right)\right)^{N_c}. \tag{6.3.7}$$

Hence, in this case, the CDF can be evaluated using Gil-Peláez inversion theorem expression (see section 3.2.4) and can be expressed as

$$F_{\beta^{ZF}}\left(\beta^{ZF}\right) = \frac{1}{2} - \frac{1}{2\pi}\int_0^\infty \left(\frac{\Phi_{\beta^{ZF}}(\omega)}{\jmath\,\omega}e^{-\jmath\beta^{ZF}\omega} - \frac{\Phi_{\beta^{ZF}}(-\omega)}{\jmath\,\omega}e^{\jmath\beta^{ZF}\omega}\right)d\omega. \tag{6.3.8}$$

Plugging this last expression into (6.3.4), we can compute the spectral efficiency values numerically by means of the double exponential integration [Mori 01].

6.4 Spectral Efficiency Analysis for MMSE-FDE

For MMSE-FDE in SC-FDMA the instantaneous SNR is expressed as eq. (5.4.22), that is,

$$\gamma_{MMSE} = \frac{E_S}{\beta^M N_0} - 1, \tag{6.4.1}$$

where

$$\beta^M = \frac{1}{N_c} \sum_{j=1}^{N_c} \frac{1}{|h_j|^2 + N_0/E_S}. \tag{6.4.2}$$

The parameter β^M determines the SNR and, consequently, the corresponding constellation to be used, that is,

$$\gamma_i < \frac{E_S}{\beta^M N_0} - 1 < \gamma_{i+1}. \tag{6.4.3}$$

In this case the inequality resulting after redefining the L regions to discretize the values of β^{ZF} is

$$\beta^M_{i+1} = \frac{E_S}{N_0} \frac{1}{\gamma_{i+1} + 1} < \beta^M < \frac{E_S}{N_0} \frac{1}{\gamma_i + 1} = \beta^M_i, \tag{6.4.4}$$

where β^M_i and β^M_{i+1} are the modified thresholds that depend on the SNR.

The average spectral efficiency can be calculated as

$$\begin{aligned} \frac{R}{B} = &\sum_{i=1}^{L-1} \log_2(M_i)\, p_{\beta^M}\left(\beta^{ZF}_{i+1} < \beta^M < \beta^M_i\right) = \\ &\sum_{i=1}^{L-1} \log_2(M_i) \left[F_{\beta^M}\left(\beta^M_i\right) - F_{\beta^M}\left(\beta^M_{i+1}\right)\right]. \end{aligned} \tag{6.4.5}$$

where L is the number of regions. This expression also requires $F_{\beta^M}(\beta^M)$ that, for a selective Rayleigh fading channel, is the sum of N_c identical weighted inverse-chi-square random variables (D.5.2.10) shifted N_0, each of them with the following PDF

$$f_Y(y) = f_X(x - N_0) = \frac{e^{\frac{-1}{(x-N_0)N_c}}}{(x-N_0)^2 N_c}. \tag{6.4.6}$$

Applying Fourier transform properties, the expression for the CHF of a single term is given by

$$\Phi_Y(\omega) = e^{\jmath N_0 \frac{\omega}{N_c}} \Phi_X(\omega) = 2\sqrt{\frac{-\omega}{N_c}\jmath} K_1\left(2\sqrt{\frac{-\omega}{N_c}\jmath}\right) e^{\jmath N_0 \frac{\omega}{N_c}}. \tag{6.4.7}$$

Under the assumption of independence among the allocated sub-carriers, the CHF of β^M yields

$$\Phi_{\beta^M}(\omega) = \left(2\sqrt{\frac{-\omega}{N_c}\jmath} K_1\left(2\sqrt{\frac{-\omega}{N_c}\jmath}\right) e^{\jmath N_0 \frac{\omega}{N_c}}\right)^{N_c}, \tag{6.4.8}$$

and can be evaluated using Gil-Peláez inversion theorem expression as

$$F_{\beta^M}\left(\beta^M\right) = \frac{1}{2} - \frac{1}{2\pi}\int_0^\infty \left(\frac{\Phi_{\beta^M}(\omega)}{\jmath\,\omega} e^{-\jmath\beta^M\omega} - \frac{\Phi_{\beta^M}(-\omega)}{\jmath\,\omega} e^{\jmath\beta^M\omega}\right) d\omega. \tag{6.4.9}$$

Plugging this last expression into (6.4.5), we can use again the double exponential integration [Mori 01] compute the spectral efficiency values.

6.5 Simulation and Numerical Results

In the following, we validate the expressions (6.3.4) and (6.4.5) through simulations. First, we consider an ideal scenario in which the channel frequency responses for allocated sub-carriers are independent: an interleaved SC-FDMA transmission. Then, more realistic scenarios based on channel models defined by ITU and 3GPP are considered. Our aim is to determine in which situations the provided analytical expressions can be used as an approximation for spectral efficiency values in actual selective Rayleigh fading channels. In both cases, we use a semi-analytical model in which complex channel frequency responses, generated for the different allocated sub-carriers, are used to calculate the conditional probability for ZF (5.4.21) and MMSE (5.4.10).

6.5.1 Validation of Closed-form Expressions

In order to validate the provided expressions for spectral efficiency (6.3.4) and (6.4.5), we evaluate them for different numbers of sub-carriers and compare the

values to those obtained from simulations. We consider a channel model in which the channel frequency response for the N_c allocated sub-carriers are modeled as i.i.d. complex Gaussian random variables. Fig. 6.2 shows the spectral efficiency with $BER_T = 10^{-3}$ and different values of N_c for ZF-FDE. OFDM spectral efficiency ($N_c = 1$) is also included to serve as a reference. By simple inspection, it can be concluded that whenever the assumption of independence among the frequency responses of the allocated sub-carriers holds, analytical values are matched by those obtained by simulations. From Fig. 6.2 it can be also concluded that an increment of the number of allocated sub-carriers reduces the spectral efficiency in SC-FDMA, whereas the spectral efficiency in OFDM is known to be independent of this value. This rate loss, already predicted in the previous section chapter (see section 5.3), increases with the number of allocated sub-carriers. Note that AM is employed here for OFDM in a sub-carrier basis and that implies a greater signalling overhead than that of SC-FDMA. In real systems the Channel Quality Indicators (CQIs) are provided for chunks of sub-carriers and it is not possible to perform a fine adaptation.

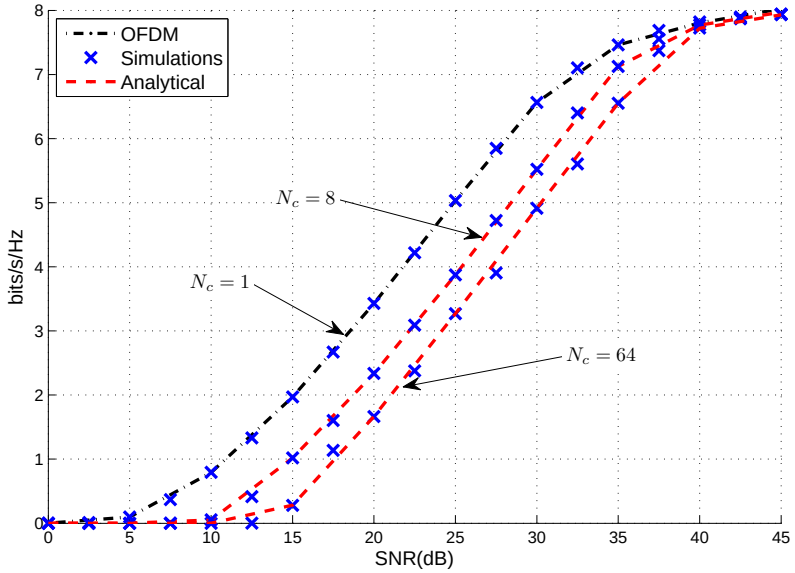

Figure 6.2: Spectral Efficiency for $BER_T = 10^{-3}$ (ZF)

These results are consistent with those presented by Wu et al. [Wu 09] using

simulation and Shannon's formula. In order to make a fair comparison between them, it must be taken into account that there is an effective power loss (i.e., power gap) due to the use of M-QAM [Goldsmith 05]. Furthermore, here we consider a maximum spectral efficiency of 8 bits/s/Hz.

For MMSE-FDE Figs. 6.3a and 6.3b shown results for different number of sub-carriers. In both cases, the analytical spectral efficiency calculated with eq. (6.4.5) matches the values obtained through simulations showing that the approximation made is valid.

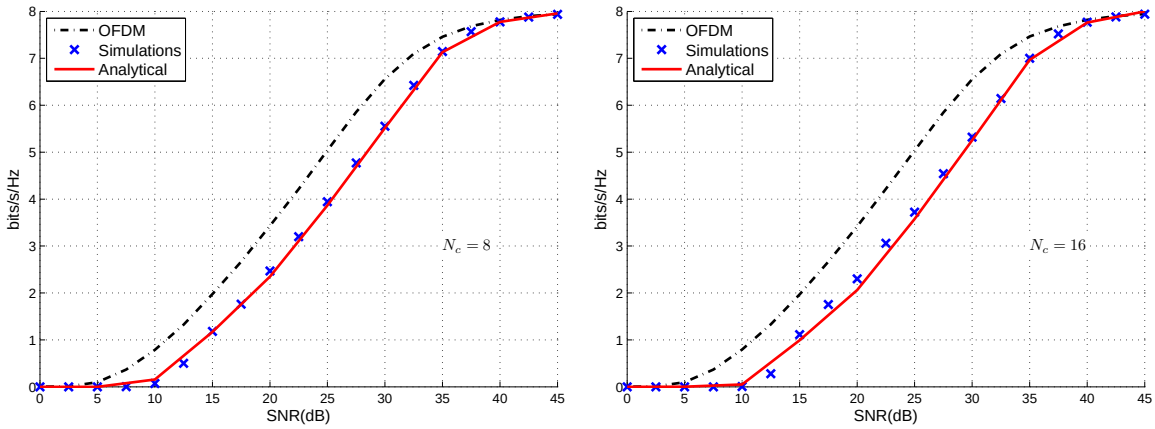

Figure 6.3: Spectral Efficiency for $BER_T = 10^{-3}$ (MMSE)

Comparing the spectral efficiency results for OFDM and MMSE-FDE (see Fig. 6.3) we can observe that the aforementioned reduction of the spectral efficient also appears for MMSE-FDE. The reason behind this reduction was hinted before: for OFDMA it is possible to consider a per sub-carrier AM whereas for SC-FDMA such a fine level of granularity it is not possible. Lastly, it must be noted that spectral efficiency values for MMSE-FDE are similar to those obtained for ZF-FDE as depicted in Fig. 6.4.

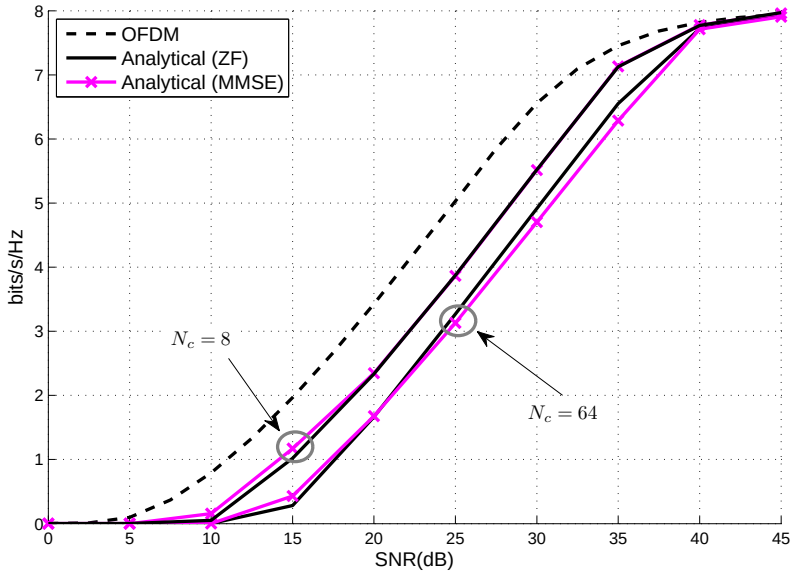

Figure 6.4: Spectral Efficiency Comparison with $BER_T = 10^{-3}$

6.5.2 Application to Realistic Scenarios

In this subsection we check the suitability of the presented closed-form expressions to evaluate the spectral efficiency for actual selective fading channels with a certain coherence bandwidth. The scenario under study is a SC-FDMA transmission over the different channel impulse response models already used in the previous chapter, that is, ITU [ITU-R 97] and 3GPP [3GPP 10] channel models. The values of the taps for the different channels considered are collected in Table 6.1.

As in the previous chapter, the coefficients for multipath fading model taps are assumed to be mutually independent zero-mean complex-valued Gaussian random variables whose real and imaginary parts are also independent and the total power is unitary. The delay spread and 50% coherence bandwidth for each test environment is presented in Table 6.2. The representative simulations parameters for the channel models under consideration are presented in Table 6.3. Through Figs. 6.5a to 6.6b, we present analytical values of the spectral efficiency for ZF and MMSE, which are calculated for a BER_T of 10^{-3} with the proposed expressions (6.3.4) and (6.4.5), besides actual ones obtained through simulations. In each figure, we include results

Table 6.1: Tapped delay line parameters for considered channel models

PA		VB		ETU		EVA	
dB	ns	dB	ns	dB	ns	dB	ns
0	0	-2.5	0	-1	0	0	0
-9.7	110	0	300	-1	50	-1.5	30
-19.2	190	-12.8	8900	-1	120	-1.4	150
-22.8	4100	-10	12900	0	200	-3.6	310
-	-	-25.2	17100	0	230	-0.6	370
-	-	-16	20000	0	500	-9.1	710
-	-	-	-	-3	1600	-7	1090
-	-	-	-	-5	2300	-12	1730
-	-	-	-	-7	5000	-16.9	2510

Table 6.2: Delay Spread, Coherence Bandwidth and Coherence Ratio for considered channels

Channel Model	Delay Spread (rms)	Coherence BW (50%)	CR Localized	CR Interleaved 16/2048	CR Interleaved 64/2048
PA	46ns	4.35MHz	290	2.264	9.06
VB	4001ns	50KHz	3.33	0.026	0.104
ETU	990.93ns	160.6KHz	13.45	0.105	0.420
EVA	356.65ns	560.8KHz	37.8	0.292	1.168

for both ZF and MMSE FDE for the specific channel and for a given number of allocated sub-carriers (16 or 64).

By a simple inspection of these figures, we can see that SC-FDMA spectral efficiency results obtained with MMSE-FDE are similar to those obtained with ZF-FDE for a given target BER (see Fig. 6.4). Scenarios with the highest values of coherence ratio[1], such as localized SC-FDMA transmission for PA channel model, present a spectral efficiency similar to that of OFDM as the channel frequency response is likely to be similar for all allocated sub-carriers as depicted in Fig. 6.5a. In this case, our expressions are not a good approximation for actual spectral efficiency values.

[1]Recall that this ratio provides information about the similarity between channel responses for

Table 6.3: Simulation Parameters

Parameter	Value
Carrier Frequency	2.5GHz
System Bandwidth	20MHz
Sampling Frequency	30.72MHz
Sub-carrier Spacing ($\leq \Delta F$)	15KHz
FFT Size	2048
Data Carriers	16 & 64

However, when the coherence bandwidth is small, the obtained analytical spectral efficiency expression serves as an approximation of actual values. The accuracy of such approximations increases when CR $\ll 1$. Thus, for interleaved transmission over VB channel, simulations results are close to the values obtained using the proposed analytical expressions (see Fig. 6.5b). Note that, for a greater number of allocated sub-carriers in a system with fixed bandwidth, the sub-carrier spacing is reduced resulting in a worsening of the accuracy of the approximation.

It must be noted that values obtained with the provided expression for extended channels (EVA and ETU) are the ones that fit best the simulation values for interleaved transmission as depicted in Figs. from 6.6a and 6.6b as $CR \ll 1$.

Several additional conclusions can be extracted from the simulation results that must be noted. First, there is a rate loss in SC-FDMA compared to that of OFDM (as stated in section 6.2 for independent sub-carriers). That implies that the spectral efficiency values for SC-FDMA are upper bounded by those of OFDM. Second, the closed-form expression we present here serves as a lower bound for the spectral efficiency in SC-FDMA. Such a lower bound becomes an accurate approximation of the spectral efficiency in SC-FDMA for low values of CR as it provides the worst spectral efficiency values reachable with SC-FDMA and serves to consider the worst case scenario for this transmission technology.

consecutive allocated sub-carriers: the higher its value, the more similar their channel responses are.

Lastly, it can be deduced that for greater values of CR (i.e., when there is a strong correlation among channel frequency responses) the spectral efficiency increases. The best values achievable in SC-FDMA for the spectral efficiency are those of OFDM[2]; that happens for flat or almost flat fading channels in which the channel frequency response is the same for all sub-carriers. That is, they are completely correlated and β becomes the enhancement factor for OFDM.

6.6 Conclusions

This chapter gathers the results obtained and the insights inferred from our analytical study of the spectral efficiency for SC-FDMA when a linear zero forcing FDE, either ZF or MMSE, is applied. First, under the assumption of independence among the channel frequency responses for the allocated sub-carriers, we derived closed-form expressions to compute spectral efficiency for ZF and MMSE-FDE. Then, we checked the suitability of those expressions to describe the spectral efficiency in actual fading channels through simulations over ITU channel models. The results obtained show how, for small coherence ratio values, provided expression approximates actual values for IFDMA. Additionally, we demonstrate that spectral efficiency values for SC-FDMA are upper bounded by those of OFDM and show through simulations that are lower bounded by those obtained with the provided closed-form expression.

From the results presented here, we can conclude that the performance in terms of spectral efficiency of SC-FDMA is slightly worse than the one obtained with OFDM. However, we also show that OFDM implies a greater signalling overhead to use AM in a sub-carrier basis that must not be neglected when comparing the technologies. Although taking into account this aspect was beyond the purpose of this dissertation, it is an interesting research topic and has been included in the

[2]As mentioned before, we are assuming in this study a sub-carrier basis adaptation for OFDM that implies a greater signalling overhead.

future work lines. Additionally, we show how the provided expressions, derived under the assumption of independence among the frequency responses of the allocated sub-carriers, are a good approximation to actual spectral efficiency values for EVA and ETU channels. Moreover, in general, these expressions serve as a lower bound for the spectral efficiency. That is, they provide the worst spectral efficiency values reachable with SC-FDMA and serve to considered the worst case scenario for this transmission technology.

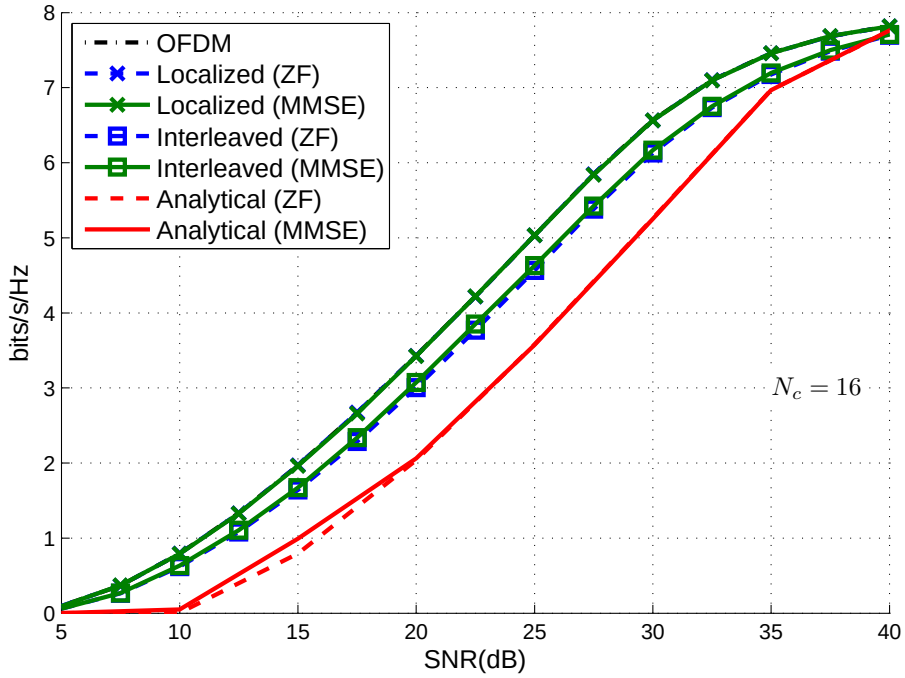

(a) PA channel

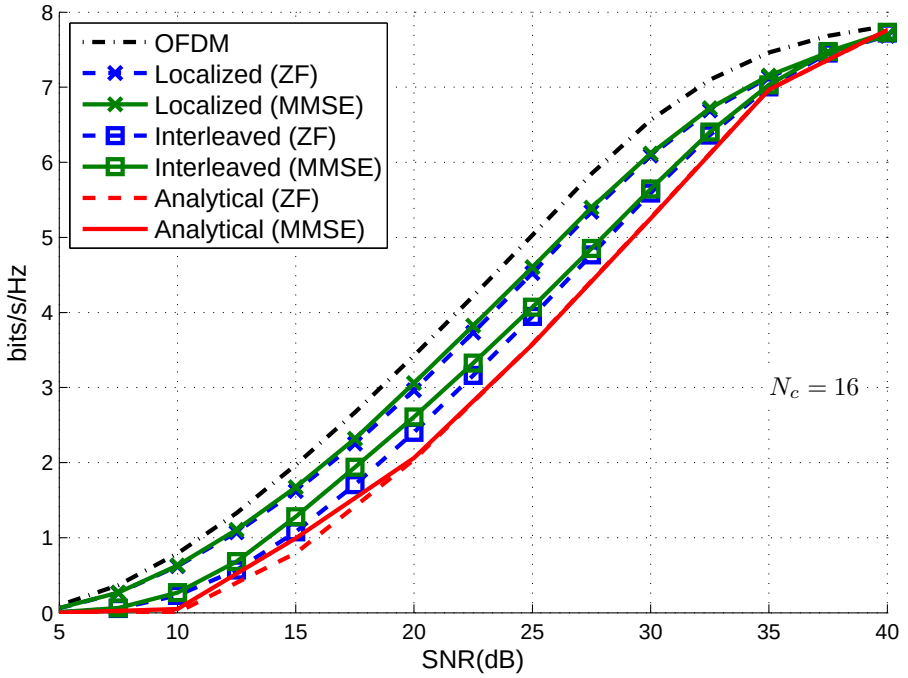

(b) VB channel

Figure 6.5: ZF vs. MMSE Spectral Efficiency (PA and VB)

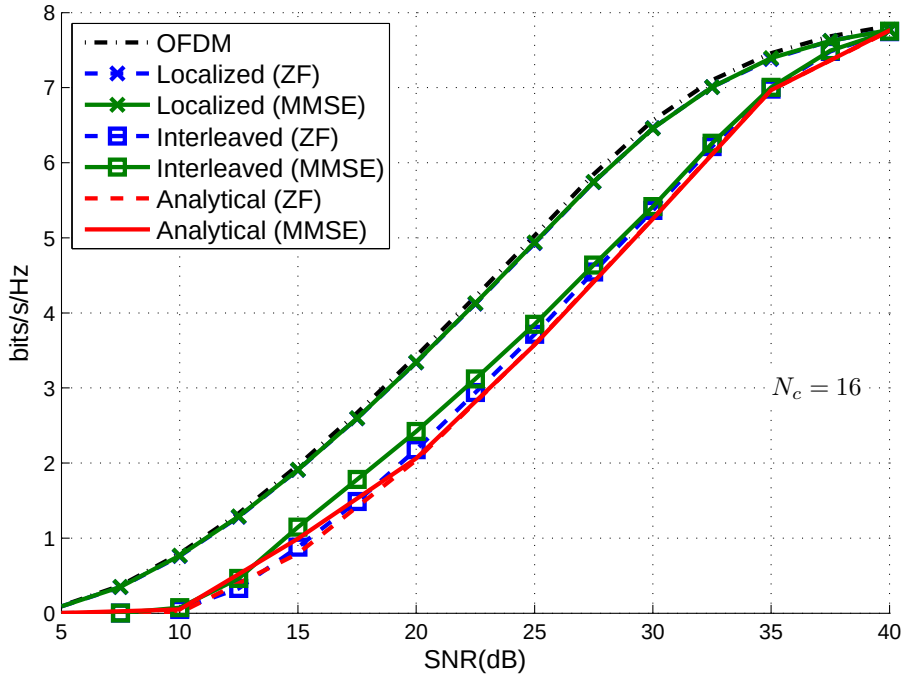

(a) EVA channel

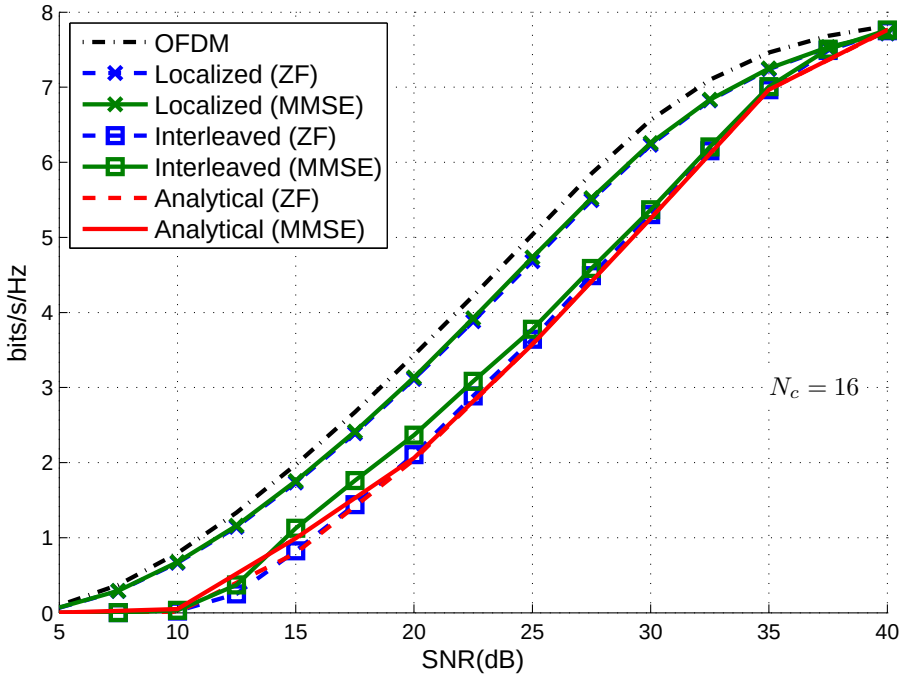

(b) ETU channel

Figure 6.6: ZF vs. MMSE Spectral Efficiency (EVA and ETU)

Chapter 7

Conclusions

Along this dissertation, we have presented the work developed during our analysis of the performance, in terms of BER and spectral efficiency, of an SC-FDMA system. First, we introduced the technologies considered and the mathematical grounds to perform the aforementioned analysis. Then, we focused on the effects of linear equalization in the frequency domain on the noise component for OFDM and SC-FDMA. Once this enhanced noise was characterized, we derived expressions for the BER and the spectral efficiency in SC-FDMA. After each step in our study, we discussed the conclusions inferred from this analysis and presented the contributions derived. In this final chapter, we include a brief summary of the previous chapters in which we remark the more significant insights. In addition, we also provide some future lines and applications regarding this work.

7.1 Synthesis of the Dissertation

An outline of the dissertation follows:

We devoted chapter 1 to introduce the motivation of this work which is to provide a mathematical analysis of the performance of an SC-FDMA system over a Rayleigh

fading channel. With this aim, we provided in chapter 2 an overview of this new radio interface technique and described its transmission and reception processes, focusing in the similarities and differences with OFDMA. For the sake of clarity, we collected in chapter 3 all the mathematical concepts regarding probability distributions which are needed to perform the aforementioned analyses.

In chapter 4 we applied the mathematical framework in order to carry out a rigorous study of the detection noise after equalization for different fading channels in OFDM. Additionally, we derived the density function of the random variable which models that noise. Concretely, we considered zero forcing equalization for an OFDM signal transmitted over different fading channels (i.e., Rayleigh, Rice and Nakagami-m).

In chapter 5 we used previous results to conduct the study of the stochastic nature of noise in SC-FDMA systems with ZF and MMSE-FDE. For ZF-FDE we showed how, for SC-FDMA transmissions over independent sub-carriers, effective noise is related to the Pearson type VII family of distributions. For MMSE we derived an approximation for the density of the effective noise applying the CLT. In both cases, closed-form expressions for BER values in SC-FDMA transmissions over Nakagami-μ fading channels, which includes Rayleigh fading channels as a particular case, with BPSK and M-QAM modulations were presented and validated by means of simulations. These expression were derived assuming independence among the channel frequency response for the allocated sub-carriers. We showed how their suitability to approximate the BER depends on the ratio between coherence bandwidth and frequency spacing among consecutive allocated sub-carriers. We also concluded that for small values of this ratio, close to or smaller than 1, provided expressions can safely be used to accurately approximate BER values for SC-FDMA. Additionally, it was shown that OFDM BER curves serve as lower bounds for BER values in SC-FDMA with different constellations when ZF-FDE is applied whereas they are an upper bound for those obtained with MMSE-FDE.

Finally, we extended our study to the analysis of the spectral efficiency for SC-FDMA in chapter 6. First, under the assumption of independence among the channel frequency responses for the allocated sub-carriers, we derived closed-form expressions to compute spectral efficiency for ZF and MMSE-FDE. Then, we showed how, for small coherence ratio values, provided expressions approximate actual values for IFDMA. Additionally, we demonstrated that spectral efficiency values for SC-FDMA are upper bounded by those of OFDM and showed through simulations that they are lower bounded by those obtained with the provided closed-form expression.

7.2 Contributions

The main contribution of this thesis is the analysis of the performance, in terms of BER and spectral efficiency, of a SC-FDMA system over Nakagami-μ fading channels. We paid special attention to the Rayleigh fading channel, which can be seen as a particular case of Nakagami-μ fading channel. The obtained results were first validated through simulations and, then, compared to those obtained with OFDMA. These comparisons allow us to determine the difference in performance between both technologies. Other contributions made during the development of this thesis are listed next.

- *Statistical study of the enhanced noise after linear equalization in frequency domain in OFDM and SC-FDMA.* We carry out a rigorous study of enhanced noise, after linear equalization for different fading channels, at the detection stage for OFDM and SC-FDMA. Additionally, we derived the density function of the random variable which models that noise.

- *Analysis of BER for OFDMA and SC-FDMA over Nakagami-μ fading channels.* Based on the aforementioned study, we obtained closed-form BER expressions for SC-FDMA transmissions over Nakagami-μ fading channels when linear frequency domain equalization is performed. Specifically, under the

assumption of independence among allocated sub-carriers, we derived closed-form expressions for the BER in the case of ZF-FDE; for MMSE-FDE we obtained a pessimist approximation in the form of a lower bound.

- *Analysis of spectral efficiency for SC-FDMA*. We extended our analytical study to the spectral efficiency when frequency-domain equalizer is applied for a SC-FDMA transmission over Rayleigh fading channels with adaptive modulation. Again, ZF and MMSE-FDE were considered and independence among allocated sub-carriers assumed. In both cases we derived closed-form expressions for the spectral efficiency; those expressions proved themselves useful to fit actual spectral efficiency values obtained thought simulation for more realistic channel models (e.g., EVA and ETU channel models). We also show how they provided the worst case scenario results for any SC-FDMA transmission.

7.3 Future Work

The results of this dissertation point to several interesting directions for future work. Some of them follow:

- Using some of the partial results obtained from the study of ZF-FDE in OFDM, we intent to extend the study of BER performance in SC-FDMA to other fading channels as Rice.

- Most of our study is developed under the assumption of independence among allocated sub-carriers. In the next stage of our research, we aim to include the effect of correlation in the study in order to derive expressions for more general scenarios.

- We also plan to study the impact of limited CQI feedback on spectral efficiency for OFDMA and SC-FDMA in order to make a fairer comparison.

- The results presented in this dissertation can be applied to channel state dependent scheduling. Results presented in this dissertation regarding the random variables used to model the SNR at the receiver can be used for the mathematical analysis of scheduling algorithms.

- Presented results are obtained assuming that there is perfect synchronization at the receiver side and there is neither ISI nor ICI. It may result interesting to include the effect of these impairments in the analyses here presented.

- Last but not least, we intend to extend this study with the inclusion of several MIMO techniques in the model; that will allow us to evaluate the performance, in terms of BER and spectral efficiency, for more realistic systems.

Appendix A

Pearson Type VII Distributions

A.1 Characteristic Function

The CHF of an even PDF can be computed as

$$G(\omega) = \int_{-\infty}^{\infty} f_X(x)\, e^{j\omega x} dx = 2\int_0^{\infty} f_X(x)\, \cos(\omega x)\, dx. \tag{A.1.1}$$

In the case under study

$$f_X(x) = \frac{\Gamma(m-1/2)}{\Gamma(m-1)\,\Gamma(1/2)} \frac{a}{(1+a^2x^2)^{m-1/2}} \tag{A.1.2}$$

and letting $t = \omega x$ the integral may be rewritten as

$$G(\omega) = \frac{2\Gamma(m-1/2)}{\Gamma(m-1)\,\Gamma(1/2)} \int_0^{\infty} \frac{a\cos(t)}{(\omega^2+a^2t^2)^{m-1/2}} \omega^{2m} dt. \tag{A.1.3}$$

According to Abramowitz and Stegun [Abramowitz 64] in 9.6.25

$$K_n(s) = \frac{\Gamma(n+1/2)}{\pi}(2s)^n \int_0^{\infty} \frac{\cos(t)}{(s^2+t^2)^{n+1/2}}\, dt \tag{A.1.4}$$

for $s \geq 0$. Therefore, letting $s = \dfrac{\omega}{a}$ and $m = n+1$

$$G(\omega) = \frac{s^n}{2^{n-1}\Gamma(n)} K_n(s) = \frac{1}{2^{n-1}\Gamma(n)} \left(\frac{|\omega|}{a}\right)^n K_n\left(\frac{|\omega|}{a}\right). \tag{A.1.5}$$

In the case under study, that is, letting $a = \sigma^{-1}$, $m = 2$ and $n = 1$, the final expression results

$$G(\omega) = \sigma|\omega| K_1(\sigma|\omega|). \tag{A.1.6}$$

A.2 Convolution

Let x and y two independent Pearson type VII random variables with the same PDF

$$p_t(t;a,N) = \frac{\Gamma\left(m-\frac{1}{2}\right)}{\sqrt{a}\Gamma(m-1)\Gamma(1/2)}\left(\frac{t^2}{a}+1\right)^{-(m-\frac{1}{2})} \tag{A.2.1}$$

and same CHF

$$G(\omega;a,m) = \frac{2^{2-m}\left(a\omega^2\right)^{\frac{m-1}{2}}}{\Gamma(m-1)}K_{m-1}\left(\sqrt{a}|\omega|\right). \tag{A.2.2}$$

Let $s = x+y$, then the PDF corresponding to s can be computed as the convolution of the PDFs of x and y

$$p_s(s;a,m_1,m_2) = \int_{-\infty}^{\infty} p_x(x;a_1,m_1)p_y(x-s;a_1,m_2)dx. \tag{A.2.3}$$

Equivalently, that PDF can be expressed as

$$p_s(s;a,m_1,m_2) = \int_{-\infty}^{\infty} G(\omega;a,m_1)G(\omega;a,m_2)e^{jx\omega}d\omega. \tag{A.2.4}$$

The solution of this integral results

$${}_3F_2(m_1-\tfrac{1}{2}, m_2-\tfrac{1}{2}, m_1+m_2-\tfrac{3}{2}; \tfrac{m_1+m_2-1}{2}, \tfrac{m_1+m_2}{2}; \tfrac{-x^2}{4a})T \tag{A.2.5}$$

where

$$T = \frac{(m_1+m_2-1)\Gamma(m_1-\frac{1}{2})\Gamma(m_2-\frac{1}{2})\Gamma(m_1+m_2-\frac{3}{2})}{\sqrt{\pi a}\Gamma(m_1-1)\Gamma(m_2-1)\Gamma(m_1+m_2)}, \tag{A.2.6}$$

and ${}_3F_2$ is a particular case of the generalized hypergeometric function ${}_pF_q$ with $p = 3$ and $q = 2$ [Abramowitz 64]). For half integer values of m_1 and m_2 it is possible to obtain a polynomial expression for $p_s(s;a,m_1,m_2)$. Several examples are presented in table A.1.

Table A.1: List of analytical expressions of $p_s(s; a, m_1, m_2)$ for half integer values of m_1 and m_2.

m_1	m_2	$p_s(s; a, m_1, m_2)$
$\frac{3}{2}$	$\frac{3}{2}$	$\frac{2\sqrt{a}}{\pi\left(4a+x^2\right)}$
$\frac{5}{2}$	$\frac{3}{2}$	$\frac{\sqrt{a}\left(12a+x^2\right)}{\pi\left(4a+x^2\right)^2}$
$\frac{5}{2}$	$\frac{5}{2}$	$\frac{4a^{3/2}\left(20a+x^2\right)}{\pi\left(4a+x^2\right)^3}$
$\frac{7}{2}$	$\frac{3}{2}$	$\frac{160a^3+36a^2x^2+3ax^4}{3\sqrt{a}\pi\left(4a+x^2\right)^3}$
$\frac{7}{2}$	$\frac{5}{2}$	$\frac{2a^{3/2}\left(560a^2+56ax^2+3x^4\right)}{3\pi\left(4a+x^2\right)^4}$
$\frac{7}{2}$	$\frac{7}{2}$	$\frac{16a^{5/2}\left(336a^2+24ax^2+x^4\right)}{3\pi\left(4a+x^2\right)^5}$

Appendix B

Probability Expressions for Enhanced Noise after ZF-FDE in OFDM

In this appendix we collect the expressions obtained in chapter 4 for the random variable that describes the enhanced noise resulting after applying ZF-FDE for different fading channels.

Table B.1: Enhanced Noise Densities after equalization in Rayleigh fading channels.

Function	Expression	
Joint Density (Polar)	$\frac{1}{\pi}\frac{\sigma r}{(\sigma + r^2)^2}$	(4.5.5)
Joint Density (Cartesian)	$\frac{1}{\pi}\frac{\sigma^2}{(\sigma^2 + (x^2 + y^2))^2}$	(4.5.6)
Marginal Density	$\frac{1}{2}\frac{\sigma^2}{(\sigma^2 + x^2)^{3/2}}$	(4.5.7)
Marginal Distribution	$\frac{1}{2} + \frac{x}{2\sqrt{x^2 + \sigma^2}}$	(4.5.8)
Characteristic Function	$\sigma\lvert\omega\rvert K_1(\sigma\lvert\omega\rvert)$	(4.5.10)

Table B.2: Enhanced Noise Densities after equalization in Rice fading channels.

Function	Expression	
Joint Density (Polar)	$\frac{r\sigma\left(\alpha^2\sigma+2\left(\sigma+r^2\right)\right)}{2\pi\left(\sigma+r^2\right)^3}e^{-\frac{\alpha^2 r^2}{2(\sigma+r^2)}}$	(4.5.13)
Joint Density (Cartesian)	$\frac{(x^2+y^2)\alpha^2\sigma+2\left((x^2+y^2)\sigma+1\right)}{2\pi\left((x^2+y^2)\sigma+1\right)^3}\sigma e^{-\frac{\alpha^2}{2((x^2+y^2)\sigma+1)}}$	(4.5.14)
Marginal Density	–	
Marginal Distribution	$\int_{-\infty}^{t}\int_{-\infty}^{\infty} f_{\hat{\eta}_r,\hat{\eta}_i}(x,y)dydx$	(4.5.15)
Characteristic Function	–	

Table B.3: Enhanced Noise Densities after equalization in Nakagami-μ fading channels.

Function	Expression	
Joint Density (Polar)	$\frac{1}{2\pi}\frac{\mu^{\mu+1}}{\sigma^2} r \left(\frac{r^2}{2\sigma^2}+\mu\right)^{-1-\mu}$	(4.5.18)
Joint Density (Cartesian)	$\frac{\mu^{\mu+1}}{2\pi\sigma^2}\left(\frac{x^2+y^2}{2\sigma^2}+\mu\right)^{-1-\mu}$	(4.5.19)
Marginal Density	$\sqrt{\frac{1}{\pi}}\frac{\Gamma\left(\mu+\frac{1}{2}\right)2^{\mu}\mu^{\mu}\sigma^{2\mu}}{\Gamma(\mu)\left(2\mu\sigma^2+z^2\right)^{\mu-\frac{1}{2}}}$	(4.5.20)
Marginal Distribution	$\frac{(-1)^{-\mu}\Gamma\left(\mu+\frac{1}{2}\right)}{2\sqrt{\pi}\Gamma(\mu)} B_{-\frac{2\mu\sigma^2}{x^2}}\left(\mu,\frac{1}{2}-\mu\right)$	(4.5.22)
Characteristic Function	$\frac{\sigma^{\mu}\lvert\omega\rvert^{\mu}}{2^{1-\mu/2}\Gamma(\mu)}\mu^{\mu/2}K_{\mu}\left(\sigma\sqrt{2\mu}\lvert\omega\rvert\right)$	(4.5.21)

Appendix C

Distribution of the Minimum of a Set of Chi-Square Random Variables

---

Let $X_1, X_2, ..., X_{N_c}$ be a set of N_c independent chi-square random variables with two degrees of freedom

$$f_{X_j}(x_j) = \frac{1}{2} e^{-x_j/2}, \tag{C.1}$$

and $X_{\min}$ the minimum value in this set

$$X_{\min} = \min\left[X_1, X_2, \ldots, X_{N_c}\right], \tag{C.2}$$

then, the distribution of X_{min} yields

$$f_{X_{\min}}(x) = \frac{N_c}{2} e^{-\frac{x}{2}N_c}, \tag{C.3}$$

and $Z = N_c X_{min}$ follows a the same chi-square distribution as that of X_j

$$f_Z(z) = \frac{1}{2} e^{-\frac{z}{2}}. \tag{C.4}$$

Proof. The CDF corresponding to this X_{min}, where all X_i are independent, may be expressed as

$$P(X_{\min} \leq x) = 1 - \prod_{j=1}^{N_c} P(X_j > x) = 1 - P(X > x)^{N_c}, \tag{C.5}$$

since $P(X_j > x) = P(X > x) \ \forall j \in \{1, 2, ..., N_c\}$. Thus, as $P(X > x) = 1 - P(X \leq x)$

$$F_{X_{\min}}(x) = 1 - (1 - F_X(x))^{N_c}, \tag{C.6}$$

where $F_X(x) = 1 - e^{-x/2}$ is the distribution function for a chi-square random variable. Then the density can be computed as

$$f_{X_{\min}}(x) = F'_{X_{\min}}(x) = \frac{N_c}{2} e^{-\frac{x}{2}N_c}, \tag{C.7}$$

and $Z = N_c X_{min}$ has the following PDF

$$f_Z(z) = f_{X_{\min}}(x)\,|_{x=z/N_c} \left|\frac{dx}{dy}\right| = \frac{e^{-\frac{z}{2}}}{2}, \tag{C.8}$$

which is the same expression that in eq. (C.1). □

Appendix D

Recapitulación

D.1 Motivación

Los sistemas de comunicaciones móviles e inalámbricas de la próxima generación facilitarán la provisión de servicios multimedia avanzados de manera ubicua gracias a las elevadas velocidades de transmisión ofrecidas. Para ello, es necesario que las tecnologías de transmisión empleadas sean capaces de resolver los problemas derivados de la transmisión de altas tasas de datos sobre canales limitados en ancho de banda y potencia.

Hasta el momento, OFDM (*Frequency-Division Multiplexing*) ha sido la técnica de transmisión más empleada debido a su robustez frente a canales con desvanecimientos selectivos en frecuencia. Sin embargo, esta tecnología sufre de una alta tasa de potencia pico a potencia media (*Peak-to-Average Power Ratio*, PAPR), una característica no deseable para la transmisión en el enlace ascendente ya que son necesarios costosos amplificadores de potencia en los terminales de usuario. Esta problemática también aparece cuando se combina esta tecnología con acceso múltiple en OFDMA (*Orthogonal Frequency-Division Multiple Access*).

Recientemente SC-FDMA (*Single Carrier Frequency-Division Multiple Access*)

se ha convertido en una atractiva alternativa a OFDMA debido a su baja PAPR. Esta característica ha hecho que fuera elegida para su implantación en el enlace ascendente de la especificación *Long Term Evolution* (LTE) [3GPP 08] del *3rd Generation Partnership Project* (3GPP). Se puede describir esta técnica como una versión de OFDMA en la que las etapas de precodificación y precodificación inversa se añaden respectivamente al transmisor y al receptor. La reducción de la PAPR en la transmisión en el enlace ascendente se traduce en una relajación en las restricciones en cuanto a eficiencia de potencia en los terminales de usuario y, por tanto, en una menor coste de fabricación de los mismos.

El objetivo de esta tesis es realizar un análisis matemático de las prestaciones de SC-FDMA en términos de tasa de error de bit (*Bit Error Rate*, BER) y eficiencia espectral cuando se emplea esta tecnología para transmitir sobre un canal con desvanecimientos selectivos en frecuencia.

D.2 Técnicas para el análisis de la BER

En la literatura se pueden encontrar diferentes aproximaciones para calcular la BER a partir del símbolo recibido tras la ecualización eq. (D.3.1.1) en sistemas de comunicaciones digitales coherentes. La más clásica se basa en promediar la BER condicionada, que normalmente implica la función $Q(\ )$ [Abramowitz 64], sobre la función densidad de probabilidad (*Probability Density Function*, PDF) de la relación señal a ruido instantánea (*Signal to Noise Ratio*, SNR) por bit $f_\gamma(\gamma)$.

$$BER = \int_0^\infty Q(a\sqrt{\gamma}) f_\gamma(\gamma) d\gamma, \tag{D.2.0.1}$$

donde a es una constante que depende de la combinación de esquemas de modulación y detección específica [Simon 05]. El principal inconveniente de este método es que normalmente no permite obtener una expresión cerrada para la BER media.

Otro método elegante consiste en usar la función generadora de momentos (*Moment Generating Function*, MGF) de la SNR condicionada a la respuesta del canal [Simon 98b]. A partir de una expresión alternativa para la función $Q(\ )$, permite obtener una representación integral de la BER condicional [Simon 05]

$$BER = \frac{1}{\pi} \int_0^{\pi/2} M_\gamma \left(\frac{-a}{2 \sin^2 \theta} \right) d\theta, \tag{D.2.0.2}$$

donde $M_\gamma(\ )$ es la MGF de $f\gamma$.

Este último método permite llegar a expresiones de la BER media que implican una sola integral finita cuyo integrando contiene sólo funciones elementales y que puede evaluarse computacionalmente con facilidad [Simon 98a].

Sin embargo, no siempre es posible derivar una expresión de la MGF para la SNR instantánea. Uno de los objetivos de esta tesis es proponer un método que pueda ser aplicado en estos casos. Para ello se emplea en esta tesis el método propuesto en [López-Martínez 10] con el cual es posible obtener expresiones cerradas para la BER con QAM multinivel (M-QAM). Este método asume que se realiza un mapeado independiente de bit para las componentes en fase y en cuadratura como ocurre, por ejemplo, cuando se emplea codificación Gray. La expresión general para la BER puede simplificarse si el ruido complejo que afecta al símbolo recibido en la etapa de decisión es circularmente simétrico ya que, en ese caso, solo se necesita la distribución marginal de su parte real (o de su parte imaginaria).

La expresión de la BER resulta

$$BER = \sum_{n=1}^{L-1} w(n) I(n), \tag{D.2.0.3}$$

donde $I(n)$ son los llamados Componentes de Probabilidad de Error (*Components of Error Probability*, CEP), $w(n)$ son coeficientes que dependen del mapeo de la constelación, $L = 2$ para BPSK, y $L = \sqrt{M}$ para M-QAM. Es posible expresar los CEPs en función de la distribución de probabilidad (*Cumulative Distribution*

Function, CDF) del ruido que afecta la señal en la etapa de decisión F_{η_r}, esto es,

$$I(n) = Pr\{\Re\{\eta\} > (2n-1)d\} = 1 - F_{\eta_r}((2n-1)d) \tag{D.2.0.4}$$

donde d es la distancia máxima entre cada símbolo y la frontera de decisión (p.ej., $d = \sqrt{E_s}$ para BPSK y $d = \sqrt{\frac{3E_s}{2\,(M-1)}}$ para M-QAM), y los coeficientes $w(n)$ se pueden calcular directamente [López-Martínez 10].

La expresión final depende de la CDF de la parte real (o imaginaria) del ruido complejo que afecta a la señal recibida en la etapa de detección. Así, esta tesis se centra en el estudio de la naturaleza estocástica de dicho ruido complejo a partir del cual es posible derivar funciones con las que evaluar las distribuciones requeridas en (D.2.0.4) para diferentes canales con desvanecimiento.

D.3 Análisis de la BER en OFDMA

El primer objetivo de esta tesis es estudiar la distribución de probabilidad del ruido mejorado tras realizar un ecualización lineal en el dominio de la frecuencia en OFDMA. Con este propósito se deriva la densidad del ruido resultante tras ecualizar para compensar los efectos de canales con desvanecimientos Rayleigh, Rice y Nakagami-μ. A partir de estas densidades es posible derivar la expresión de la BER para una transmisión sin codificación de canal.

El análisis se centra en la ecualización zero-forcing en el dominio de la frecuencia (*Zero-Forcing Frequency Domain Equalization*, ZF-FDE) ya que los resultados obtenidos para MMSE-FDE (*Minimum Mean Square Error* FDE) en cuanto a rendimiento son similares en ambos casos aunque, en este último, el error cuadrático medio es menor. Tanto en [Wang 04] como en la sección 4.2.3 de [Wang 05] se proporciona una justificación detallada de este comportamiento.

Tras una extensiva búsqueda bibliográfica, el autor ha encontrado que existe muy

poca literatura en la que se realicen análisis similares. Solo en [Aghamohammadi 90], [Shayesteh 95] y [Wilson 99], en los que se obtiene la densidad de probabilidad para señales moduladas linealmente sobre canales Rayleigh y Rice, puede encontrarse un estudio similar. Además, la literatura concerniente al rendimiento de OFDM sobre canales con desvanecimiento selectivo tipo Nakagami-μ no es abundante y se centra principalmente en expresiones semi-analíticas ([Count 01], [Subotic 07]). Los resultados de este análisis se usan para obtener expresiones cerradas para la BER en un sistema OFDM.

D.3.1 Modelo de sistema para OFDMA

En la Fig. D.1 se muestra el diagrama de bloques simplificado para un sistema OFDM en el cual el ancho de banda disponible se divide en sub-portadoras ortogonales. En OFDMA, la secuencia de símbolos modulados complejos x se mapea en paralelo sobre el subconjunto de sub-portadoras asignadas al usuario mientras que el resto se fuerzan a cero.

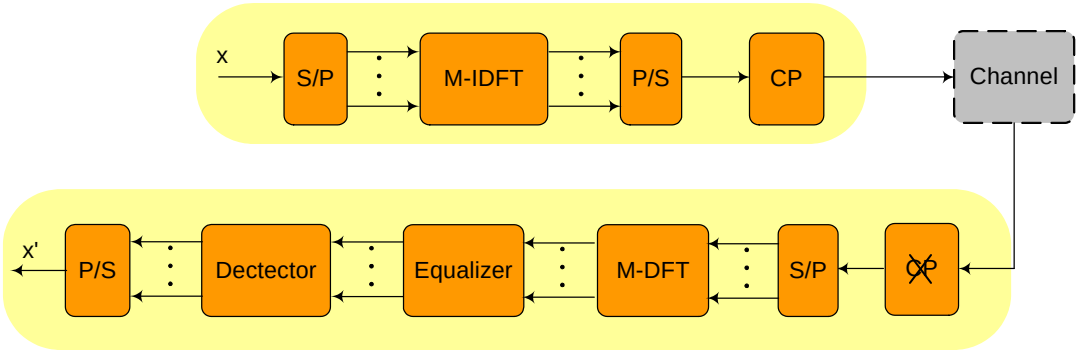

Figure D.1: Transmisor y receptor OFDM

Debido a las operaciones duales de transformada discreta de Fourier inversa (*Inverse Discrete Fourier Transform*, IDFT) y transformada de Fourier discreta (*Discrete Fourier Transform*, DFT), realizadas en el transmisor y en el receptor respectivamente, y a la adición del prefijo cíclico la señal recibida se puede expresar como una versión de la transmitida tras ser transformada por la respuesta del canal

y contaminada con ruido AWGN (*Additive White Gaussian Noise*).

$$\mathbf{r} = \mathbf{Hx} + \boldsymbol{\eta}, \tag{D.3.1.1}$$

donde $\mathbf{H}$ es una matrix diagonal de tamaño NxN cuyos elementos h_k $(k = 1, \ldots, N)$ son las respuestas en frecuencia del canal, $\boldsymbol{\eta}$ es un vector con las componentes de ruido complejo AWGN para cada sub-portadora η_k. La variable aleatoria compleja correspondiente a la respuesta en frecuencia del canal para una portadora específica h_k se supone de media cero y con potencia normalizada mientras que los términos de ruido tienen media cero y varianza N_0. Tanto η_k como h_k son variables aleatorias con simetría circular [Gubner 06].

Para el sistema analizado, la señal recibida es la suma de todos los caminos de visibilidad directa (*Line of Sight*, LOS) y todas las componentes multicamino resolubles. En este estudio solo se considera el desvanecimiento multicamino debido a las combinaciones constructivas y destructivas de versiones retardadas, reflejadas, dispersadas y difractadas de la señal transmitida. Este tipo de desvanecimiento es relativamente rápido y es responsable de las variaciones a corto plazo de señal.

Tres diferentes escenarios son considerados en esta sección dependiente de que distribución siga el desvanecimiento rápido: Rayleigh, Rice o Nakagami-μ. Tanto la distribución de Rayleigh como la de Rice se basan en modelos matemáticos que capturan el comportamiento subyacente los canales reales. Se emplean para modelar el desvanecimiento multicamino (sin y con visibilidad directa, respectivamente) [Simon 05]. La distribución Nakagami-μ aventaja a las anteriores ya que se ajusta mejor a resultados basados en medidas empíricas [Goldsmith 05] por lo que es utilizada con frecuencia [Beaulieu 05].

En este punto debe tenerse en cuenta que la transformada Fourier preserva la normalidad de las variables [Ghosh 69] al tratarse de una transformación lineal. De este modo, si las variables aleatorias subyacentes a la respuesta al impulso del canal son gaussianas, las correspondientes a la respuesta en frecuencia del canal siguen la

misma distribución. Por ejemplo, para canales con desvanecimiento Rayleigh, las variables subyacentes para la respuesta en frecuencia son gaussianas complejas de media cero y varianza unidad [Ohno 04]. Para canales con desvanecimiento Rice, las gaussianas complejas no tienen media cero. Por otro lado, en canales selectivos en frecuencia con una distribución Nakagami-μ, el módulo de la respuesta en frecuencia se puede aproximar como variables aleatorias que también siguen una distribución Nakagami-μ aunque los parámetros de la misma pueden ser diferentes [Kang 03].

D.3.2 Análisis de ruido para ZF-FDE

En un sistema de comunicaciones basado en OFDM, la ecualización ZF-FDE conlleva el cociente entre dos variables aleatorias complejas: la correspondiente al AWGN en el receptor y la correspondiente a la respuesta en frecuencia del canal. Esta última depende de la naturaleza de la propagación multicamino; en este estudio se considera los casos de distribuciones Rayleigh, Rice o Nakagami-μ.

Tras realizar la ecualización ZF-FDE y asumiendo un conocimiento ideal de la respuesta en frecuencia del canal, la expresión para el símbolo recibido se puede derivar de (D.3.1.1) como

$$\hat{\mathbf{x}} = \mathbf{x} + (\mathbf{H}^H\mathbf{H})^{-1}\mathbf{H}^H\eta \tag{D.3.2.2}$$

La expresión para el k-ésimo símbolo recibido resulta

$$\hat{x}_k = x_k + \frac{\eta_k}{h_k} = x_k + \hat{\eta}_k, \tag{D.3.2.3}$$

donde h_k es la respuesta en frecuencia del canal para la sub-portadora k.

El término de ruido mejorado $\hat{\eta}_k$ es el cociente entre dos variables aleatorias complejas independientes e idénticamente distribuidas (i.i.d.) con simetría circular. El subíndice k es omitido de aquí en adelante para lograr una mayor claridad en las expresiones.

Canal con desvanecimiento Rayleigh

Para un canal con desvanecimiento Rayleigh la densidad de probabilidad del término de ruido mejorado $\hat{\eta}$ se puede expresar como

$$f_{\hat{\eta}}(r,\theta) = \frac{1}{\pi}\frac{\sigma^2 r}{\left(\sigma^2 + r^2\right)^2} \qquad r \in \mathbb{R}\ ,\ r \geq 0. \tag{D.3.2.4}$$

En coordenadas cartesianas la densidad de probabilidad resulta

$$f_{\hat{\eta}_r,\hat{\eta}_i}(x,y) = \frac{1}{\pi}\frac{\sigma^2}{\left(\sigma^2 + (x^2+y^2)\right)^2} \qquad x,y \in \mathbb{R}, \tag{D.3.2.5}$$

donde $\hat{\eta}_r$ y $\hat{\eta}_i$ son las componentes real e imaginaria del término elemental de ruido.

La expresión eq. (D.3.2.5) es la función de densidad de probabilidad de una Student t bivariable con 2 grados de libertad, media $(0,0)$, matrix de escalado $\frac{\sigma^2}{2}I_2$, donde I_2 es la matrix identidad de tamaño 2.

La densidad de probabilidad de las componentes reales e imaginarias son idénticas y vienen dadas por

$$f_{\hat{\eta}_r}(x) = f_{\hat{\eta}_i}(x) = \frac{1}{2}\frac{\sigma^2}{\left(\sigma^2 + x^2\right)^{3/2}} \qquad x \in \mathbb{R}. \tag{D.3.2.6}$$

Se trata de una distribución de cola pesada cuyas colas decaen siguiendo una ley de potencia x^{-3} y tiene varianza infinita.

La CDF marginal correspondiente a $\hat{\eta}_r$ resulta

$$F_{\hat{\eta}_r}(x) = \frac{1}{2} + \frac{x}{2\sqrt{x^2+\sigma^2}} \qquad x \in \mathbb{R}. \tag{D.3.2.7}$$

y función característica (*Characteristic Function*, CHF) puede expresarse por

$$\Psi_{\hat{\eta}_r}(\omega) = \sigma|\omega| K_1(\sigma|\omega|) \qquad \omega \in \mathbb{R}, \tag{D.3.2.8}$$

donde $|\omega|$ es el valor absoluto de ω y $K_1(\ )$ es la función modificada de Bessel de segunda especie y primer orden [Bocher 92].

Canal con desvanecimiento Rice

Para un canal con desvanecimiento Rice la densidad del ruido mejorado $\hat{\eta}$ puede expresarse como

$$f_{\hat{\eta}}(r) = \frac{r\sigma\left(\alpha^2\sigma + 2\left(\sigma + r^2\right)\right)}{2\pi\left(\sigma + r^2\right)^3} e^{-\frac{\alpha^2 r^2}{2(\sigma + r^2)}} \qquad r \in \mathbb{R}\ ,\ r \geq 0. \tag{D.3.2.9}$$

donde $\sigma^2 = \dfrac{N_0}{E_s}$. Para $\alpha = 0$ la expresión se convierte en la derivada en la sección previa (D.3.2.4).

De nuevo con un cambio a coordenadas cartesianas, se puede expresar la densidad anterior en función de las componentes reales e imaginarias del término de ruido $\hat{\eta}_r$ y $\hat{\eta}_i$ como

$$f_{\hat{\eta}_r,\hat{\eta}_i}(x,y) = \frac{(x^2+y^2)\alpha^2\sigma + 2\left((x^2+y^2)\sigma + 1\right)}{2\pi\left((x^2+y^2)\sigma + 1\right)^3} \sigma e^{-\frac{\alpha^2}{2((x^2+y^2)\sigma+1)}} \qquad x, y \in \mathbb{R}. \tag{D.3.2.10}$$

Se trata de nuevo de una variable aleatoria circularmente simétrica. En este caso los autores no tienen conocimiento de que sea posible encontrar una expresión cerrada para las distribuciones marginales. Sin embargo, sí que es posible evaluar la CDF mediante integración numérica de la siguiente expresión,

$$F_{\hat{\eta}_r}(t) = F_{\hat{\eta}_i}(t) = \int_{-\infty}^{t}\int_{-\infty}^{\infty} f_{\hat{\eta}_r,\hat{\eta}_i}(x,y)dydx \qquad x, y \in \mathbb{R}. \tag{D.3.2.11}$$

Este método de cálculo es similar al propuesto en [Shayesteh 95] para obtener la función de densidad de señales moduladas linealmente transmitidas sobre canales con desvanecimiento Rice. Debido a la necesidad de realizar una doble integral numérica y a los errores que dicha operación puede acarrear, se ha descartado emplear esta expresión para realizar el análisis de BER para canales con desvanecimiento Rice.

Canal con desvanecimiento Nakagami-μ

Si el canal sigue un desvanecimiento en frecuencia tipo Nakagami-μ, la densidad de probabilidad en coordenadas polares del ruido mejorado $\hat{\eta}$ puede expresarse como

$$f_{R_{\hat{\eta}},\Phi_{\hat{\eta}}}(r,\phi) = \frac{1}{2\pi}\frac{\mu^{\mu+1}}{\sigma^2} r \left(\frac{r^2}{2\sigma^2}+\mu\right)^{-1-\mu} \qquad r \in \mathbb{R}\ y\ r \geq 0, \tag{D.3.2.12}$$

donde $\sigma = \dfrac{N_0}{E_s}$.

Es fácil comprobar cómo para $\mu = 1$ la expresión coincide con la obtenida para desvanecimientos tipo Rayleigh.

La PDF conjunta en coordenadas cartesianas resulta

$$f_{\hat{\eta}_r,\hat{\eta}_i}(x,y) = \frac{\mu^{\mu+1}}{2\pi\sigma^2}\left(\frac{x^2+y^2}{2\sigma^2}+\mu\right)^{-1-\mu} \qquad x,y \in \mathbb{R}, \tag{D.3.2.13}$$

donde de nuevo $\hat{\eta}_r$ y $\hat{\eta}_i$ son las componentes reales e imaginarias del término de ruido elemental. En este caso se trata de una variable aleatoria con distribución Pearson tipo VII. Las densidades marginales correspondientes resultan

$$f_{\hat{\eta}_r}(x) = f_{\hat{\eta}_i}(x) = \sqrt{\frac{1}{\pi}}\frac{\Gamma\left(\mu+\frac{1}{2}\right)2^{\mu}\mu^{\mu}\sigma^{2\mu}}{\Gamma(\mu)\left(2\mu\sigma^2+z^2\right)^{\mu-\frac{1}{2}}} \qquad z \in \mathbb{R}, \tag{D.3.2.14}$$

donde $\Gamma(n)$ es la denominada función Gamma [Abramowitz 64].

La densidad marginal anterior tiene media cero y varianza $\sigma^2_{\hat{\eta}_r} = \dfrac{\mu\sigma^2}{\mu-1}$ siempre que $\mu > 1$. Si $\mu \leq 1$ no tiene varianza finita ni momentos de orden superior y, por tanto, no tiene MGF. No obstante, no sucede lo mismo con su CHF que puede expresarse como

$$\Psi_{\hat{\eta}_r}(\omega) = \frac{\sigma^{\mu}|\omega|^{\mu}}{2^{\mu/2-1}\Gamma(\mu)}\mu^{\mu/2}K_{\mu}\left(\sigma\sqrt{2\mu}|\omega|\right) \qquad \omega \in \mathbb{R}, \tag{D.3.2.15}$$

donde $|\omega|$ es el valor absoluto de ω y $K_{\mu}(\ )$ es la función modificada de Bessel de segunda especie y orden μ-ésimo [Bocher 92].

La CDF correspondiente vienen dada por

$$F_{\hat{\eta}_r}(x) = \frac{(-1)^{-\mu}\Gamma\left(\mu+\frac{1}{2}\right)}{2\sqrt{\pi}\Gamma(\mu)}B_{-\frac{2\mu\sigma^2}{x^2}}\left(\mu,\frac{1}{2}-\mu\right) \qquad x \in \mathbb{R}, \tag{D.3.2.16}$$

donde $B(\ )$ es la función incompleta de Beta [Abramowitz 64].

D.3.3 Valores de la BER

Combinando las expresiones (D.3.2.7) y (D.2.0.4) es posible calcular las CEPs para un canal con desvanecimiento Rayleigh y, partir de ellos, se puede expresar la BER como

$$BER = \sum_{n=1}^{L-1} w(n) \left(\frac{1}{2} - \frac{2n-1)d}{2\sqrt{(2n-1)d)^2 + \sigma^2}} \right). \qquad \text{(D.3.3.17)}$$

De manera similar se obtiene una expresión para canales con desvanecimiento Nakagami-μ que viene dada por

$$BER = \sum_{n=1}^{L-1} w(n) \left(1 - \frac{(-1)^{-\mu}\Gamma\left(\mu + \frac{1}{2}\right)}{2\sqrt{\pi}\Gamma(\mu)} B_{-\frac{2\mu\sigma^2}{((2n-1)d)^2}} \left(\mu, \frac{1}{2} - \mu \right) \right). \qquad \text{(D.3.3.18)}$$

Como ya fue mencionado antes, el análisis de la BER para canales con desvanecimiento Rice es omitido al no ser posible obtener expresiones cerradas para las PDF marginales.

Las expresiones anteriores han sido validadas mediante simulaciones para canales con desvanecimiento Nakagami para los cuales la respuesta en frecuencia sigue una distribución Nakagami-μ con valores enteros y semienteros de μ. En la Fig. D.2 se presentan los resultados para diferentes valores de μ; para $\mu = 1$ los resultados coinciden con los de un canal con desvanecimiento Rayleigh. Para $\mu < 1$ los valores de la BER empeoran respecto a los obtenidos para Rayleigh mientras que para $\mu > 1$ se obtienen valores menores de la BER. El mismo comportamiento se produce para constelaciones más densas como puede observarse en Fig. D.3 y D.4 para 4QAM y 16QAM respectivamente.

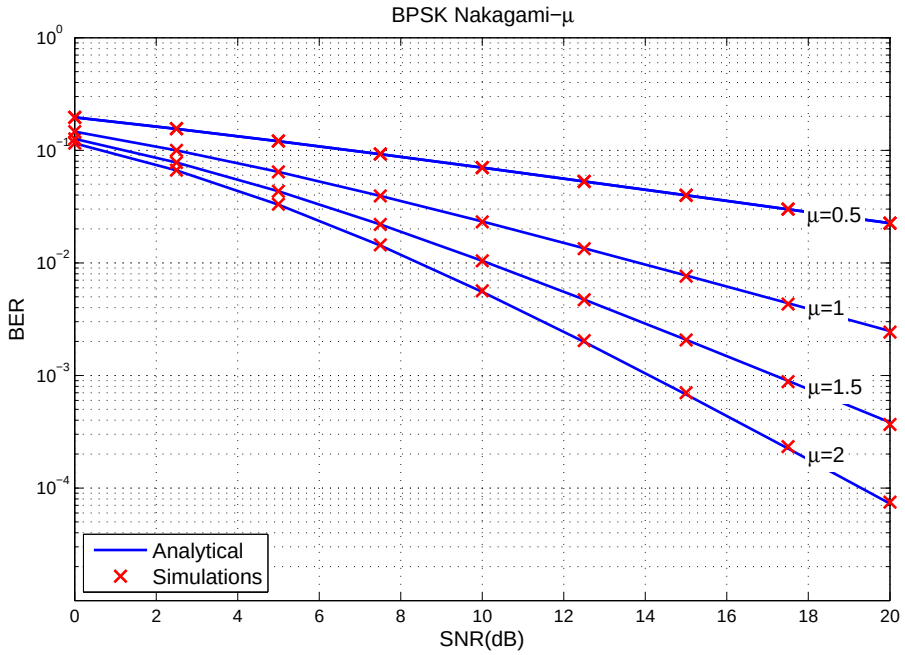

Figure D.2: Valores de BER para diferentes canales con desvanecimiento Nakagami-μ, incluido el caso Rayleigh ($\mu = 1$), para BPSK

D.4 Análisis de la BER en SC-FDMA

A partir de los resultados obtenidos en la sección anterior, es posible analizar el rendimiento en términos de BER de una transmisión SC-FDMA sin codificación de canal sobre un canal con desvanecimiento Nakagami. Estos resultados incluyen los correspondientes a un desvanecimiento Rayleigh como caso particular.

El análisis permite obtener expresiones cerradas para aproximar la BER que son validadas mediante simulaciones para el escenario analizado. También se comprueba su validez para aproximar valores reales de BER obtenidos para diferentes canales con desvanecimiento Rayleigh propuestos por la ITU [ITU-R 97] y el 3GPP [3GPP 10].

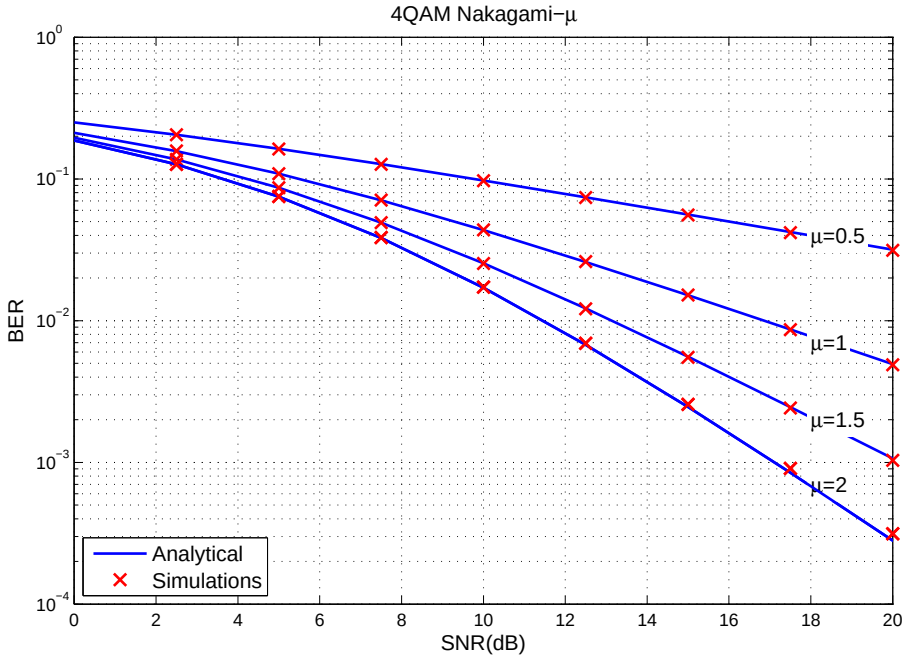

Figure D.3: Valores de BER para diferentes canales con desvanecimiento Nakagami-μ, incluido el caso Rayleigh ($\mu = 1$), para 4QAM

D.4.1 Modelo de sistema SC-FDMA

El proceso de transmisión en SC-FDMA es similar al de OFDMA como se muestra en la Fig. D.5. Para un usuario determinado, se mapea la secuencia de bits transmitidos a una constelación de símbolos complejos (p.ej., BPSK o M-QAM). La secuencia compleja resultante $\mathbf{x}$ es transformada por un bloque de precodificación, consistente en una DFT, antes de ser mapeado sobre el subconjunto de N_c portadoras asignadas. Para un vector de información de N_c símbolos complejos $\mathbf{x}$, el símbolo complejo precodificado $\mathbf{X_{N_c}}$ se obtienen multiplicando por la matrix unitaria de Fourier $\mathbf{F}$ que realiza la N_c-DFT antes mencionada. Cada elemento en $\mathbf{F}$ se define como $F_{j,k} = e^{\frac{2\pi i}{N_c}jk}/\sqrt{N_c}$ con $\mathbf{F}\mathbf{F}^H = \mathbf{I}$.

La precodificación supone la mayor diferencia entre SC-FDMA y OFDMA, ya que los símbolos complejos se transmite ahora de forma secuencial en lugar de en paralelo. La secuencia precodificada, representada por el vector columna $\mathbf{X_{N_c}}$, es

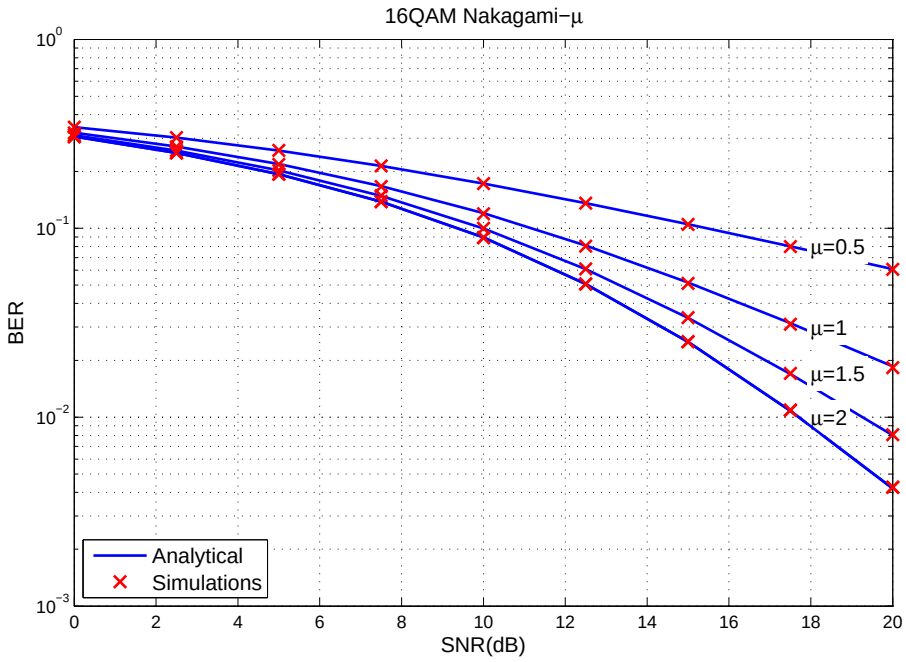

Figure D.4: Valores de BER para diferentes canales con desvanecimiento Nakagami-μ, incluido el caso Rayleigh ($\mu = 1$), para 16QAM

mapeada en el subconjunto de sub-portadoras asignadas, es decir, sobre N_c de las M sub-portadoras que componen el ancho de banda total del sistema. El subconjunto puede consistir en un grupo de sub-portadoras adyacentes (*Localized Frequency Domain Multiple Access*, LFDMA) o entrelazadas (*Interleaved FDMA*, IFDMA) [Myung 06] y es determinado por la matrix de mapeo $\mathbf{L}$ de tamaño $M \times N_c$ para la cual $L_{i,j} = 1$ si el símbolo precodificado j es transmitido sobre la sub-portadora i y cero en otro caso.

El símbolo en el dominio de la frecuencia es definido como $\mathbf{X_M} = \mathbf{LX_{N_c}}$; en consecuencia, las sub-portadoras no asignadas son forzadas a cero. A partir de este punto, el proceso de transmisión es similar al de OFDMA: mediante una M-IDFT se convierte cada símbolo en el dominio de la frecuencia $\mathbf{X_M}$ en un símbolo en el dominio del tiempo al que posteriormente se le añade un prefijo cíclico. La longitud de este prefijo debe ser mayor que la respuesta al impulso del canal para evitar la interferencia intersimbólica (*InterSymbol Interference*, ISI).

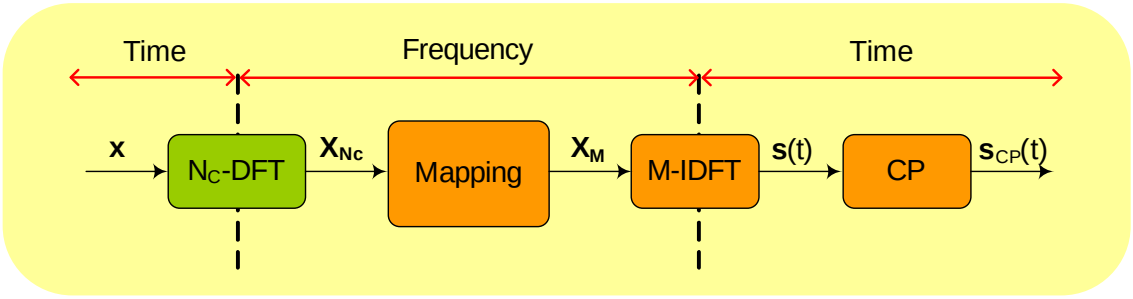

(a) Transmisor SC-FDMA

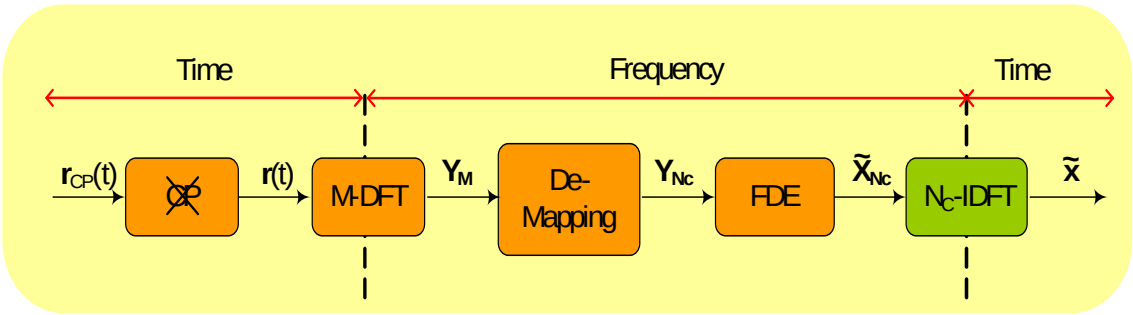

(b) Receptor SC-FDMA

Figure D.5: Esquemas de transmisor y receptor para SC-FDMA

En esta disertación, se asume una canal selectivo en frecuencia Nakagami-μ, para el cual el módulo de los caminos que componen las respuesta al impulso $|h(n)|$, $n = 1, \ldots, L-1$, se modelan como variables aleatorias Nakagami-μ i.i.d. cuya función de densidad de probabilidad viene dada por

$$f_{|h(n)|}(x) = \frac{2}{\Gamma(\mu_n)} \left(\frac{\mu_n}{\Omega_n}\right)^{\mu_n} x^{2\mu_n - 1} e^{-\frac{x^2 \mu_n}{\Omega_n}} \qquad x \in \mathbb{R}\ y\ x \geq 0, \tag{D.4.1.1}$$

donde para el n-ésimo camino $\mu_n > 1/2$ es el parámetro que determina el desvanecimiento y Ω_n la potencia. A lo largo de esta tesis, se asume un perfil de intensidad multicamino exponencial con una tasa de decaimiento δ ($\Omega_n = \Omega_t e^{-\delta n}$) y el mismo factor de desvanecimiento μ_t para todos los caminos.

En el receptor (see Fig. D.5b) se asume que, gracias a una estimación perfecta del canal y a que el sistema está sincronizado, se evitan interferencias entre usuarios. Tras suprimir la parte correspondiente al prefijo cíclico, el símbolo en el dominio del tiempo es convertido mediante una M-DFT en un símbolo en el dominio de la

frecuencia $\mathbf{Y_M}$. Se aplica entonces la matrix $\mathbf{L}^H$ para realizar el demapeo y las N_c sub-portadoras asignadas $\mathbf{Y_{N_c}}$ en el receptor pueden expresarse como

$$\mathbf{Y_{N_c}} = \mathbf{L}^H\mathbf{H_M}\mathbf{LFx} + \mathbf{L}^H\boldsymbol{\eta_M}, \tag{D.4.1.2}$$

donde $\boldsymbol{\eta_M}$ es el vector de ruido cuyas entradas son variables aleatorias gaussianas complejas $\mathcal{CN}(0, N_0)$ i.i.d. y la respuesta en frecuencia del canal para cada sub-portadora está representada por la matrix diagonal $\mathbf{H_M}$ de tamaño $M \times M$ cuyos elementos son variables aleatorias complejas y circularmente simétricas [Kang 03]. El módulo de la respuesta en frecuencia puede aproximarse con una distribución Nakagami-μ con parámetros μ y Ω; dichos parámetros son en general diferentes de aquellos de sus homólogos en el dominio del tiempo [Nakagami 58]. Para un canal plano $\mu = \mu_t$, mientras que si $\mu_t \geq 1$ entonces $1 \leq \mu < \mu_t$, y si $1/2 \leq \mu_t < 1$ entonces $1 > \mu > \mu_t$ [Kang 03]. Aunque se ha demostrado que esta aproximación tiene limitaciones para canales con dos caminos [Du 06], se puede considerar válida para casos más generales y es una suposición habitual [Wang 07]. Para un canal con desvanecimiento Rayleigh (es decir, con $\mu = 1$), la aproximación es exacta para cualquier valor de L.

La expresión para el símbolo recuperado en el dominio de la frecuencia tras la ecualización FDE $\widetilde{\mathbf{X}}_{\mathbf{N_c}}$ resulta

$$\widetilde{\mathbf{X}}_{\mathbf{N_c}} = \mathbf{W}\mathbf{Y_{N_c}} = \mathbf{WHFx} + \mathbf{WL}^H\boldsymbol{\eta_M}, \tag{D.4.1.3}$$

donde $\mathbf{H} = \mathbf{L}^H\mathbf{H_M}\mathbf{L}$ es una matrix diagonal de tamaño $N_c \times N_c$ cuyos elementos no nulos $\mathbf{h} = diag(\mathbf{H})$ son las respuestas en frecuencia del canal para cada una de las sub-portadoras asignadas y $\boldsymbol{\eta} = \mathbf{L}^H\boldsymbol{\eta_M}$ es un vector con los valores de ruido complejo correspondientes. Los elementos de $\mathbf{h}$ se asume que son variables aleatorias complejas i.i.d.; tal asunción es válida siempre que la separación entre sub-portadoras asignadas de manera consecutiva sea mayor que el ancho de banda de coherencia del canal con desvanecimientos considerado.

La matrix de ecualización $\mathbf{W}$ tiene tamaño $N_c \times N_c$ y se define para ZF-FDE

como

$$\mathbf{W}_{ZF} = (\mathbf{H}^H\mathbf{H})^{-1}\mathbf{H}^H, \tag{D.4.1.4}$$

mientras que para MMSE-FDE resulta

$$\mathbf{W}_{MMSE} = \left(\frac{N_0}{E_S}\mathbf{I} + \mathbf{H}^H\mathbf{H}\right)^{-1}\mathbf{H}^H, \tag{D.4.1.5}$$

donde E_S y N_0 son la potencia de señal y de ruido respectivamente.

Previamente a la etapa de detección, se realiza una precodificación inversa mediante una N_c-IDFT. De este modo, para ZF-FDE, el símbolo ecualizado se puede expresar en el dominio del tiempo como

$$\widetilde{\mathbf{x}} = \underbrace{\mathbf{F}^H}_{\text{Precoding Inverso}}\underbrace{(\mathbf{H}^H\mathbf{H})^{-1}\mathbf{H}^H}_{\text{FDE}}\mathbf{H}\mathbf{F}\mathbf{x} + \underbrace{\mathbf{F}^H}_{\text{Precoding Inverso}}\underbrace{(\mathbf{H}^H\mathbf{H})^{-1}\mathbf{H}^H}_{\text{FDE}}\boldsymbol{\eta}, \tag{D.4.1.6}$$

mientras que para MMSE resulta

$$\widetilde{\mathbf{x}} = \underbrace{\mathbf{F}^H}_{\text{Precoding Inverso}}\underbrace{\left(\frac{N_0}{E_S}\mathbf{I} + \mathbf{H}^H\mathbf{H}\right)^{-1}\mathbf{H}^H}_{\text{FDE}}\mathbf{H}\mathbf{F}\mathbf{x} + \underbrace{\mathbf{F}^H}_{\text{Precoding Inverso}}\underbrace{\left(\frac{N_0}{E_S}\mathbf{I} + \mathbf{H}^H\mathbf{H}\right)^{-1}\mathbf{H}^H}_{\text{FDE}}\boldsymbol{\eta}. \tag{D.4.1.7}$$

Para MMSE-FDE, la expresión para el k-ésimo símbolo recibido viene dada por

$$\widetilde{x}_k = x_k + \sum_{j=1}^{N_c}\frac{F_{j,k}^*}{h_j}\eta_j = x_k + \sum_{j=1}^{N_c}\hat{\eta}_{j,k} = x_k + \tilde{\eta}_k \tag{D.4.1.8}$$

donde $\hat{\eta}_{j,k} = \dfrac{F_{j,k}^*\eta_j}{h_j}$.

Puede observarse que, tras la ecualización ZF-FDE, cada símbolo recibido es el resultado de añadir un término de ruido efectivo $\tilde{\eta}_k$ al símbolo transmitido originalmente (eq. (D.4.1.8)). Por tanto, cuando se aplica ZF-FDE, el ruido efectivo es la suma de términos de ruido elementales $\hat{\eta}_{j,k}$ (ruido mejorado) para cada subportadora asignada, siendo cada uno de esos términos elementales equivalente al ruido mejorado en OFDM cuando se aplica ZF-FDE.

Para MMSE-FDE, la expresión en el dominio del tiempo para el k-ésimo símbolo recibido tras la ecualización resulta

$$\widetilde{x}_k = x_k T_{k,k} + \sum_{\substack{l \neq k \\ l=1}}^{N_c} x_l T_{k,l} + \sum_{j=1}^{N_c} \frac{F_{j,k}^* h_j^*}{|h_j|^2 + N_0/E_S} \eta_j \tag{D.4.1.9}$$

donde los elementos de $\mathbf{T} = \mathbf{F}^H \mathbf{W}_{MMSE} \mathbf{H} \mathbf{F}$ pueden expresarse como

$$T_{k,l} = \frac{1}{N_c} \sum_{j=1}^{N_c} \frac{F_{k,j}^* F_{l,j} |h_j|^2}{|h_j|^2 + N_0/E_S}. \tag{D.4.1.10}$$

La principal diferencia entre esta expresión y (D.4.1.8) radica en que para MMSE-FDE existe, además de un término correspondiente al ruido, una componente de interferencia debido a los otros símbolos. Además, el símbolo recibido tras FDE se ve atenuado por el término $T_{k,k}$. Cuando la respuesta en frecuencia del canal es tal que $\frac{\sigma_\eta^2}{\sigma_s^2} \ll |h_j|^2$, el término de interferencia desaparece y el de ruido es igual al correspondiente a (D.4.1.8). Tras compensar el símbolo recibido, se obtiene el símbolo transmitido contaminado por los términos correspondientes al ruido equivalente $\tilde{\eta}_k$ y a la interferencia δ_k

$$\hat{x}_k = x_k + \underbrace{T_{k,k}^{-1} \sum_{\substack{l \neq k \\ l=1}}^{N_c} x_l T_{k,l}}_{\text{Interferencia Efectiva}} + \underbrace{T_{k,k}^{-1} \sum_{j=1}^{N_c} \frac{F_{j,k}^* h_j^*}{|h_j|^2 + N_0/E_S} \eta_j}_{\text{Ruido Efectivo}} = x_k + \delta_k + \tilde{\eta}_k = x_k + \xi_k, \tag{D.4.1.11}$$

donde el término ξ_k recoge los efectos del ruido y la interferencia que son inherentemente independientes [Nisar 07].

D.4.2 Caracterización del ruido efectivo para ZF-FDE

Antes se demostró que el ruido efectivo tras ZF-FDE es el resultado de la suma de varios términos de ruido elemental, cada uno de ellos es una variable aleatoria compleja que sigue una distribución Pearson tipo VII. En la sección 3.4.1, se obtuvo la siguiente expresión para calcular la PDF de la suma de variables Pearson type

VII independientes

$$f_{\tilde{\eta}_r}(x) = \frac{1}{2\pi}\int_{-\infty}^{\infty}\left(\frac{\sigma^{\mu}|\omega|^{\mu}}{2^{1-\mu/2}\Gamma(\mu)}\mu^{\mu/2}K_{\mu}\left(\sigma\sqrt{2\mu}|\omega|\right)\right)^{N_c} e^{-j\omega x}d\omega. \qquad \text{(D.4.2.12)}$$

Para $N_c = 2$ es posible resolver la integral (D.4.2.12) y obtener la siguiente expresión analítica

$$p_{\tilde{\eta}_r}(x) = \frac{2^{-2\mu-\frac{1}{2}}\Gamma\left(\mu+\frac{1}{2}\right)\Gamma\left(2\mu+\frac{1}{2}\right)}{\sigma\Gamma(\mu)^2\Gamma(\mu+1)}\sqrt{\frac{1}{\mu}}\ {}_2F_1\left(\mu+\frac{1}{2}, 2\mu+\frac{1}{2}; \mu+1; -\frac{x^2 1}{8\mu\sigma^2}\right), \qquad \text{(D.4.2.13)}$$

donde ${}_2F_1(\ )$ es la función hipergeométrica gaussian (consultar 15.1.1 in [Abramowitz 64]).

También es posible calcular la CDF en este caso

$$F_{\tilde{\eta}_r}(x) = \frac{1}{2} + \frac{x\Gamma\left(\mu+\frac{1}{2}\right)\Gamma\left(2\mu+\frac{1}{2}\right)\sqrt{\frac{1}{\mu}}}{2^{2\mu+\frac{1}{2}}\sigma\Gamma(\mu)^2\Gamma(\mu+1)}\ {}_3F_2\left(\frac{1}{2}, \mu+\frac{1}{2}, 2\mu+\frac{1}{2}; \frac{3}{2}, \mu+1; \frac{-x^2 1}{8\mu\sigma^2}\right), \qquad \text{(D.4.2.14)}$$

donde ${}_3F_2(\ )$ es una particularización de la función geométrica generalizada ${}_pF_q$ [Daalhuis 10].

Aunque no sea posible obtener una expresión analítica de $F_{\tilde{\eta}_r}(x)$ para $N_c \geq 2$, es posible aplicar la fórmula del teorema de inversión propuesta por Gil-Peláez (ver seción 3.2.4) para evaluar dicha distribución como

$$F_{\tilde{\eta}_r}(x) = \frac{1}{2} + \frac{1}{2\pi}\int_0^{\infty}\frac{e^{ix\omega}\Psi_{\tilde{\eta}_r}(-\omega) - e^{-ix\omega}\Psi_{\tilde{\eta}_r}(\omega)}{i\omega}\,d\omega \qquad \text{(D.4.2.15)}$$

donde $\Psi_{\tilde{\eta}_r}(\omega)$ corresponde a la CHF definida en eq. (D.3.2.15).

En el caso particular de un canal con desvanecimiento Rayleigh, es posible particularizar la expresión anterior usando la CHF correspondiente a la distribución Student t (D.3.2.8); la expresión resultante es

$$f_{\tilde{\eta}_r}(\tilde{\eta}) = \frac{1}{2\pi}\int_{-\infty}^{\infty}\left(\sigma|\omega|K_1(\sigma|\omega|)\right)^{N_c} e^{-j\omega\tilde{\eta}}d\omega. \qquad \text{(D.4.2.16)}$$

En general, la evaluación de la eq. (D.4.2.16) requiere integración numérica. Sin embargo, es posible usar los resultados recogidos en el apéndice B para obtener el

siguiente resultado analítico para su evaluación con $N_c = 2$

$$f_{\tilde{\eta}_r}(\tilde{\eta}) = \frac{3\pi}{16\sqrt{2}\sigma}\,{}_2F_1\left(\frac{3}{2},\frac{5}{2};2;-\frac{x^2}{2\sigma^2}\right). \tag{D.4.2.17}$$

Se obtiene entonces una distribución de Behrens-Fisher (ver sección 3.4.1) que tiene también media cero y varianza infinita. También es posible obtener la siguiente expresión para la CDF correspondiente

$$F_{\tilde{\eta}_r}(x) = \frac{1}{2} + \frac{3\pi x}{16\sqrt{2}\sigma}\,{}_2F_1\left(\frac{1}{2},\frac{5}{2},2,-\frac{x^2}{2\sigma^2}\right). \tag{D.4.2.18}$$

Conviene reseñar que, aunque el ruido efectivo tras aplicar ZF-FDE es una suma de variables aleatorias independientes, no fue posible aplicar el CLT (consultar sección 3.5.1). Esto es debido a que canal con desvanecimientos Rayleigh (Nakagami-μ con $\mu = 1$) el ruido sigue una distribución Student t que no tiene varianza finita. Se recurrió entonces al GCLT. Para ello se estudió la cola de la distribución para determinar su exponente de decaimiento como

$$f_{\hat{\eta}_r}(x) = \frac{1}{2}\frac{\sigma^2}{(\sigma^2+x^2)^{3/2}} \simeq A|x|^{-(3)} \qquad |x| \to \infty, \tag{D.4.2.19}$$

Por tanto, el exponente característico resulta $\alpha = 2$. En la sección 3.5.2 se explicó como para $\alpha < 2$, la distribución de la suma entra en el dominio de atracción de las leyes estables. Sin embargo, no es posible determinar el dominio de atracción para el caso considerado ($\alpha = 2$).

D.4.3 Caracterización de Ruido e Interferencia para MMSE-FDE

Para MMSE-FDE el símbolo recuperado antes de la etapa de detección viene dado por

$$\hat{x} = x + \delta + \tilde{\eta} = x + \xi, \tag{D.4.3.20}$$

donde los efectos del ruido $\tilde{\eta}$ y de la interferencia δ se encuentran recogidos en el término de ruido efectivo ξ.

La densidad de probabilidad del ruido condicionada a la respuesta en frecuencia del canal $\mathbf{h} = [h_1 \dots h_{N_c}]$ puede expresarse como

$$p\left(\tilde{\eta}/\mathbf{h}\right) \sim \mathcal{CN}\left(0, \sigma_{\tilde{\eta}}^2\right), \tag{D.4.3.21}$$

donde $\sigma_{\tilde{\eta}}^2$ se define como

$$\sigma_{\tilde{\eta}}^2 = \sigma_{\eta}^2 \frac{\frac{1}{N_c}\sum_{j=1}^{N_c}\left(\frac{|h_j|}{|h_j|^2+N_0/E_S}\right)^2}{\left(\frac{1}{N_c}\sum_{j=1}^{N_c}\frac{|h_j|^2}{|h_j|^2+N_0/E_S}\right)^2}. \tag{D.4.3.22}$$

El término correspondiente a la interferencia puede asumirse que sigue una distribución gaussiana compleja con simetría circular [Nisar 07]. Su media es 0 y su varianza σ_{δ}^2 resulta

$$\sigma_{\delta}^2 = \sigma_s^2 \frac{\frac{1}{N_c}\sum_{j=1}^{N_c}\left(\frac{|h_j|^2}{|h_j|^2+N_0/E_S}\right)^2 - \left(\frac{1}{N_c}\sum_{j=1}^{N_c}\frac{|h_j|^2}{|h_j|^2+N_0/E_S}\right)^2}{\left(\frac{1}{N_c}\sum_{j=1}^{N_c}\frac{|h_j|^2}{|h_j|^2+N_0/E_S}\right)^2}. \tag{D.4.3.23}$$

Como los componentes de ruido e interferencia son variables aleatorias independientes, su suma es otra distribución gaussiana compleja que tiene media cero y cuya varianza puede expresarse como

$$\sigma_{\xi}^2 = \frac{\frac{E_S}{N_c}\sum_{j=1}^{N_c}\frac{|h_j|^2}{|h_j|^2+N_0/E_S} - E_S\left(\frac{1}{N_c}\sum_{j=1}^{N_c}\frac{|h_j|^2}{|h_j|^2+N_0/E_S}\right)^2}{\left(\frac{1}{N_c}\sum_{j=1}^{N_c}\frac{|h_j|^2}{|h_j|^2+N_0/E_S}\right)^2} = E_S\frac{\frac{N_0}{E_S}\beta^M}{1-\frac{N_0}{E_S}\beta^M}, \tag{D.4.3.24}$$

con

$$\beta^M = \frac{1}{N_c}\sum_{j=1}^{N_c}\frac{1}{|h_j|^2+N_0/E_S}. \tag{D.4.3.25}$$

[0]Debe tenerse en cuenta que

$$\frac{1}{N_c}\sum_{j=1}^{N_c}\frac{|h_j|^2}{|h_j|^2+N_0/E_S} = 1 - \frac{1}{N_c}\sum_{j=1}^{N_c}\frac{N_0/E_S}{|h_j|^2+N_0/E_S}$$

El término j-ésimo en la suma (D.4.3.26) se define como

$$Z_j = \frac{1}{|h_j|^2 + N_0/E_S}. \tag{D.4.3.26}$$

y es el inverso de una variable chi cuadrado desplazada una constante N_0. Su densidad de probabilidad resulta

$$f_{Z_j}(z) = f_{|h_j|^2}\left(\frac{1 - z\frac{E_S}{N_0}}{z}\right)\frac{1}{z^2} = \frac{1}{z^2\Gamma(\mu)}\left(\frac{\mu}{\Omega}\right)^{\mu}\left(\frac{1}{z} - \frac{E_S}{N_0}\right)^{\mu-1} e^{\frac{\mu\left(\frac{E_S}{N_0}z - 1\right)}{\Omega z}}. \tag{D.4.3.27}$$

Se ha comprobado que es posible obtener expresiones analíticas para la media y la varianza de Z_j para valores arbitrarios de Ω siempre que μ sea un entero. En otros casos, sería posible emplear técnicas de integración numérica para realizar el cálculo. Un vez que se obtienen los valores de media y varianza, al aplicación del CLT para aproximar la función de densidad de β^M is directa. Dicha aproximación se puede usar entonces para calcular la BER para canales Nakagami-μ arbitrario.

Tras caracterizar Z_j, es posible reescribir la expresión (D.4.3.24) de una manera elegante

$$\sigma_\xi^2 = \sigma_{\tilde{\eta}}^2 + \sigma_\delta^2 = E_S\frac{\frac{N_0}{E_S}\beta^M}{1 - \frac{N_0}{E_S}\beta^M}, \tag{D.4.3.28}$$

y la densidad del término ξ condicionado a la respuesta en frecuencia del canal resulta

$$f(\xi/\mathbf{h}) = f\left(\xi/\beta^M\right) \sim \mathcal{CN}\left(0, \sigma_\xi^2\right). \tag{D.4.3.29}$$

Como se asume mapeado independiente de bit para las señales en fase y cuadratura y la variable es circularmente simétrica, es posible considerar solo su componente real

$$f(\xi_r/\mathbf{h}) = p(\xi_r/\beta^M) \sim \mathcal{N}\left(0, \sigma_{\xi_r}^2/2\right) \tag{D.4.3.30}$$

De esta forma, la densidad del ruido efectivo en MMSE se puede expresar como[1]

$$f_{\xi_r}(x) = \int_0^{E_S/N_0} \sqrt{\frac{\frac{1}{E_S}\left(\frac{E_S}{\beta^M N_0} - 1\right)}{\pi}}\, e^{-x^2\frac{1}{E_S}\left(\frac{E_S}{\beta^M N_0} - 1\right)} p_{\beta^M}(\beta^M) d\beta^M. \tag{D.4.3.31}$$

En los casos en los que Z_j tiene un varianza finita y asumiendo independencia entre los términos en la suma (D.4.3.26), es posible aplicar the CLT (ver section 3.5.1). Así, como (D.4.3.26) es la media de una secuencia de N_c variables aleatorias i.i.d. con media $\overline{Z}$ y varianza $\sigma^2_{Z_j}$, la PDF de β^M se puede aproximar madiante la siguiente función gaussiana

$$f_{\beta^M}(\beta^M) \approx \hat{f}_{\beta^M}(\beta^M) = \frac{1}{\sqrt{2\pi\sigma_Z^2/N_c}}\, e^{-\frac{(\beta^M-\overline{Z_j})^2}{2\sigma_Z^2/N_c}}, \tag{D.4.3.32}$$

con media $\overline{Z_j}$ y varianza $\sigma^2_{Z_j}/N_c$.

Existe una restricción adicional que hay que tener en cuenta: la variable β^M se encuentra limitada por definición en el intervalo the interval $[0, E_S/N_0]$. Para incorporar esta restricción al modelo, la densidad se aproxima ahora por una versión acotada de (D.4.3.32), es decir, por

$$f_{\beta^M}(\beta^M) \approx p_{\beta^M}(\beta^M) = \frac{1}{\hat{F}(\frac{E_S}{N_0}) - \hat{F}(0)} \frac{1}{\sqrt{2\pi\sigma_Z^2/N_c}}\, e^{-\frac{(\beta^M-\bar{Z})^2}{2\sigma_Z^2/N_c}} \quad \beta^M \in [0, E_S/N_0], \tag{D.4.3.33}$$

donde $\hat{F}(x)$ es la CDF obtenida mediante integración a partir de (D.4.3.32).

La expresión de la CDF para el ruido efectivo tras aplicar MMSE-FDE se puede

[1]No debe olvidarse que

$$f_{\xi_r}(x) = \int_{-\infty}^{\infty} \frac{e^{-\frac{x^2}{2\sigma^2_{\xi_r}}}}{\sqrt{2\pi\sigma^2_{\xi_r}}} p_{\sigma^2_{\xi_r}}(\sigma^2_{\xi_r}) d\sigma^2_{\xi_r} = \int_0^{E_S/N_0} \sqrt{\frac{\frac{1}{E_S}\left(\frac{E_S}{\beta^M N_0} - 1\right)}{\pi}} e^{-x^2 \frac{1}{E_S}\left(\frac{E_S}{\beta^M N_0}-1\right)} p_{\beta^M}(\beta^M) d\beta^M.$$

obtener a partir de la eq. (D.4.3.31) mediante integración, es decir,

$$F_{\xi_r}(x) = \int_{-\infty}^{x} \left(\int_0^{E_S/N_0} \sqrt{\frac{\frac{1}{E_S}\left(\frac{E_S}{\beta^M N_0} - 1\right)}{\pi}} e^{-x^2 \frac{1}{E_S}\left(\frac{E_S}{\beta^M N_0} - 1\right)} p_{\beta^M}(\beta^M) d\beta^M \right) dt$$
$$= \int_0^{E_S/N_0} p_{\beta^M}(\beta^M) \left(\int_{-\infty}^{x} \sqrt{\frac{\frac{1}{E_S}\left(\frac{E_S}{\beta^M N_0} - 1\right)}{\pi}} e^{-x^2 \frac{1}{E_S}\left(\frac{E_S}{\beta^M N_0} - 1\right)} dt \right) d\beta^M. \tag{D.4.3.34}$$

La integral interior puede reescribirse empleando la función $Q(\ )$ como

$$\int_{-\infty}^{x} \sqrt{\frac{\frac{1}{E_S}\left(\frac{E_S}{\beta^M N_0} - 1\right)}{\pi}} e^{-x^2 \frac{1}{E_S}\left(\frac{E_S}{\beta^M N_0} - 1\right)} dt = \left\{ \begin{array}{l} u = \sqrt{\frac{2}{E_S}\left(\frac{E_S}{\beta^M N_0} - 1\right)} t \\ du = \sqrt{\frac{2}{E_S}\left(\frac{E_S}{\beta^M N_0} - 1\right)} dt \end{array} \right\}$$
$$= \frac{1}{\sqrt{2\pi}} \int_{-\infty}^{xA(\beta^M)} e^{-\frac{u^2}{2}} du = \frac{1}{\sqrt{2\pi}} \int_{-xA(\beta^M)}^{\infty} e^{-\frac{u^2}{2}} du = Q\left(-xA(\beta^M)\right) = 1 - Q\left(xA(\beta^M)\right),$$

con

$$A(\beta^M) = \sqrt{\frac{2}{E_S}\left(\frac{E_S}{\beta^M N_0} - 1\right)}.$$

Por tanto, la CDF del ruido efectivo tras MMSE-FDE resulta

$$F_{\xi_r}(x) = 1 - \int_0^{E_S/N_0} p_{\beta^M}(\beta^M) Q\left(x\sqrt{\frac{2}{E_S}\left(\frac{E_S}{\beta^M N_0} - 1\right)}\right) d\beta^M. \tag{D.4.3.35}$$

Por ultimo, se muestra a continuación cómo se puede obtener las expresiones anteriores para un canal Nakagami-μ concreto. En concreto, se obtienen las expresiones analíticas para el caso en el que el módulo de la respuesta en frecuencia del canal sigue una distribución de Rayleigh y se encuentra normalizada, es decir, $\Omega = 1$. Para tales valores, la función de densidad puede reducirse a

$$f_{Z_j}(z) = \frac{e^{\frac{E_S}{N_0} - \frac{1}{z}}}{z^2} \quad \forall z \in [0, E_S/N_0]. \tag{D.4.3.36}$$

La expresión correspondiente para la media resulta

$$\overline{Z_j} = e^{\frac{E_S}{N_0}}\Gamma(0,1), \tag{D.4.3.37}$$

donde $\Gamma(z,x)$ es la función Gamma incompleta definida en [Abramowitz 64] como

$$\Gamma(z,x) = \int_x^\infty t^{z-1}e^{-t}dt. \tag{D.4.3.38}$$

La varianza viene dada por

$$\sigma^2_{Z_j} = \frac{E_S}{N_0} - e^{\frac{E_S}{N_0}}\Gamma\left(0,\frac{E_S}{N_0}\right) - e^{2\frac{E_S}{N_0}}\Gamma\left(0,\frac{E_S}{N_0}\right)^2. \tag{D.4.3.39}$$

D.4.4 Expresiones para la BER

El análisis de la BER para SC-FDMA también asume, por un lado, el uso de constelaciones M-QAM cuadradas con mapeado de bit independiente para las componentes en fase y en cuadratura y, por otro, que el término de ruido efectivo $\bar{\eta}$ (i.e., $\tilde{\eta}$ o ξ) es circularmente simétrico. Así puede usarse eq. (D.2.0.3) para expresar la BER como una suma de componentes de probabilidad que dependen de la CDF del ruido efectivo.

Para el caso de ZF-FDE, la integral (D.4.2.15) puede resolverse aplicando la regla trapezoidal compuesta. De este modo la CDF es calculada con

$$F_{\tilde{\eta}_r}(x) \approx \frac{1}{2} + \frac{1}{2\pi}\left(\frac{\omega_{\max}-\omega_{\min}}{n}\left[\frac{\Upsilon\left(x,\omega_{\min}\right)+\Upsilon\left(x,\omega_{\max}\right)}{2} + \sum_{k=1}^{n-1}\Upsilon\left(x,\omega_{\min}+k\frac{\omega_{\max}-\omega_{\min}}{n}\right)\right]\right), \tag{D.4.4.40}$$

donde la función auxiliar $\Upsilon\left(x,\omega\right)$ se define como

$$\Upsilon\left(x,\omega\right) = \frac{e^{ix\omega}\Psi_{\tilde{\eta}_r}(-\omega) - e^{-ix\omega}\Psi_{\tilde{\eta}_r}(\omega)}{i\omega}. \tag{D.4.4.41}$$

Haciendo uso de esas expresiones es posible obtener la siguiente expresión cerrada

para aproximar la BER

$$BER_{ZF} = \sum_{n=1}^{L-1} w(n) \left(\frac{1}{2} - \frac{\omega_{\max}}{2\pi n} \left(\frac{1 + \Upsilon\left((2n-1)d, \omega_{\max}\right)}{2} + \sum_{k=1}^{n-1} \Upsilon\left((2n-1)d, k\frac{\omega_{\max}}{n}\right) \right) \right). \quad \text{(D.4.4.42)}$$

En el caso de MMSE-FDE los CEPs se calculan directamente usando eq. (D.4.3.34). Sustituyéndolos en la suma (D.2.0.3) se obtiene la siguiente expresión para calcular los valores de la BER

$$BER_M = \sum_{n=1}^{L-1} w(n) \int_0^{E_S/N_0} p_{\beta^M}(\beta^M)\, Q\left((2n-1)d \sqrt{\frac{2}{E_S}\left(\frac{E_S}{\beta^M N_0} - 1\right)} \right) d\beta^M. \quad \text{(D.4.4.43)}$$

D.4.5 Resultados de las simulaciones

Las expresiones cerradas (D.4.4.42) y (D.4.4.43) han sido validadas mediante simulaciones considerando un modelo de canal en el cual la respuesta en frecuencia para las N_c sub-portadoras asignadas son modeladas como variables aleatorias complejas i.i.d. con distribución gaussianas.

En el caso de ZF-FDE se presentan los resultados para BPSK en la Fig. D.6. Puede observarse como para valores bajos de la SNR, las curvas de BER están por encima de la correspondiente a OFDM y la diferencia es mayor conforme aumenta N_c. Sin embargo, a medida se incrementa la SNR, todas las curvas convergen a la de OFDM independientemente del número de portadoras.

Para MMSE-FDE se presentan resultados para 4QAM . Se observa que la validez de la expresión propuesta depende del número de sub-portadoras asignadas N_c y en la potencia de ruido N_0. Para valores de la SNR pequeños, la expresión proporciona resultados de BER consistentes con los obtenidos mediante simulaciones, mientras que, para valores altos de SNR, se produce una divergencia cuando N_c es pequeño.

Independientemente de la SNR, la aproximación es válida para valores más realistas de N_c ($N_c \geq 64$).

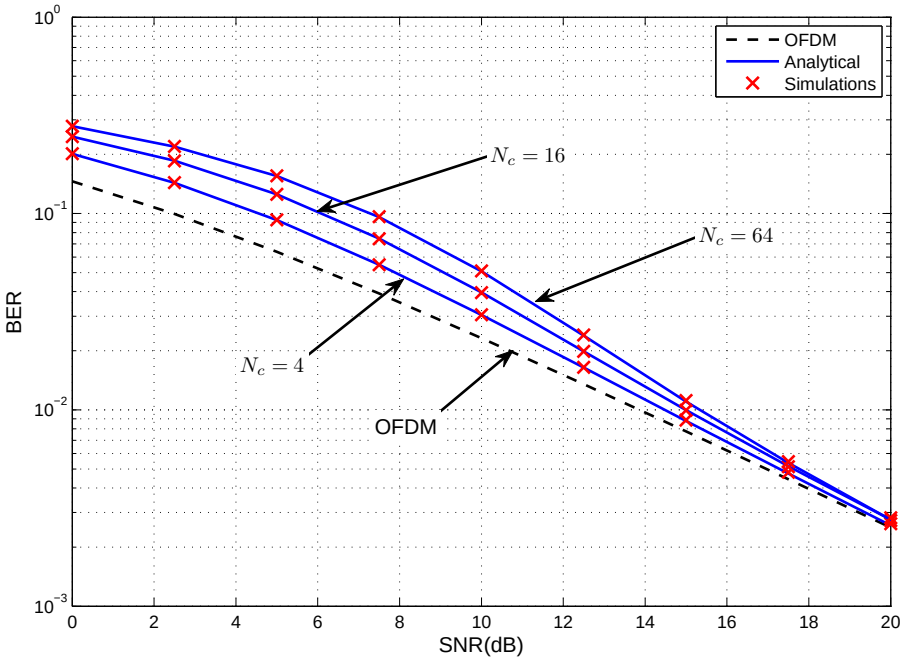

Figure D.6: Resultadqos analítico y de simulaciones para portadoras independientes (BPSK) ZF-FDE

Las expresiones propuestas han sido también comparadas con valores de BER realistas obtenidos para una transmisión SC-FDMA con BPSK sobre diferente modelos de canal definidos por el ITU [ITU-R 97] y el 3GPP [3GPP 10]. En la tesis se muestra como el cociente de coherencia (*Coherence Ratio*, CR) entre el ancho de banda de coherencia (*Coherence Bandwidth*, CB) y el espaciado en frecuencia entre portadoras asignadas consecutivas influye en la bondad de las aproximaciones propuesta. Para CR ≤ 1, se obtienen valores aproximados a los obtenidos mediante simulaciones para tanto para ZF-FDE como para MMSE-FDE en SC-FDMA entrelazado.

De los resultados presentados se puede deducir que OFDM establece un límite inferior para SC-FDMA en términos de BER. También se observa que tanto los valores de BER obtenidos para MMSE-FDE con (D.4.4.43) y como los obtenidos

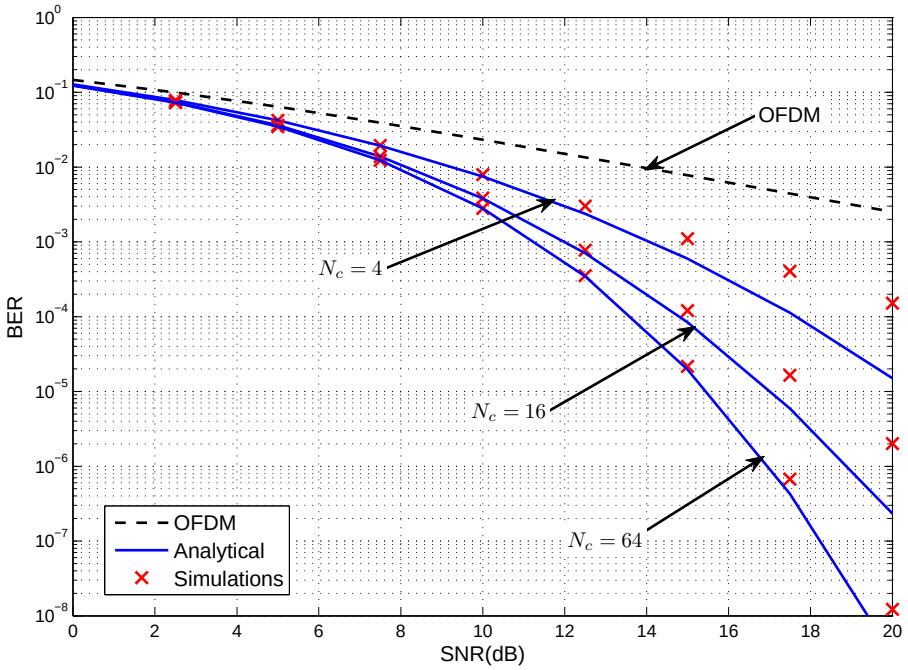

Figure D.7: Resultados analítico y de simulaciones para portadoras independientes (BPSK) MMSE-FDE

mediante simulaciones están por debajo de los de OFDM. Este comportamiento es consistente con los resultados en [Ciochina 07] e implica que los valores de OFDM suponen un límite superior.

D.5 Análisis de la eficiencia espectral

La calidad de la señal recibida en los sistemas celulares depende de varios factores tales como las pérdidas de propagación, *shadowing* log-normal o el desvanecimiento rápido y el ruido. La utilización de modulación adaptativa (Adaptive Modulation, AM) permite mejorar la eficiencia espectral de la señal transmitida compensando los efectos anteriores. Así, usuarios con buenas condiciones emplean constelaciones más densas (p.ej., 64 QAM) mientras que el orden de modulación decrece para usuarios con peores condiciones de canal. En esta disertación se analiza la eficiencia espectral para un transmisión SC-FDMA sin codificación sobre un canal con desvanecimiento

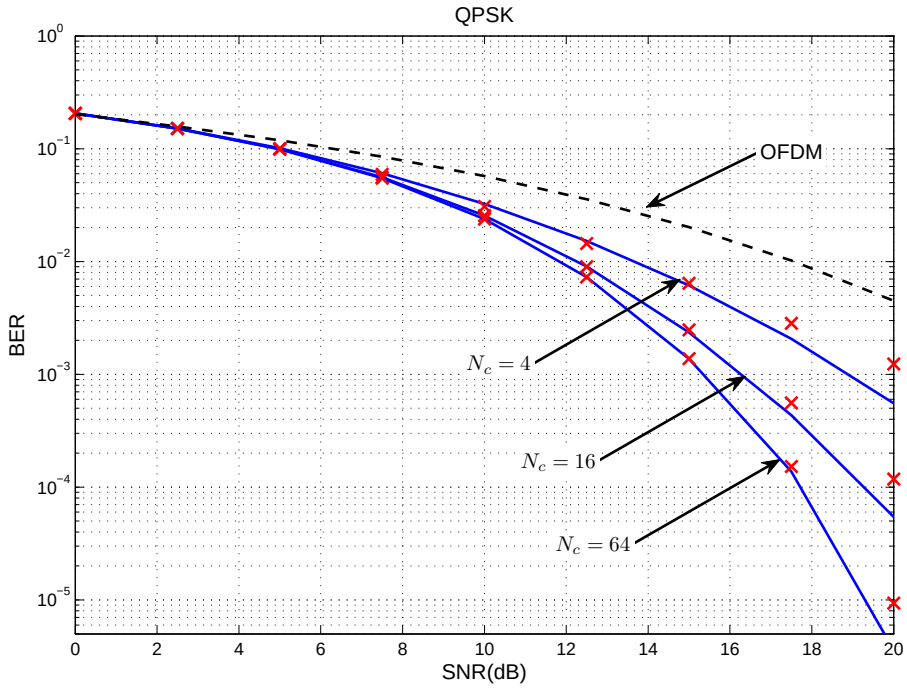

Figure D.8: Resultados analítico y de simulaciones para portadoras independientes 4QAM) MMSE-FDE

Rayleigh tanto para ZF-FDE como para MMSE-FDE.

D.5.1 Análisis de la eficiencia espectral para ZF-FDE

El valor de la SNR en el receptor para SC-FDMA con ZF-FDE viene dado por $\frac{E_S}{\beta^{ZF} N_0}$, donde β^{ZF} se define como

$$\beta^{ZF} = \frac{1}{N_c} \sum_{j=1}^{N_c} \frac{1}{|h_j|^2}. \tag{D.5.1.1}$$

La constelación correspondiente a la i-ésima region se aplica cuando el valor de la SNR se encuentra entre las fronteras de la mimas, es decir,

$$\gamma_i < \frac{E_S}{\beta^{ZF} N_0} < \gamma_{i+1}. \tag{D.5.1.2}$$

La expresión anterior puede reescribirse si se redefinen las L regiones para discretizar los valores de β^{ZF}

$$\beta^{ZF}_{i+1} = \frac{1}{\gamma_{i+1}} \frac{E_S}{N_0} < \beta^{ZF} < \frac{1}{\gamma_i} \frac{E_S}{N_0} = \beta^{ZF}_i, \tag{D.5.1.3}$$

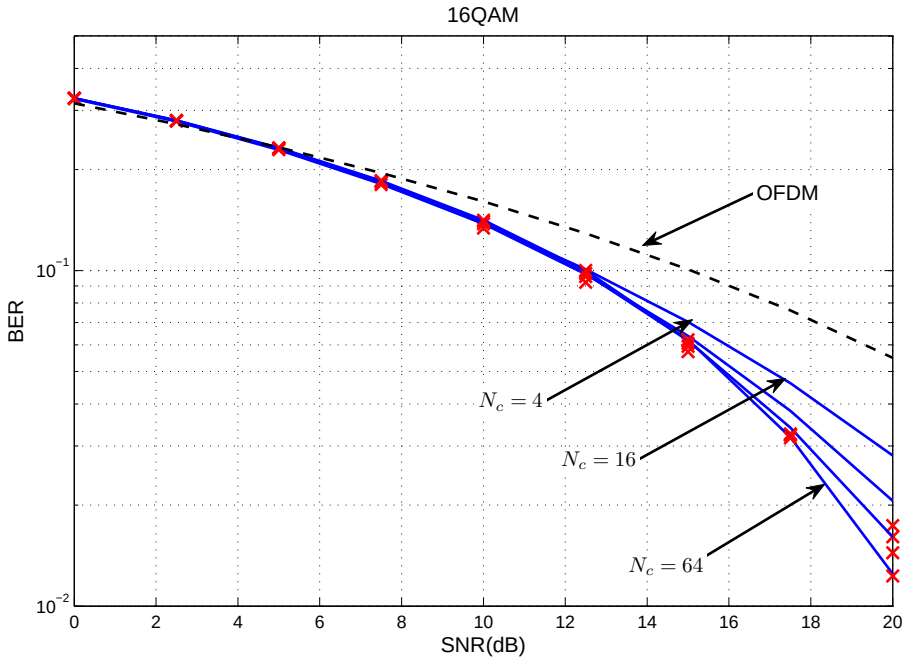

Figure D.9: Resultados analítico y de simulaciones para portadoras independientes (16QAM) MMSE-FDE

donde β_i^{ZF} y β_{i+1}^{ZF} son los umbrales modificados que dependen de la SNR.

La eficiencia espectral media se puede calcular como

$$\frac{R}{B} = \sum_{i=1}^{L-1} \log_2(M_i)\, p_{\beta^{ZF}}\left(\beta_{i+1}^{ZF} < \beta^{ZF} < \beta_i^{ZF}\right) = \sum_{i=1}^{L-1} \log_2(M_i)\left[F_{\beta^{ZF}}\left(\beta_i^{ZF}\right) - F_{\beta^{ZF}}\left(\beta_{i+1}^{ZF}\right)\right]. \quad \text{(D.5.1.4)}$$

donde L es el número de regiones.

Por tanto, es necesario conocer $F_{\beta^{ZF}}(\beta^{ZF})$ para calcular la eficiencia espectral media. Para una canal con desvanecimiento selectivo en frecuencia de tipo Rayleigh, es la CDF correspondiente a la suma de N_c variables aleatorias idénticas con una distribución inversa chi-cuadrado ponderada (D.5.1.1), cada una con la siguiente PDF

$$f_X(x) = \frac{e^{-\frac{1}{xN_c}}}{x^2 N_c}. \quad \text{(D.5.1.5)}$$

A partir de la expresión anterior, es posible calcular CHF usando (3.471.9) en

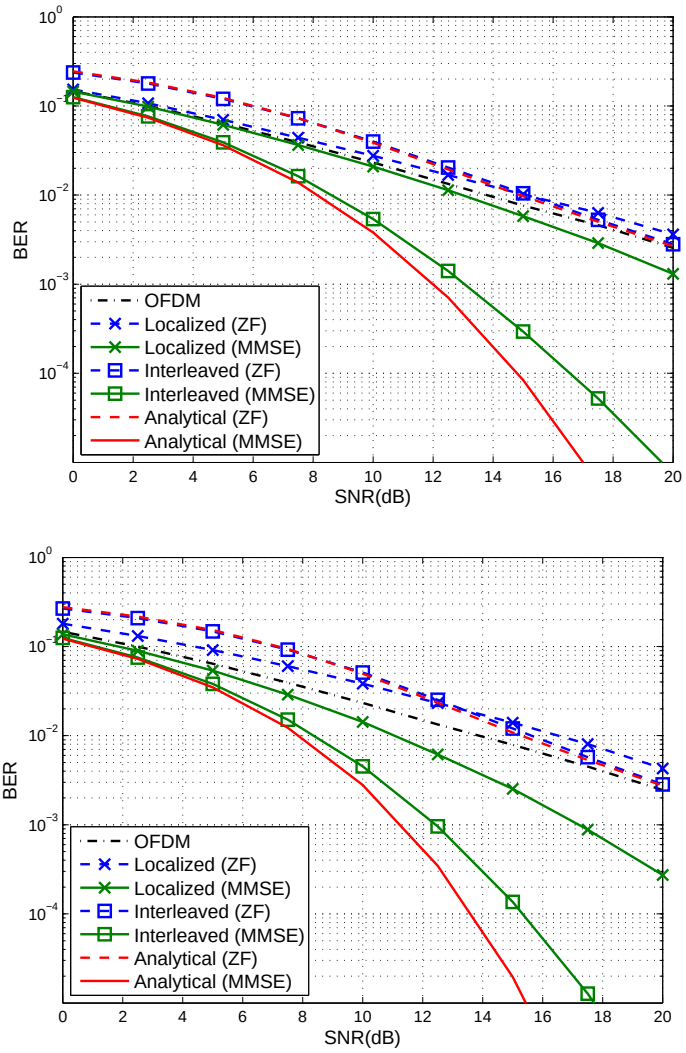

Figure D.10: BER para canal Extended VA ($N_c = 16$ y $N_c = 64$)

[Grinstead 97] como

$$\Phi_X(\omega) = 2\sqrt{\frac{-\omega}{N_c}\jmath}K_1\left(2\sqrt{\frac{-\omega}{N_c}\jmath}\right). \tag{D.5.1.6}$$

Como la respuesta en frecuencia del canal para cada una de las portadoras asignadas se supone independiente, la CHF de β^{ZF} resulta

$$\Phi_{\beta^{ZF}}(\omega) = 2\left(\sqrt{\frac{-\omega}{N_c}\jmath}K_1\left(2\sqrt{\frac{-\omega}{N_c}\jmath}\right)\right)^{N_c}. \tag{D.5.1.7}$$

De nuevo se puede emplear la expresión de Gil-Peláez del teorema de inversión para

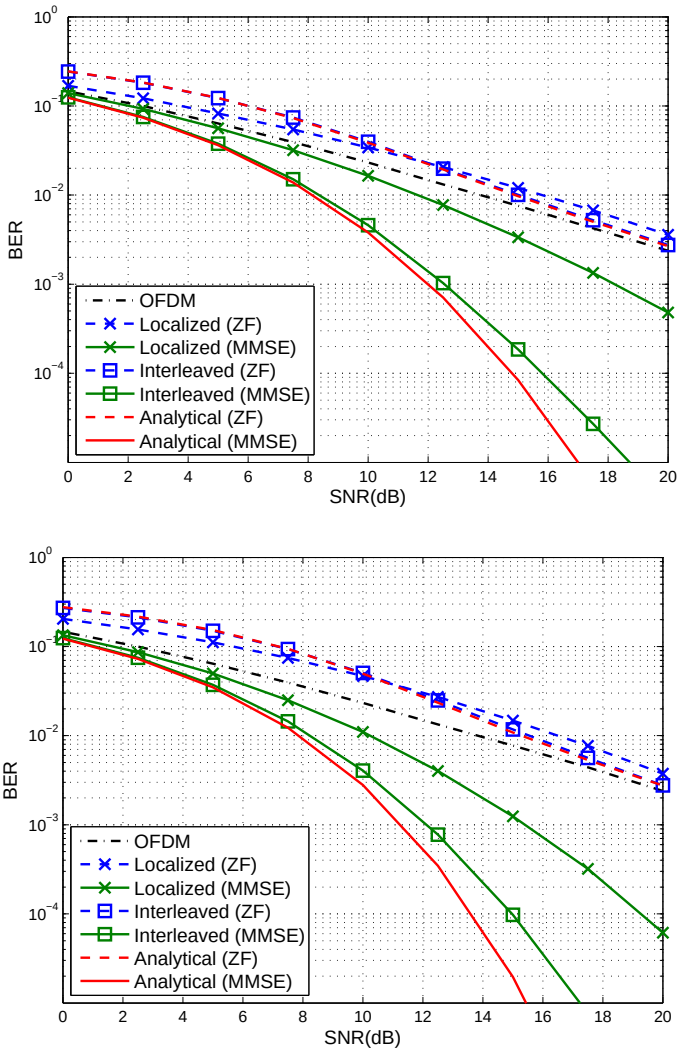

Figure D.11: BER para canal Extended TU ($N_c = 16$ y $N_c = 64$)

evaluar la correspondiente CDF

$$F_{\beta^{ZF}}\left(\beta^{ZF}\right) = \frac{1}{2} - \frac{1}{2\pi}\int_0^{\infty}\left(\frac{\Phi_{\beta^{ZF}}(\omega)}{\jmath\,\omega}e^{-\jmath\beta^{ZF}\omega} - \frac{\Phi_{\beta^{ZF}}(-\omega)}{\jmath\,\omega}e^{\jmath\beta^{ZF}\omega}\right)d\omega. \quad \text{(D.5.1.8)}$$

Sustituyendo esta expresión en (D.5.1.4) se pueden calcular los valores de eficiencia espectral.

D.5.2 Análisis de la eficiencia espectral para MMSE-FDE

En el caso en el que se aplica MMSE-FDE para compensar los efectos del canal sobre la transmisión SC-FDMA, la SNR instantánea se puede expresar como

$$\gamma_{MMSE} = \frac{E_S}{\beta^M N_0} - 1, \tag{D.5.2.9}$$

donde

$$\beta^M = \frac{1}{N_c} \sum_{j=1}^{N_c} \frac{1}{|h_j|^2 + N_0/E_S}. \tag{D.5.2.10}$$

El parámetro β^M determina la SNR y, en consecuencia, la constelación a emplear en cada caso. Formalmente,

$$\gamma_i < \frac{E_S}{\beta^M N_0} - 1 < \gamma_{i+1}. \tag{D.5.2.11}$$

En este caso la desigualdad resultante tras redefinir las L regiones para discretizar el valor de β^{ZF} es

$$\beta_{i+1}^M = \frac{E_S}{N_0} \frac{1}{\gamma_{i+1} + 1} < \beta^M < \frac{E_S}{N_0} \frac{1}{\gamma_i + 1} = \beta_i^M, \tag{D.5.2.12}$$

donde β_i^M y β_{i+1}^M son los umbrales modificados que dependen de la SNR.

Para MMSE-FDE la eficiencia espectral media se puede expresar como

$$\begin{aligned} \frac{R}{B} = & \sum_{i=1}^{L-1} \log_2(M_i)\, p_{\beta^M}\left(\beta_{i+1}^{ZF} < \beta^M < \beta_i^M\right) = \\ & \sum_{i=1}^{L-1} \log_2(M_i) \left[F_{\beta^M}\left(\beta_i^M\right) - F_{\beta^M}\left(\beta_{i+1}^M\right)\right]. \end{aligned} \tag{D.5.2.13}$$

donde L es el número de regiones.

De nuevo se necesita $F_{\beta^M}(\beta^M)$ que en este caso es la suma de N_c variables aleatorias idénticas de tipo chi-cuadrado inversa ponderadas y desplazadas N_0. Cada una de ellas con una PDF

$$f_Y(y) = f_X(x - N_0) = \frac{e^{-\frac{1}{(x-N_0)N_c}}}{(x - N_0)^2 N_c}. \tag{D.5.2.14}$$

La CHF correspondiente viene dada por

$$\Phi_Y(\omega) = \Phi_X(\omega) e^{\jmath N_0 \frac{\omega}{N_c}} = 2\sqrt{\frac{-\omega}{N_c}\jmath} K_1\left(2\sqrt{\frac{-\omega}{N_c}\jmath}\right) e^{\jmath N_0 \frac{\omega}{N_c}}. \quad \text{(D.5.2.15)}$$

Bajo la asunción de independencia entre las respuestas en frecuencia del canal, la CHF de β^M resulta

$$\Phi_{\beta^M}(\omega) = \left(2\sqrt{\frac{-\omega}{N_c}\jmath} K_1\left(2\sqrt{\frac{-\omega}{N_c}\jmath}\right) e^{\jmath N_0 \frac{\omega}{N_c}}\right)^{N_c}, \quad \text{(D.5.2.16)}$$

y se puede evaluar usando la fórmula de Gil-Peláez como

$$F_{\beta^M}\left(\beta^M\right) = \frac{1}{2} - \frac{1}{2\pi}\int_0^\infty \left(\frac{\Phi_{\beta^M}(\omega)}{\jmath\,\omega} e^{-\jmath\beta^M\omega} - \frac{\Phi_{\beta^M}(-\omega)}{\jmath\,\omega} e^{\jmath\beta^M\omega}\right) d\omega. \quad \text{(D.5.2.17)}$$

Combinando la expresión anterior con (D.5.2.13) se pueden calcular los valores de eficiencia espectral para MMSE-FDE.

D.5.3 Validación de las expresiones

La validez de (D.5.1.4) y (D.5.2.13) realizando simulaciones con los mismo modelos de canal que en el apartado anterior. En Fig. D.12 se presentan resultados de eficiencia espectral para $BER_T = 10^{-3}$ y diferentes valores de N_c para ZF-FDE. Puede observarse que, siempre que se cumpla la condición de independencia entre las respuestas en frecuencia del canal para las sub-portadoras asignadas, los valores de eficiencia espectral calculados con eq. (D.5.1.4) y los obtenidos mediante simulaciones coinciden. También se puede observar que el número de sub-portadoras asignadas reduce la eficiencia espectral en SC-FDMA.

Los resultados obtenidos son consistentes con los obtenidos en [Wu 09] donde emplean la fórmula de Shannon. A la hora de hacer comparaciones debe tenerse en cuenta que hay un pérdida efectiva de potencia debida al uso de M-QAM [Goldsmith 05].

Para MMSE-FDE se presentan las Figs. D.13a y D.13b donde se muestran resultados para diferentes número de sub-portadoras asignadas. En ambos casos,

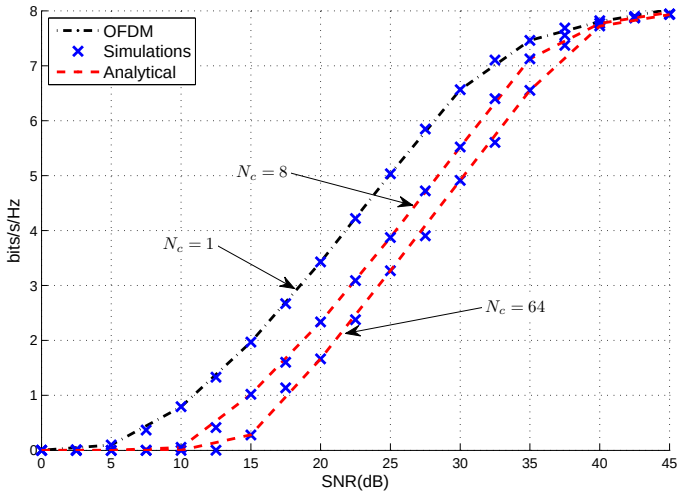

Figure D.12: Eficiencia espectral para $BER_T = 10^{-3}$ (ZF)

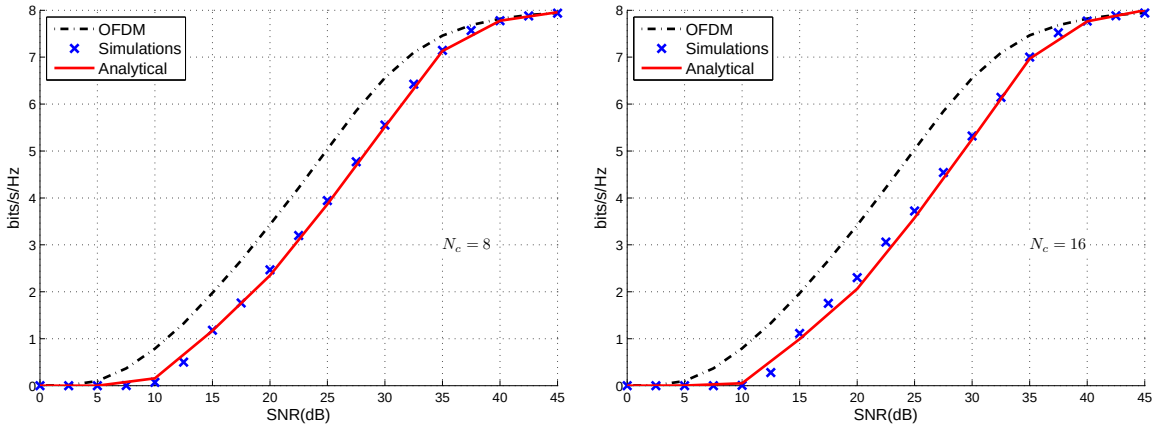

Figure D.13: Eficiencia espectral para $BER_T = 10^{-3}$ (MMSE)

los valores de eficiencia espectral calculados con (D.5.2.13) están muy próximos a los obtenidos mediante simulaciones lo que demuestra la validez de la aproximación empleada.

Al igual que en el análisis de BER, se ha estudiado la bondad de las expresiones obtenidas a la hora de aproximar resultados obtenidos con modelos de canal más realistas. Las figuras Figs. D.14a a D.14a muestran los resultados para canales EVA y ETU. Se observa que para estos canales las expresiones permiten aproximar los valores reales de la eficiencia espectral para SC-FDMA entrelazado.

Además, se observa que la eficiencia espectral para SC-FDMA tiene la correspondiente a OFDMA como límite superior. También, se puede concluir que las expresiones propuestas pueden servir para definir los valores de eficiencia espectral en SC-FDMA asumiendo el caso peor. Es decir, la expresiones son un límite inferior para los valores reales.

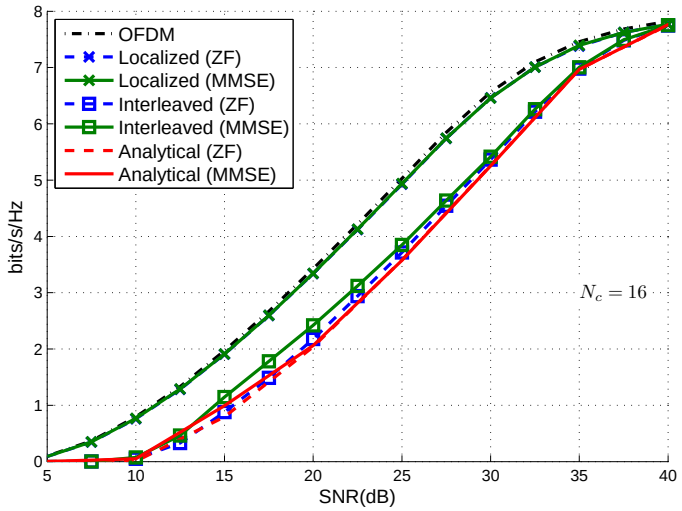

(a) Canal EVA

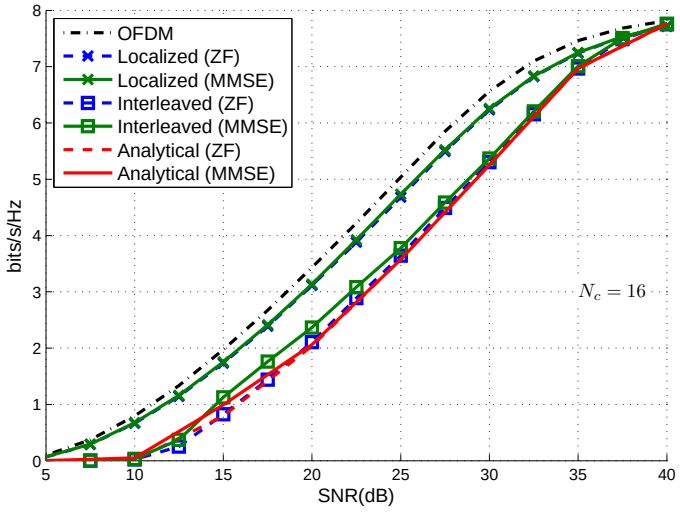

(b) Canal ETU

Figure D.14: Comparación de eficiencia espectral para canales EVA y ETU

D.6 Conclusiones

En esta tesis se recoge el trabajo realizado durante el análisis del rendimiento de SC-FDMA en términos de BER y eficiencia espectral. Se ha prestado especial atención a los efectos de la ecualización lineal en frecuencia sobre el ruido mejorado. Las principales contribuciones de esta tesis se enumeran a continuación.

- *Estudio estadístico del ruido mejorado tras la ecualización lineal en el dominio de la frecuencia para OFDM y SC-FDMA*. Considerando diferentes canales con desvanecimiento selectivo en frecuencia, se ha realizado un riguroso estudio del ruido mejorado tras ecualización a la entrada del detector para OFDM y SC-FDMA. Además, se ha derivado la función densidad de probabilidad para la variable aleatoria que modelo dicho ruido.

- *Análisis de la BER para la transmisión SC-FDMA sobre canales Nakagami-μ con desvanecimientos*. A partir de el estudio mencionado en el apartado anterior, se han obtenido expresiones cerradas de la BER para transmisiones SC-FDMA sobre canales Nakagami-μ con desvanecimientos cuando se aplica ecualización lineal en el dominio de la frecuencia. Concretamente, asumiendo independencia entre las sub-portadoras asignadas, se han obtenido expresiones cerradas de la BER para ecualización ZF-FDE; para MMSE-FDE se ha derivado una aproximación pesimista que funciona como límite inferior.

- *Análisis de la eficiencia espectral para SC-FDMA*. La eficiencia espectral lograda tras aplicar ecualización lineal en el dominio de la frecuencia ha sido también objeto de estudio. En concreto se considerado una transmisión SC-FDMA con modulación adaptativa sobre un canal con desvanecimiento. De nuevo se consideran los algoritmos de ecualización en frecuencia antes mencionados (ZF y MMSE-FDE) y se asume independencia entra las sub-portadoras asignadas. En ambos casos, se hallaron expresiones cerradas para la eficiencia espectral que han demostrado su validez al ser comparadas con valores obtenidos con

simulaciones para modelos de canal realistas (p.ej., EVA y ETU). También se ha demostrado que dichas expresiones ofrecen resultados para el caso peor en cualquier transmisión SC-FDMA.

Bibliography

[3GPP 08] 3GPP. *36series: Evolved Universal Terrestrial Radio Access (E-UTRA).* Ts, 3rd Generation Partnership Project (3GPP), http://www.3gpp.org/ftp/Specs/html-info/36-series.htm, 2008.

[3GPP 10] 3GPP. *36.104: Evolved Universal Terrestrial Radio Access (E-UTRA); Base Station (BS) radio transmission and reception.* Ts, 3rd Generation Partnership Project (3GPP), http://www.3gpp.org/ftp/Specs/html-info/36-series.htm, 2010.

[Abe 00] S. Abe & A. K. Rajagopal. *Justification of power law canonical distributions based on the generalized central-limit theorem.* Europhysics Letters, vol. 52, no. 6, pages 610–614, 2000.

[Abramowitz 64] M. Abramowitz & I. A. Stegun. Handbook of mathematical functions with formulas, graphs, and mathematical tables. Dover, New York, ninth dover printing, tenth gpo printing edition, 1964.

[Aghamohammadi 90] A. Aghamohammadi & H. Meyr. *On the error probability of linearly modulated signals on Rayleigh frequency-flat fading channels.* IEEE Transactions on Communications, vol. 38, no. 11, pages 1966–1970, nov 1990.

[Balakrishnan 09] N. Balakrishnan & C.-D. Lai. Continuous Bivariate Distributions, chapitre Elliptically Symmetric Bivariate and Other Symmetric Distributions, pages 591–622. Springer, 2009.

[Bardou 02] F. Bardou, J.-P. Bouchaud, A. Aspect & C. Cohen-Tannoudji. Lévy Statistics and Laser Cooling, chapitre Broad distributions and Levy statistics: a brief overview, pages 42–59. Cambridge University Press, 2002.

[Baxley 10] R. J. Baxley, B. Walkenhorst & G. Acosta-Marum. *Complex Gaussian Ratio Distribution with Applications for Error Rate Calculation in Fading Channels with Imperfect CSI.* In IEEE Global Telecommunications Conference, GLOBECOM 2010, 2010.

[Beaulieu 05] N. Beaulieu & C. Cheng. *Efficient Nakagami-m fading channel Simulation.* IEEE Transactions on Vehicular Technology, vol. 54, no. 2, pages 413 –424, march 2005.

[Berger 63] J. M. Berger & B. Mandelbrot. *A new model for error clustering in telephone circuits.* IBM Journal, vol. 7, pages 224–236, July 1963.

[Bocher 92] M. Bocher. *On Bessel's Functions of the Second Kind.* The Annals of Mathematics, vol. 6, no. 4, pages 85–90, 1892.

[Box 73] G. E. P. Box & G. Tiao. Bayesian Inference in Statistical Analysis. AddissonWesley, 1973.

[Brcic 02] R. F. Brcic. *Some aspects of signal processing in heavy tailed noise.* PhD thesis, Curtin University of Technology, Australian Telecommunications Research Institute, 2002.

[Brown 10] R. J. Brown & B. Rimmer. *Generalized Central Limit Theorem.* Demostration, The Wolfram Demonstrations Project, 2010.

[Cambanis 81] S. Cambanis, S. Huang & G. Simons. *On the theory of elliptically contoured distributions.* Journal of Multivariate Analysis, vol. 11, no. 3, pages 368–385, 1981.

[Cedilnik 06] A. Cedilnik, K. Kovsmelj & A. Blejec. *Ratio of Two Random Variables: A Note On The Existence of Its Moments.* metodološki zvezki - Advances in Methodology and Statistics, vol. 3, pages 1–7, 2006.

[Chang 66] R. W. Chang. *Synthesis of band-limited orthogonal signals for multi-channel data transmission.* Bell System Technical Journal, vol. 46, pages 1775–1796, 1966.

[Chmielewski 81] M. A. Chmielewski. *Elliptically Symmetric Distributions: A Review and Bibliography.* International Statistical Review / Revue Internationale de Statistique, vol. 49, no. 1, pages 67–74, 1981.

[Cimini 85] L. Cimini. *Analysis and Simulation of a Digital Mobile Channel Using Orthogonal Frequency Division Multiplexing.* IEEE Transactions on Communications [legacy, pre - 1988], vol. 33, no. 7, pages 665–675, 1985.

[Ciochina 07] C. Ciochina, D. Castelain, D. Mottier & H. Sari. *Single-Carrier Space-Frequency Block Coding: Performance Evaluation.* In IEEE 66th Vehicular Technology Conference, 2007. VTC-2007 Fall, pages 715 –719, 302007-oct.3 2007.

[Cooper 62] P. W. Cooper. *The Hypersphere in pattern recognition.* Information and Control, vol. 5, pages 324–346, 1962.

[Count 01] P. A. Count. *Performance analysis of OFDM in frequency-selective, slowly fading Nakagami channels.* PhD thesis, Naval Postgraduate School, 2001.

[Daalhuis 10] A. B. O. Daalhuis & R. A. Askey. Digital library of mathematical functions. National Institute of Standards and Technology, 2010.

[DasGupta 10] A. DasGupta. Fundamentals of Probability: A First Course. Springer Texts in Statistics. Springer, 2010.

[Davenport 52] W. B. Davenport. *An Experimental Study of Speech-Wave Probability Distributions.* The Journal of the Acoustical Society of America, vol. 24, pages 390–399, 1952.

[David 95] H. A. David. *First (?) Occurrence of Common Terms in Mathematical Statistics.* The American Statistician, vol. 49, no. 2, pages 121–133, 1995.

[del Castillo 01] C. del Castillo. *La Distribución de Behrens-Fisher Multivariante. Aplicación al Problema de Behrens-Fisher Multivariante.* PhD thesis, Servicio de Publicaciones de la Universidad de Málaga, 2001.

[Du 06] Z. Du, J. Cheng & N. Beaulieu. *Accurate error-rate performance analysis of OFDM on frequency-selective Nakagamim fading channels.* Communications, IEEE Transactions on, vol. 54, no. 2, pages 319 – 328, 2006.

[Dugué 06] D. Dugué. Encyclopedia of statistical sciences, volume 3, chapitre Lévy, Paul-Pierre, pages 4143–4144. John Wiley and Sons, 2nd edition, 2006.

[DuMouchel 75] W. H. DuMouchel. *Stable Distributions in Statistical Inference: 2. Information from Stably Distributed Samples.* Journal of the American Statistical Association, vol. 70, no. 350, pages 386–393, 1975.

[Eisenhart 06] C. Eisenhart. Encyclopedia of statistical sciences, volume 6, chapitre Laws of Error – II: The Gaussian Distribution, pages 4068–4082. John Wiley and Sons, 2nd edition, 2006.

[Ergen 09] M. Ergen. Mobile Broadband Including WiMAX and LTE. Springer Science+Business Media, LLC, 1st edition edition, 2009. ISBN: 0387681892.

[Falconer 02] D. Falconer, S. L. Ariyavisitakul, A. Benyamin-Seeyar & B. Eidson. *Frequency Domain Equalization for Single-Carrier Broadband Wireless Systems*. IEEE Commun. Mag, vol. 40, pages 58–66, 2002.

[Fang 90a] K. T. Fang, S. Kotz & K. Ng. Symmmetric Multivariate and Related Distributions. Chapman and Hall, 1990.

[Fang 90b] K.-T. Fang, S. Kotz & K. W. Ng. Symmetric Multivariate and Related Distributions. Chapman and Hall, 1990.

[Fang 06] K. Fang. Encyclopedia of statistical sciences, volume 3, chapitre Elliptically contoured distributions, pages 1910–1918. John Wiley and Sons, 2nd edition, 2006.

[Fazel 03] K. Fazel & S. Kaiser. Multi-Carrier and Spread Spectrum Systems, chapitre Chapter 5: Applications. Wiley, 2003.

[Feller 71] W. Feller. An introduction to probability theory and its applications, vol. 2. Wiley, 3 edition, January 1971.

[Gazor 03] S. Gazor & W. Zhang. *Speech probability distribution*. IEEE Signal Processing Letters, vol. 10, no. 7, pages 204–207, July 2003.

[Ghosh 69] J. K. Ghosh. *Only Linear Transformations Preserve Normality.* Sankhyā: The Indian Journal of Statistics, Series A, vol. 31, no. 3, pages pp. 309–312, 1969.

[Gil-Peláez 51] J. Gil-Peláez. *Note on the Inversion Theorem.* Biometrika, vol. 38, no. 3/4, pages 481–482, 1951.

[Girón 99] F. J. Girón, M. L. Martínez & L. Imlahi. *A characterization of the Behrens–Fisher distribution with applications to Bayesian inference.* Comptes Rendus de l'Académie des Sciences - Series I - Mathematics, vol. 328, no. 8, pages 701 – 706, 1999.

[Girón 01] F. J. Girón & C. del Castillo. *A note on the convolution of inverted-gamma distributions with applications to the Behrens-Fisher distribution.* Rev. R. Acad. Cien. Serie A. Mat., vol. 95, no. 1, pages 39–44, 2001.

[Gnedenko 54] B. V. Gnedenko & A. N. Kolmogorov. Limit distributions for sums of independent random variables. Addison-Wesley, 1954.

[Goldsmith 05] A. Goldsmith. Wireless communications. Cambridge University Press, New York, NY, USA, 2005.

[Gradshteyn 07] I. Gradshteyn & I. Ryzhik. Table of integrals, series, and products. Elsevier Academic Press, 2007.

[Grinstead 97] C. M. Grinstead & L. J. Snell. Introduction to probability. American Mathematical Society, July 1997.

[Gubner 06] J. A. Gubner. Probability and Random Processes for Electrical and Computer Engineers. Cambridge University Press, New York, NY, USA, 2006.

[Hara 03] S. Hara & R. Prasad. Multicarrier Techniques for 4G Mobile Communications. Universal Personal Communications. Artech House, 2003.

[Hasna 03] M. Hasna & M.-S. Alouini. *End-to-end performance of transmission systems with relays over Rayleigh-fading channels.* IEEE Transactions on Wireless Communications, vol. 2, no. 6, pages 1126–1131, 2003.

[Hayya 75] J. Hayya, D. Armstrong & N. Gressis. *A Note on the Ratio of Two Normally Distributed Variables.* Management Science, vol. 21, no. 11, pages 1338–1341, 1975.

[Heyde 06a] C. C. Heyde. Encyclopedia of statistical sciences, volume 10, chapitre Probability Theory: An Outline, pages 6492–6496. John Wiley and Sons, 2nd edition, 2006.

[Heyde 06b] C. C. Heyde. Encyclopedia of statistical sciences, volume 6, chapitre Limit Theorem, Central, pages 4183–4187. John Wiley and Sons, 2nd edition, 2006.

[IEEE 09] IEEE. *IEEE Standard for Local and metropolitan area networks Part 16: Air Interface for Broadband Wireless Access Systems.* IEEE Std 802.16-2009 (Revision of IEEE Std 802.16-2004), vol. 0, page 0, 29 2009.

[ITU-R 97] ITU-R. *M.1225, Guidelines for Evaluation of Radio Transmission Technologies for IMT-2000.* Recommendation ITU-R M, no. 1225, 1997.

[Johnson 87] M. E. Johnson. Multivariate statistical simulation, chapitre Chapter 6: Elliptical Contoured Distributions, pages 106–124. John Wiley & Sons, Inc., 1987.

[Johnson 95] N. Johnson, S. Kotz & N. Balakrishnan. Continuous Univariate Distributions, volume 2. Wiley Series in Probability and Statistics, 1995.

[Kang 03] Z. Kang, K. Yao & F. Lorenzelli. *Nakagami-m fading modeling in the frequency domain for OFDM system analysis.* IEEE Communications Letters, vol. 7, no. 10, pages 484 – 486, oct. 2003.

[Kelker 70] D. Kelker. *Distribution theory of spherical distributions and a location-scale parameter generalization.* Sankhya: The Indian Journal of Statistics. Series A, vol. 32, pages 419–430, 1970.

[Kotz 04] S. Kotz & N. Balakrishnan. Multivariate t Distributions and their Applications. Cambridge University Press, 2004.

[Lam 00] E. Lam & J. Goodman. *A mathematical analysis of the DCT coefficient distributions for images.* IEEE Transactions on Image Processing, vol. 9, no. 10, pages 1661–1666, Oct 2000.

[Lawrey 97] E. Lawrey. *The suitability of OFDM as a modulation technique for wireless telecommunications, with a CDMA comparison.* PhD thesis, James Cook University, 1997.

[Lévy 24] P. Lévy. *Théorie des erreurs. La loi de Gauss et les lois exceptionnelles.* Bulletin de la Société Mathématique de France, vol. 52, pages 49–85, 1924.

[López-Martínez 10] F. López-Martínez, E. Martos-Naya, J. Paris & U. F. Plazaola. *Generalized BER Analysis of QAM and Its Application to MRC Under Imperfect CSI and Interference in Ricean Fading Channels.* IEEE Transactions on Vehicular Technology, vol. 59, no. 5, pages 2598–2604, jun 2010.

[Mandelbrot 60] B. Mandelbrot. *The Pareto-Lévy Law and the Distribution of Income.* International Economic Review, vol. 1, no. 2, pages 79–106, 1960.

[McGraw 68] D. McGraw & J. Wagner. *Elliptically symmetric distributions.* IEEE Transactions on Information Theory, vol. 14, no. 1, pages 110–120, Jan 1968.

[Monrad 06] D. Monrad & W. Stout. Encyclopedia of statistical sciences, volume 3, chapitre Stable Distributions, pages 7974–7978. John Wiley and Sons, 2nd edition, 2006.

[Mori 01] M. Mori & M. Sugihara. *The double-exponential transformation in numerical analysis.* Journal of Computational and Applied Mathematics, vol. 127, page 287âĂŞ296, 2001.

[Myung 06] H. G. Myung, J. Lim & D. J. Goodman. *Single carrier FDMA for uplink wireless transmission.* IEEE Vehicular Technology Magazine, vol. 1, no. 3, pages 30–38, Sept. 2006.

[Myung 07] H. G. Myung. *Single Carrier Orthogonal Multiple Access Technique for Broadband Wireless Communications.* PhD thesis, Polytechnic University, Brooklyn, NY, USA, January 2007.

[Myung 08] H. G. Myung & D. J. Goodman. Single Carrier FDMA: A New Air Interface for Long Term Evolution. Wiley Series on Wireless Communications and Mobile Computing. Wiley, first edition, October 2008.

[Nadarajah 08] S. Nadarajah. *A Review of Results on Sums of Random Variables.* Acta Applicandae Mathematicae, vol. 103, pages 131–140, 2008.

[Nakagami 58] M. Nakagami. *The m-Distribution, a general formula of intensity of rapid fading.* Statistical Methods in Radio Wave Propagation: Proceedings of a Symposium held June 18-20, pages 3–36, 1958.

[Nee 00] R. v. Nee & R. Prasad. Ofdm for wireless multimedia communications. Artech House, Inc., Norwood, MA, USA, 2000.

[Nisar 07] M. Nisar, H. Nottensteiner & T. Hindelang. *On Performance Limits of DFT Spread OFDM Systems.* In 16th IST Mobile and Wireless Communications Summit, pages 1 –4, 2007.

[Nolan 11] J. P. Nolan. Stable distributions - models for heavy tailed data. Birkhäuser, Boston, 2011. In progress, Chapter 1 online at academic2.american.edu/∼jpnolan.

[Ohno 04] S. Ohno & G. Giannakis. *Capacity maximizing MMSE-optimal pilots for wireless OFDM over frequency-selective block Rayleigh-fading channels.* IEEE Transactions on Information Theory, vol. 50, no. 9, pages 2138 – 2145, sep. 2004.

[Ollila 08] E. Ollila. *On the Circularity of a Complex Random Variable.* IEEE Signal Processing Letters, vol. 15, pages 841 –844, 2008.

[Ollila 11] E. Ollila, J. Eriksson & V. Koivunen. *Complex Elliptically Symmetric Random Variables - Generation, Characterization, and Circularity Tests.* IEEE Transactions on Signal Processing, vol. 59, no. 1, pages 58 –69, 2011.

[Owen 83] J. Owen & R. Rabinovitch. *On the Class of Elliptical Distributions and their Applications to the Theory of Portfolio*

Choice. The Journal of Finance, vol. 38, no. 3, pages 745–752, June 1983.

[Pancaldi 08] F. Pancaldi, G. M. Vitetta, N. Al-Dhahir, M. Uysal, S. Muhaidat & R. Kalbasi. *Single-Carrier Frequency Domain Equalization: A Review*. IEEE Signal Processing Magazine, vol. 25, no. 5, pages 37–56, 2008.

[Pearson 16] K. Pearson. *Mathematical Contributions to the Theory of Evolution. XIX. Second Supplement to a Memoir on Skew Variation*. Philosophical Transactions of the Royal Society of London. Series A, Containing Papers of a Mathematical or Physical Character, vol. 216, pages 429–457, 1916.

[Pham-Gia 06] T. Pham-Gia, N. Turkkan & E. Marchand. *Density of the Ratio of Two Normal Random Variables and Applications*. Communications in Statistics - Theory and Methods, vol. 35 (9), pages 1569–1591, 2006.

[Picinbono 94] B. Picinbono. *On circularity*. IEEE Transactions on Signal Processing, vol. 42, no. 12, pages 3473 –3482, December 1994.

[Pierce 96] R. Pierce. *RCS characterization using the alpha-stable distribution*. In IEEE National Radar Conference, pages 154–159, May 1996.

[Pierce 97] R. Pierce. *Application of the positive alpha-stable distribution*. In IEEE Signal Processing Workshop on Higher-Order Statistics, pages 420–424, Jul 1997.

[Prasad 03] R. Prasad & M. Ruggieri. Technology Trends In Wireless Communications. Universal Personal Communications. Artech House, 2003.

[Proakis 00] J. G. Proakis. Digital communications / john g. proakis. McGraw-Hill, New York, 4 edition, 2000.

[Rappaport 66] S. Rappaport & L. Kurz. *An Optimal Nonlinear Detector for Digital Data Transmission Through Non-Gaussian Channels.* IEEE Transactions on Communication Technology, vol. 14, no. 3, pages 266–274, June 1966.

[Read 06] C. B. Read. Encyclopedia of statistical sciences, volume 8, chapitre Normal Distributions, pages 5652–5663. John Wiley and Sons, 2nd edition, 2006.

[Reiss 07] R.-D. Reiss & M. Thomas. Statistical Analysis of Extreme Values, chapitre Elliptical and Related Distributions, pages 279 – 290. Springer, 3rd edition, 2007.

[Samorodnitsky 94] G. Samorodnitsky & M. S. Taqqu. Stable non-gaussian random processes: Stochastic models with infinite variance. Chapman and Hall, London, 1994.

[Sánchez-Sánchez 09a] J. J. Sánchez-Sánchez, M. C. Aguayo-Torres & U. Fernández-Plazaola. *On the bivariate Pearson type VII and its application to the BER analysis for SC-FDMA.* In 2nd International Symposium on Applied Sciences in Biomedical and Communication Technologies (Isabel 2009), 2009. Bratislava, Slovak Republik.

[Sánchez-Sánchez 09b] J. J. Sánchez-Sánchez, U. Fernández-Plazaola, M. C. Aguayo-Torres & J. Entrambasaguas. *Closed-form BER expression for interleaved SC-FDMA with M-QAM.* In IEEE 70th Vehicular Technology Conference, 2009. VTC 2009 Fall, 2009.

[Sánchez-Sánchez 11] J. J. Sánchez-Sánchez, M. C. Aguayo-Torres & U. Fernández-Plazaola. *BER Analysis for Zero-Forcing SC-FDMA over Nakagami-m Fading Channels.* IEEE Transactions on Vehicular Technology, 2011.

[Sari 95] H. Sari, G. Karam & I. Jeanclaude. *Transmission techniques for digital terrestrial TV broadcasting.* IEEE Signal Processing Letters, vol. 33, no. 2, pages 100 –109, feb 1995.

[Sari 96] H. Sari, Y. Lvy & G. Karam. *Orthogonal frequency-division multiple access for the return channel on CATV networks.* In International Conference on Telecommunications (ICT 96), 1996.

[Seneta 06] E. Seneta. Encyclopedia of statistical sciences, volume 10, chapitre History of Probability, pages 6469–6472. John Wiley and Sons, 2nd edition, 2006.

[Shao 93a] M. Shao & C. Nikias. *Signal processing with fractional lower order moments: stable processes and their applications.* Proceedings of the IEEE, vol. 81, no. 7, pages 986–1010, Jul 1993.

[Shao 93b] M. Shao & C. Nikias. *Signal detection in impulsive noise based on stable distributions.* In Conference Record of The Twenty-Seventh Asilomar Conference on Signals, Systems and Computers, pages 218–222 vol.1, Nov 1993.

[Shayesteh 95] M. Shayesteh & A. Aghamohammadi. *On the error probability of linearly modulated signals on frequency-flat Ricean, Rayleigh, and AWGN channels.* IEEE Transactions on Communications, vol. 43, no. 234, pages 1454 –1466, feb/mar/apr 1995.

[Simon 98a] M. Simon & M. Alouini. *A unified approach to the performance analysis of digital communication over generalized fading channels.* Proceedings of the IEEE, vol. 86, no. 9, pages 1860 –1877, September 1998.

[Simon 98b] M. Simon & M.-S. Alouini. *A unified approach to the probability of error for noncoherent and differentially coherent modulations over generalized fading channels.* IEEE Transactions on Communications, vol. 46, no. 12, pages 1625 – 1638, December 1998.

[Simon 05] M. K. Simon & M.-S. Alouini. Digital communication over fading channels. Wiley series in telecommunications and signal processing. John Wiley & Sons, 2005.

[Simon 06] M. K. Simon. Probability distributions involving gaussian random variables: A handbook for engineers, scientists and mathematicians. Springer-Verlag New York, Inc., Secaucus, NJ, USA, 2006.

[Stuck 74] B. W. Stuck & B. Kleiner. *A statistical analysis of telephone noise.* Bell Syst. Tech. J., vol. 53, pages 1263–1320, 1974.

[Stuck 00] B. Stuck. *An historical overview of stable probability distributions in signal processing.* In IEEE International Conference on Acoustics, Speech, and Signal Processing, ICASSP '00, volume 6, pages 3795–3797 vol.6, 2000.

[Subotic 07] V. Subotic & S. Primak. *BER Analysis of Equalized OFDM sytems in Nakagami, $m < 1$ Fading.* Wireless Personal Communications, vol. 40, pages 281–290, 2007.

[Tsakalides 95] P. Tsakalides. *Array signal processing with alpha-stable distributions*. PhD thesis, Univ. Southern California, Los Angeles, 1995.

[Tsanakas 04] A. Tsanakas & Z. Landsman. *Elliptical distributions and stochastic orders*. In 3rd Conference in Actuarial Science & Finance in Samos, 2004.

[van de Beek 02] J. van de Beek, P. Ödling, S. Wilson & P. Börjesson. Review of Radio Science, 1996-1999, chapitre Orthogonal Frequency Division Multiplexing (OFDM). Wiley, 2002.

[Voit 05] J. Voit. The statistical mechanics of financial markets series. Theoretical and Mathematical Physics. Springer-Verlag, 3rd edition, 2005.

[Walzman 73] T. Walzman & M. Schwartz. *Automatic equalization using the discrete frequency domain*. IEEE Transactions on Information Theory, vol. 19, no. 1, pages 59 – 68, jan 1973.

[Wang 04] Z. Wang, X. Ma & G. Giannakis. *OFDM or single-carrier block transmissions?* IEEE Transactions on Communications, vol. 52, no. 3, pages 380 – 394, mar. 2004.

[Wang 05] N. Wang. *Transmit Optimization for Multicarrier and Multiple-Input Multiple-Output Wireless Communications*. PhD thesis, Queen's University, 2005.

[Wang 07] X. Wang, Q. Liu, S. Member & G. B. Giannakis. *Analyzing and optimizing adaptive modulation coding jointly with ARQ for QoS-guaranteed traffic*. IEEE Trans. Veh. Technol, vol. 56, 2007.

[Wang 08] H. Wang, X. You, B. Jiang & X. Gao. *Performance Analysis of Frequency Domain Equalization in SC-FDMA Systems.* In IEEE International Conference on Communications, ICC '08, pages 4342–4347, May 2008.

[Weinstein 71] S. Weinstein & P. Ebert. *Data Transmission by Frequency-Division Multiplexing Using the Discrete Fourier Transform.* IEEE Transactions on Communications [legacy, pre - 1988], vol. 19, no. 5, pages 628–634, 1971.

[Weisstein 99] E. W. Weisstein. The CRC concise encyclopedia of mathematics, chapitre Probability, pages 1445–1146. CRC Press, 1999.

[Wilson 99] S. Wilson & J. Cioffi. *Probability density functions for analyzing multi-amplitude constellations in Rayleigh and Ricean channels.* IEEE Transactions on Communications, vol. 47, no. 3, pages 380 –386, mar 1999.

[Wolfson 06] D. Wolfson. Encyclopedia of statistical sciences, volume 6, chapitre Lindeberg-Lévy Theorem, pages 4190–4192. John Wiley and Sons, 2nd edition, 2006.

[Wu 09] H. Wu, T. Haustein & P. A. Hoeher. *On the Information Rate of Single-Carrier FDMA Using Linear Frequency Domain Equalization and Its Application for 3GPP-LTE Uplink.* EURASIP Journal on Wireless Communications and Networking, page 11, 2009.